Clarke Lake Gas Field Reservoir Characterization

Geoscience BC Report 2018-19

Prepared by Evan Renaud, Dr. Jonathan Banks, Dr. Nicholas B. Harris and Dr. John Weissenberger

Prepared for Geoscience BC

Contents

Tables

Figures

Appendix A

Appendix B

Executive Summary

Clarke Lake field, a depleted natural gas reservoir in northeast British Columbia, is being investigated for its potential to be repurposed as a geothermal reservoir. This report evaluates key geological variables that control the flow of hot water within the reservoir. Rocks encountered within the field are described for sedimentological characteristics and interpreted for depositional environments then related to porosity and permeability data to identify, map and characterize the quality of reservoir units. We then apply flow units in flow simulations to assess the viability of 25-year geothermal power plant projects. Our primary flow unit shows relatively high average porosity (6.4%) and permeability (124md). Favorable values of porosity are due to non-touching vugs within dolomitized sections where bioclasts have been dissolved. Resulting flow simulations using our primary flow unit have shown that we are able produce 300kW of electrical power using a well doublet and 2400kW of electrical power using a four injector and eight producer well configuration.

Introduction

We report on a preliminary investigation of the geothermal energy potential of the Clarke Lake gas field, located ~10km south/southeast of Fort Nelson, B.C, and hosted within dolomitized carbonates of the Slave Point Formation (Figure 1). Hydrothermal fluids moving through the Western Canadian Sedimentary Basin created a locally pervasive body of dolomite within the Middle Devonian Presqu'ile Barrier, which extends from Pine Point, NWT to northeastern B.C (Qing, 1994). At Clarke Lake, this has allowed for porous and permeable reservoir rock to develop in otherwise tight limestone. Reservoir temperatures in the Clarke Lake field are abnormally high (Figure 2). The mature gas field is now being investigated for its potential to produce sufficient hot formation water to generate geothermal electric power. We have applied core data and well log data with advanced modelling software to provide a model of the reservoir and simulate hot water production.

Geologic Background

The oldest Devonian deposits in the Western Canadian Sedimentary Basin were deposited in the mid-Eifelian to early Givetian and are bounded by major regional unconformities at the base and top of a second order transgressional sequence (base of upper Chinchaga Formation and base of the Watt Mountain Formation, respectively) (Weissenberger, 2001, Figure 3).

At this time, the Presqu'ile Barrier and Clarke Lake field were located at approximately 5° south of the paleoequator within a shallow epicontinental sea that was favourable for carbonate deposition (Witzke, 1988). The Keg River Formation of the Elk Point Group developed as a large east to west/northwest trending carbonate barrier referred to as the Presqu'ile Barrier. The barrier restricted seawater circulation to the south, allowing for deposition of evaporites of the Muskeg and Prairie formations (Qing, 1994; Weissenberger, 2001). Reefs of the

Upper Keg River Formation developed on top of the Lower Keg River Formation in response to an overall sea level rise during the final stages of deposition of the mid-Eifelian to early Givetian second order sequence.

In the late Givetian, continued sea level rise terminated most reef growth within the Presqu'ile Barrier. This sea level rise is represented by the Evie shale (Figure 1), which was deposited over Keg River carbonates during the incursion of the epicontinental sea onto the carbonate platform. Aggradational deposits of the Sulphur Point Formation (Figure 3) also reflect this final transgression before the upper Givetian-Frasnian second order sequence (Weissenberger, 2001). The highstand portion of Beaverhill Lake Group (and beginning of the Givetian-Frasnian sequence) is first represented by the thin shale of the Watt Mountain Formation (Figure 3). The shale sits unconformably above the Elk Point Group and has been interpreted to represent an erosional and/or a transgressive event (Lonnee, 2006).

As conditions favourable for carbonate deposition persisted into the late Devonian, patch reefs of the Slave Point Formation developed on structural highs related to fault-bounded highs in the Precambrian basement (O'Connell, 1990). Shales of the Otter Park Member of the Horn River Group, deposited north of the platform margin, represent the basinal equivalent of the Slave Point Formation. Slave Point reefs continued to grow in a back-stepping nature as sea level rose until the Slave Point reefs, much like the Keg River, were eventually drowned when reef growth failed to keep up with sea level rise. This major Late Devonian sea level rise deposited a package of Muskwa Formation shale on top of the reef complex, which provided a regional seal for many Devonian oil & gas plays in Alberta and BC (Morrow, 2002).

Data Set and Methods

Twenty cores from wells within the immediate area of the Clarke Lake field were described in August of 2017 at the BC Oil and Gas Commission Core Research Facility in Fort St. John. Dunham's (1962) carbonate classification was applied to the rocks, which were divided into facies and facies associations.

Two hundred eighty two wells with well logs taken from GeoScout and IHS Markit were compared to rock descriptions in order to provide common log responses that represent specific depositional or diagenetic facies. These log signatures give the ability to interpret facies where there is no core control. The data was observed and interpreted using Schlumberger's software Petrel.

Stratigraphic cross-sections were built in order to understand the spatial variability as well as the inherent facies structure of the reservoir. Seven hundred thirty six porosity and permeability analyses for samples from the Slave Point Formation were available through the GeoScout database. These measurments were taken from analysis of small plugs and full cores taken from intervals within the Slave Point Formation. Surfaces were generated by correlating well tops and these surfaces form the basis of our static geomodels. Cells within the model

were assigned permeability and porosity values that are characteristic of particular flow units. Simulations were run using the software PetraSim to provide realistic flow cases for particular rocks at Clarke Lake field.

Results

Facies

Slave Point Formation at Clarke Lake field can be grouped into 4 facies associations. Breccia and gray matrix dolomite of Facies Association 4 represent diagenetic features due to a significant dolomitic overprint that destroyed most or all original depositional character. Facies Associations 1 to 3 are either limestone (with preserved depositional character) or partially dolomitized carbonate rock (depositional features are discernable). Depositional facies were classified based on fossil type, abundance and size; additional features noted include the presence of dolomite or limestone, sedimentary structures and pore types. Diagenetic facies were classified based on pore types and the dominance of breccia or gray matrix dolomite.

Facies Descriptions (Depositional)

Facies Association 1

1A: *Amphipora*/*Stachyodes* Wacke/Packstone

Facies 1A consists of abundant *Amphipora* and *Stachyodes* fossils in conjunction (Figure 4A). *Amphipora* fossil size never exceeds more than a few mm, but fossils are generally larger in this facies compared to facies 1B. *Stachyodes* fossil in this faces are typically between 0.5cm to 1cm in scale. The matrix is composed of a skeletal fragment mudstone. Tabular and larger formed stromatoporoids along with coral form minor but important parts of the fossil assemblage. In dolomitized sections, the rock is primarily gray in colour (Figure 4B), whereas limestone sections are darker gray. Packstone intervals vary from 10-20cm in thickness, whereas wackestone intervals are usually thicker, locally exceeding 2 meters. Primary porosity within limestone sections is poorly developed, whereas fossil dissolution gives way to mouldic and vuggy porosity within the dolomitized sections. We also see mouldic pores infilled by white saddle dolomite (Figure 4C). Intercrystalline porosity also exists in dolomitized sections showing gray matrix dolomite.

1B: *Amphipora* Wacke/Packstone

Facies 1B is dominated by small (1-2mm) *Amphipora* fossils that occur in stratigraphic association with facies 1C (Figure 5A). Minor fossil constituents include *Stachyodes*, corals, nodular and hemispherical stromatoporoids. The matrix is composed of skeletal fragments along with larger stromatoporoid fragments. Like facies 1A, dolomitic sections tend to be a gray to light gray, whereas limestone sections are dark gray. Horizons of *Amphipora* packstone are locally present within this facies as well as within facies 1C (although less common in facies 1C). Primary porosity within limestone sections is poorly developed, whereas dolomitized sections show significant

intercrystalline as well as mouldic porosity (Figure 5B).

1C: Brown Mudstone

The primary feature of facies 1C is the development of weakly laminated to unlaminated brown mudstone (Figure 6A). In instances where the fabric is strongly laminated, fossils are generally absent, whereas weakly laminated to unlaminated sections show minor occurrences of *Amphipora* as well as Ostracods (Figure 6B). Facies 1C predominantly overlies facies 1B, but it also occurs in stratigraphic association with facies 1A. Organic-rich laminae were also observed in some of the sections. Subvertical and subhorizontal fractures in this facies tend to be completely or partially filled by sparry calcite. Primary porosity is poorly developed in limestone sections. Dolomitic sections of this facies show intercrystalline porosity but this facies generally lacks the mouldic or vuggy pores that are present in facies 1A and 1B (Figure 6C).

Facies Association 2

2A: Massive Stromatoporoid Boundstone

Continuous intervals of predominantly large hemispherical stromatoporoids are representative of facies 2A (Figure 7A). This facies is up to 20cm thick in core and comprises a minor part of Facies Association 2. Tabular stromatoporoid forms are also present. Facies 2A occurs in stratigraphic association with facies 2B and 2C. Observation of this facies within dolomitized sections is difficult but possible due to dolomite selectively replacing the stromatoporoid fabric. This is especially apparent in partially dolomitized sections where white dolomite crystals are easily seen in contrast to dark gray limestone (Figure 7B). In limestone sections, this rock shows interparticle as well as intraparticle pores that are dominantly filled with sparry calcite. Sparry calcite fill is also apparent in irregular fractures and fracture swarms. Dolomitic sections show some mouldic pores but are dominated by intercrystalline porosity.

2B: *Stachyodes* Packstone

Facies 2B represents the majority of Facies Association 2 and is composed mostly of *Stachyodes* stromatoporoids (Figure 8A). The matrix is composed of a brown skeletal and crinoidal wackestone. Bioclasts include *Stachyodes*, *Amphipora*, crinoids, tabular stromatoporoids, and corals. Sections of this facies (along with facies 2A and 2B) are dark gray to black in colour, making observations difficult, whereas other intervals are light gray to brown and depositional character is easily observed. Bioclast concentration varies, and some horizons can be described as grainstone. Dolomitic sections typically show significant mouldic and vuggy porosity where large amounts of fossils have been leached. Limestone sections show significant interparticle as well as intraparticle pores that are almost always filled by sparry calcite (Figure 8B). One instance of a dark fissile shale occurs within this facies.

2C: *Stachyodes* Wackestone

Facies 2C contains a fossil assemblage similar to facies 2B but with a lower concentration of bioclasts. This facies is still dominantly composed of *Stachyodes* with minor coral, *Amphipora* and tabular stromatoporoids. The matrix is a dark gray skeletal mudstone to wackestone. Facies 2C occurs stratigraphically below facies 2B. Intervals of this facies are typically only ~10cm thick, but there are specific cases of 1-2meter thick intervals. Primary porosity within this facies is poorly developed, but some minor occurrences of intraparticle porosity do exist. Dolomitic sections show intercrystalline porosity but generally appear to have less porosity than facies 2A and 2B.

Facies Association 3

3A: Crinoidal Wackestone

Facies 3A is a dark gray/black wackestone with crinoids, skeletal fragments and large (up to 3.5cm) brachiopod shells/shell fragments (Figure 9A). There are also minor occurrences of *Stachyodes* fossils and soft sediment deformation. The matrix is a dark gray/black mudstone. Limestone sections have poor primary porosity, but where present, dolomitization produced a chaotic texture with large vugs from dissolution of large brachiopod fragments and some intercrystalline porosity. More fossiliferous sections show more mouldic porosity, whereas less fossiliferous sections show more intercrystalline porosity.

3B: Crinoidal Mudstone

Facies 3B is a dark gray/black mudstone with lower fossil density than facies 3A (Figure 9B). Minor crinoid ossicles, skeletal fragments and rare brachiopod shells constitutes the fossil assemblage. This facies occurs stratigraphically below facies 3A. Limestone porosity is again poorly developed but dolomitic sections can show some intercrystalline porosity and very small mouldic pores. Dolomitized sections of facies 3A and 3B show large veins partially to fully filled by dolomite (Figure 9C, 9D).

Facies Descriptions (Diagenetic)

Facies Association 4

4A: Breccia

Facies 4A is a breccia that shows rounded or angular clasts. The angular clasts are mudstone and are brecciated by saddle dolomite veins or gray matrix dolomite (Figure 10A, 10B), whereas rounded clasts are brecciated by large saddle dolomite veins (Figure 10C). Depositional character within this facies has been almost entirely destroyed by dolomitization. Sulfide mineralization is present with higher intensity toward the stratigraphically lower portion of cored intervals. This facies is dominated by intercrystalline porosity but also displays vugs which are partially infilled by saddle dolomite. Mouldic pores are present but rare.

4B: Gray Matrix Dolomite (GMD)

Facies 4B represents sections of rock where depositional character has been entirely destroyed and replaced with gray matrix dolomite (with minor amounts of saddle dolomite) (Figure 10D). Styolites and subvertical to subhorizontal fractures partially to fully filled by saddle dolomite are common within this facies. Compared to facies 4A, there is much less saddle dolomite and porosity is dominantly intercrystalline, although some oversized vugs do occur.

Well Log Character

Dolomite and limestone

The most effective way to distinguish dolomite from limestone is by using a photoelectric log, which give values of ~3.0 barns/electron for dolomite and ~5.0 barns/electron for limestone (Doveton, 1994). Increases in resistivity, density porosity and sonic two-way travel time also mark a transition from dolomite to limestone. The neutron log shows a decrease in porosity/neutron counts when leaving a dolomite interval and entering limestone intervals. The SP log can also show negative deflections representing less permeable limestone zones. These well log responses (aside from the sonic log) are shown in Figure 11, in which the limestone interval is present from 1990m to 2026m.

Facies

Brown mudstone of facies 1C is well represented by a high gamma ray log response within the interval 2001.82m to 2003m (Figure 12). The neutron log shows a decrease in porosity/neutron counts and an increase in sonic two-way travel time within the same interval. In comparison, the *Amphipora* packstone/wackestone of facies 1B shows low gamma ray log response, an increase in porosity/neutron counts and a decrease in sonic two-way travel time. The smaller interval of facies 1C at 2000.9m to 2001.21m also shows a subtle increase in gamma ray log response and a decrease in neutron porosity/neutron counts.

Stachyodes packstone of facies 2B can be recognized by a relatively lower gamma ray response compared to wackestones of facies 2C (Figure 13). This is shown in the interval of ~1967.5m to 1978m. The section shows a shoaling upward sequence where packstone intervals of facies 2B and intervals of facies 2C grade into a coarser grainstone/packstone section at 1962.7m to 1967.5m. Figure 14 shows a relatively coarser section of Facies Association 2, with the shale described in facies 2B represented by a high gamma ray log response at 1987m. Thinner intervals of facies 2B packstones cause slight decreases in porosity/neutron counts shown from 1974m to 1977.5m, whereas intervals of facies 2B grainstone show increases in porosity/neutron counts. Facies Association 3 deposits are demarcated by a relative increase in gamma ray log response (Figure 15). The lowest gamma ray response seen in Facies Association 3 is 15 API units compared to a minimum of ~9 API in Facies Association

1 and a minimum of ~5 API in Facies Association 2.

Petrophysical Character by Facies/Facies Association

Figure 16 shows porosity and permeability analyses by lithology (dolomite, limestone or mixed lithology). Limestone samples lay within the bottom left quadrant while dolomite and limestone dolomite mixed samples show relatively higher porosity and permeability (Figure 16). Porosity and permeability centroid values for limestone are 2.5% and 0.714md, respectively. For dolomite, the values are 6.4% and 104md. For mixed lithologies, the values are 8.4% and 81md. The majority of high perm/high porosity analyses are from dolomite samples and dolomite and limestone mixed lithologies. Figure 17 shows analyses by facies associations. Porosity and permeability centroid values for Facies Association 1 are 6.8% and 80md, respectively. For Facies Association 2, the values are 4.7% and 42md. For Facies Association 3, the values are 10% and 72md. For Facies Association 4, the values are 5.1% and 183md.

The relationships between facies and petrophysical properties are shown in Figure 18. Average porosity, permeability and densities for each facies are given in Table 1. Facies 1A and 1B display similar values of porosity and are more porous than facies 1C. However, facies 1A shows a higher average value of permeability compared to facies 1B (Figure 18A). Facies 1B shows a wide range of porosity and permeability (Figure 18B), while facies 1C shows relatively lower permeability and porosity (Figure 18C). Facies Association 2 shows clearly that limestone samples have low porosity and permeability compared to dolomite samples (Figure 18D). Facies Association 3 generally shows high porosity but low permeability, with the exception of three samples (Figure 18E) in well CANLIN CLARKE B-A018-D/094-J-16. These high permeability samples are likely due to partially filled fractures or enlarged vugs. Facies Association 4 shows a wide range of porosity values but exhibits the highest values of permeability (Figures 18F, 18G).

Interpretation

Facies Interpretation

We apply the depositional model of a rimmed carbonate platform, following Wendte's (1992) depositional model for the Swan Hills Formation at Judy Creek field (Figure 19), which is depositionally equivalent to the Clarke Lake reservoir. The model depicts a lower energy reef interior comprising lagoonal and tidal deposits and a higher energy platform margin with reef flat deposits. Beyond the reef margin is the upper slope with poorly cyclic deposits, whereas further down the slope are increasingly lower energy deposits in a basinal depositional setting (Figure 19). In the following sections, facies interpretations are compared to Wendte's facies model and Lonnee's (2006) facies model for the Slave Point Formation at Clarke Lake field.

Facies Association 1

Facies 1A

The presence of *Amphipora* implies a relatively low energy lagoonal setting. Larger *Amphipora* with *Stachyodes* indicates that deposition occurred in a higher energy section of the reef where these larger organisms could withstand increased wave energy. These features suggest that this facies represents a back reef lagoonal setting relatively near the reef margin. This facies corresponds to Wendte's (1992) reef flat shoal-margin limestone which is dominated by brecciated *Amphipora*, cylindrical and tabular stromatoporoids (Figure 19). Facies 1A did not show brecciation or significant fracturing of *Amphipora* clasts described in Wendte's (1992) model, which may be because the Swan Hills reef at Judy Creek field was subjected to higher energy at the reef margin. Lonnee's (2006) facies zone IIIb is equivalent to this facies, although he interpreted this rock to have been deposited in a relatively lower energy setting. Using the paleodepth graphic from Wendte, deposition occurred at water depths between 0-5m (Figure 19).

Facies 1B

Lower fossil concentration and diversity than in facies 1A and the presence of smaller mm-scale *Amphipora* suggests that facies 1B was deposited in a lower energy, more restricted lagoonal setting. Deposition is interpreted to have occurred farther landward from the reef margin in a deeper part of the lagoon. This facies is similar to Wendte's *Amphipora* Lagoonal Limestone facies in the Swan Hills Field, except that he recorded larger cm-scale sized fossils compared to mm-scale fossils described in this study (Figure 19). He also noted that the dark colour of the rock implies settings closer to the center of the reef complex where circulation was poor. Deposition occurred at water depths between 0-5m.

Facies 1C

Poorly developed laminae and very low fossil diversities and concentrations present in facies 1C is distinctive of a shallow tidal flat environment. Minor *Amphipora* imply that some of these rocks were deposited in a subtidal environment. Where no *Amphipora* are present, water levels may have been shallower. This facies corresponds to Wendte's tidal flat environment, which was deposited at low energy shorelines in the reef interior in 0-5m of water (Figure 19). This facies is also equivalent to Lonnee's facies zone Ib and IIb.

Facies Association 2

Facies 2A

A diverse fossil assemblage coupled with the occurrence of robust forms of hemispherical and tabular stromatoporoids imply a high energy, well oxygenated, shallow water setting at the reef margin. This facies conforms to Wendte's reef margin/upper foreslope facies (Figure 19). This facies is similar to Lonnee's facies IV/V and V.

Facies IV/V shows increasing concentrations of tabular stromatoporoids, whereas facies V corresponds to increasing concentrations of wavy and hemispherical stromatoporoids. Both of Lonne's (2006) facies are included in facies 2A, although the tabular stromatoporoids would have been deposited in somewhat deeper water than wavy and hemispherical stromatoporoids. Deposition occurred at water depths of 0-10m (Figure 19).

Facies 2B

The diverse, abundant and robust fossil assemblage in facies 2B implies a high energy, well oxygenated and shallow water setting. The absence of hemispherical and tabular stromatoporoids, with *Amphipora* and a dominance of *Stachyodes* fossils typify this facies. This is similar to Wendte's middle foreslope facies, which occurs in a slightly deeper setting than facies 2A in front of the reef margin and above fair-weather wave base (Figure 19). He notes the presence of thicker tabular stromatoporoids in stratigraphically upper (shallower) cored intervals, whereas thinner tabular stromatoporoids are present in stratigraphically lower (deeper) cored intervals. The presence of crinoids in the matrix implies that there is at least some connection with the open basin. A distinctive shale bed occurring in CANLIN CLARKE C- 094-L/094-J-09 core may represent a sequence boundary. Deposition occurred at water depths of 10-15m (Figure 19).

Facies 2C

Low fossil concentrations and increased mud content imply lower energy, less oxygenated and deeper water compared to facies 2B. Instances of this facies represent short-term development of deeper water conditions. Core from well CANLIN CLARKE B- 078-J/094-J-09 shows a shoal at the top of the Slave Point Formation interval which is interpreted to be a terminal shoal deposited before the reef was fully transgressed. This facies corresponds to Wendte's lower foreslope facies deposited at water depths of 15-22m (Figure 19).

Facies Association 3

Facies 3A

Dominance of crinoids with minor brachiopod shells/shell fragments in a muddy matrix implies a deeper, more basinal setting that is close to fair weather wave base. According to Lonnee (2006), layers of increased fossil intensities were deposited as a result of turbulent storm events, after which mud was settled out of suspension. Deposition occurred at water depths below 22m in the basinal section of the reef (Figure 19).

Facies 3B

Lower fossil concentrations and increased mud content differentiate this facies from facies 3A. Deposition is interpreted to have been in slightly deeper and less oxygenated conditions, where living fauna were sparse. This facies represents maximum paleowater depth and is congruent with Lonnee's If facies and Wendte's nodular mudstone facies in the basinal section of the reef (Figure 19).

Facies Association 4

The diagenetic history of dolomite at Clarke Lake field is interpreted by Lonnee (2006). He concluded that two separate density-driven brines, both sourced from Devonian evaporites to the south and east in the basin, were responsible for the diagenetic character at Clarke Lake. The first fluid was halite-saturated, which caused matrix dolomitization and the majority of gray matrix dolomite seen in core. A later gypsum/halite hybrid brine then altered the GMD, forming oversized pores, recrystallized GMD and the saddle dolomite seen as a cement and replacement mineral.

Flow Units

Porosity and permeability analyses show that reservoir flow properties are mainly dependent on dolomitization. Dolomites from facies 4A samples had high permeability (three highest sampled permeabilities are from this facies), which is probably due to open fractures that provide conduits for fluid flow. Porosity in this facies is relatively low, which may be due to the lack of mouldic pores. Mixed dolomite/limestone samples displayed a wide range of porosity and permeability. The mixed lithology samples showed no correlation between flow properties and depositional facies, and differences in flow properties could simply result from varying degrees of dolomitization, with more dolomitized samples showing better flow properties. Unaltered tight limestone of the Slave Point Formation as well as basinal shales of the Fort Simpson Formation and Horn River Group are considered barriers to flow and represent trapping elements at Clarke Lake field (Morrow, 2002).

High porosity samples existing within facies 1A and 1B are due to the presence of mouldic and vuggy porosity. Low permeability and porosity in some samples from these facies are due to infilling of mouldic pores and vugs by saddle dolomite. Facies 1A shows a relatively higher permeability compared to facies 1B, which may be related to larger bioclast sizes creating larger mouldic pores or vugs. Facies Association 2 shows relatively lower permeability and porosity due to the absence of the pronounced mouldic pores and vugs seen in facies 1A and 1B, although, mouldic and vuggy pores do exist locally in Facies Association 2. Likewise, Facies Association 3 locally shows vuggy porosity but less frequently than in facies 1A and 1B. Dolomitized units of Facies Association 3 show relatively high porosities, but there are few analyses, which may be skewing the mean porosity and permeability. Facies 1A is considered the primary flow unit, whereas facies 1B can be considered a secondary flow unit. Facies Association 4, displaying relatively high permeability, can also be considered a secondary flow unit.

Flow Simulations

Fourteen 25-year flow simulation cases were conducted within a 2500x2500x-250 polygonal mesh that represents a portion of the Clarke Lake reservoir. We tested models with a reservoir pressure of 28MPa and 18.5MPa at a temperature of 100°C. These values were chosen as initial conditions as part of a simulation using water

as a single phase. Boundary conditions were designated as open flow boundaries (the properties at the model boundary are assumed to continue beyond the model and to infinity). This was done because formation water within Clarke Lake field experiences hydrodynamic flow conditions and is in communication with the greater Presqu'ile Barrier aquifer system (Dave Moffatt, personal communication, June 25, 2018). The pressure of 28MPa corresponds to maximum reservoir pressure and that of 18.5MPa corresponds to the minimum reservoir pressure recorded by drill stem tests taken within the Slave Point Formation at Clarke Lake field. The temperature was selected based on Slave Point Formation reservoir temperatures from drill stem tests (Figure 2). Twelve of the fourteen simulations are doublet flow models, with one producer and one injector spaced at 500 meters distance from each other. Both the injection and production water circulation rates were 25kg/s. Two of these simulations were based on four injector wells and eight producer wells. Each injector well injected at 50kg/s, whereas producer wells produced at 25kg/s. These rates are based on observed upper limits of co-produced fluid rates within the Clarke Lake field (Petro-Canada Oil & Gas, 2009; Figure 20).

In the different model runs, reservoir cells were populated with maximum, minimum, mean, median, Q1 (the middle value between smallest value and median value in the permeability and porosity data set) and Q3 (the middle value between median and highest value in the permeability and porosity data set) values for porosity, horizontal permeability and vertical permeability. These values, along with parameters kept constant in the simulation, are shown in Table 2.

An example of a successful doublet simulation run (defined as a simulation case that shows no significant change in temperature at the producer well after 25 years) is shown in Figures 20 and 21. Figure 20 shows four images each representing a specific time in the simulation: 1500 seconds, ~76 days, 5 years and 25 years (Herein referred to as time steps). The cold water temperature plume around the injection well grows at each time step as cold water is re-injected into the reservoir. At the 25-year time step, the plume has not reached the production well, so the production well is still producing water at original reservoir temperature. Figure 21 graphs show temperature and pressure at the producer and injector well through simulation time (in seconds). Pressure decay is linear in both the injector and producer wells due to an overall drop in reservoir temperature from the reinjection of cold water. Temperature change in the producer well is linear and temperature change at the injector is exponential. The FLO(AQ.) (kg/s)(x) per m^2 value shown in Figure 22 represents water flow rates through one square meter in the x-direction of the reservoir. The water flow rate at the producer shows an immediate spike related to initial water injection into the reservoir but afterwards shows a linear increase through time. This spike also occurs at the injector well but water flow quickly stabilize at ~8.4e-5 kg/s (x) per m^2 (Figure 22). The temperature at the producer well after the 25-year simulation is 98.1°C, which doesn't constitute a sig-

nificant change in temperature (Figure 21).

Figures 23 and 24 show an example of a failed doublet simulation case. Time steps show change in reservoir pressure and after ~48 hours into the simulation, reservoir pressure at the injector is depleted (Figure 23). Failed simulations are a result of the porosity and permeability inputs not being able to sustain a 25-year simulation. The minimum high pressure case failed after 2 days while the minimum low pressure case failed after 1.89 days. The Q1 high pressure case failed after 0.73 years while the Q1 low pressure case failed after 26 days.

Simulations using four injector wells and eight producer wells were completed to demonstrate a well configuration capable of generating increased geothermal electricity output compared to the doublet models (Figures 25, 26). The doublet model is capable of producing 300kW of electrical power, whereas a four injector and eight producer well configuration is capable of producing 2400kW of electrical power.

Resulting flow simulations show that we are able to sustain 25-year geothermal projects for all simulation cases except for the minimum and Q1 cases. Simulation data for all other simulation cases are shown in Appendix A.

Conclusions

Reservoir rock at Clarke Lake gas field can be classified on the basis of depositional as well as diagenetic character. Dolomitized units of facies 1A display the best flow capabilities with an average porosity of 6.4% and an average permeability of 124md. High permeability samples exist for each facies, which may be due to presence of microfractures. The presence of dolomite appears to be the major constraint on rock flow properties although there is variation in these properties within dolomitized faces. For our purposes, facies 1A is our primary flow unit due to relatively high porosity and permeability.

Flow simulations showed that we are able to operate 25-year geothermal projects sourcing formation water from within facies 1A in the doublet and the four injector and eight producer well configurations. Electrical power output for the doublet and the four injector and eight producer configurations are 300kW and 2400kW, respectively. The 25-year simulation failed using Q1 and minimum values for facies 1A permeability and porosity.

The next steps in this study will involve applying the facies well log signatures to the rest of the field in order to delineate more completely the geological and reservoir models. From this we will be able to correlate flow units to delineate possible new well targets or targets that can be exploited with old wells. We will also use petrographic thin sections to further constrain the elements responsible for differences in flow properties within dolomitized units.

References

Doveton, J. H. (1994). The Photoelectric Index.

Dunham, R. J. (1962). Classification of carbonate rocks according to depositional textures.

Eppelbaum, Lev & Kutasov, izzy & Pilchin, Arkady. (2014). Thermal Properties of Rocks and Density of Fluids. Lecture Notes in Earth System Sciences. 99-149. 10.1007/978-3-642-34023-9_2.

Gray, F. F., & Kassube, J. R. (1963). Geology and stratigraphy of Clarke Lake gas field, British Columbia. AAPG Bulletin, 47(3), 467-483.

Lonnee, J., & Machel, H. G. (2006). Pervasive dolomitization with subsequent hydrothermal alteration in the Clarke Lake gas field, Middle Devonian Slave Point Formation, British Columbia, Canada. AAPG bulletin, 90(11), 1739-1761.

Morrow, D. W., Zhao, M., & Stasiuk, L. D. (2002). The gas-bearing Devonian Presqu'ile Dolomite of the Cordova embayment region of British Columbia, Canada: Dolomitization and the stratigraphic template. AAPG bulletin, 86(9), 1609-1638.

O'Connell, S. C., Dix, G. R., & Barclay, J. E. (1990). The origin, history, and regional structural development of the Peace River Arch, Western Canada. Bulletin of Canadian Petroleum Geology, 38(1), 4-24.

Petro-Canada Oil & Gas (2009). Clarke Lake Experimental Scheme (Annual Report #4).

Qing, H., & Mountjoy, E. W. (1994). Formation of coarsely crystalline, hydrothermal dolomite reservoirs in the Presqu'ile barrier, Western Canada sedimentary basin. AAPG bulletin, 78(1), 55-77.

Weissenberger, J. A., & Potma, K. (2001). The Devonian of western Canada—Aspects of a petroleum system: Introduction. Bulletin of Canadian Petroleum Geology, 49(1), 1-6.

Wendte, J. C. (1992). Evolution of the Judy Creek complex, a Late Middle Devonian isolate platform-reef com plex in west-central Alberta.

Witzke, B. J., & Heckel, P. H. (1988). Paleoclimatic indicators and inferred Devonian paleolatitudes of Euramerica.

Facies	Average porosity (fraction)	Average permeability (md)	Average density (kg/m³)
Facies 1A	0.064	124	2610
Facies 1B	0.074	35	n/a
Facies 1C	0.055	7	n/a
Facies 2	0.047	42	2666
Facies 3	0.1	72	n/a
Facies 4A	0.051	246	2706
Facies 4B	0.05	57	2706

Table 1: Average porosity, permeability and density by facies.

Simulation case	Horizontal permeability (md)	Vertical permeability (md)	Porosity (fraction)
Maximum	1040.00	74.00	0.17
Minimum	0.21	0.01	0.01
Mean	92.00	7.00	0.07
Median	9.30	0.52	0.07
Q1	1.50	0.18	0.05
Q3	58.00	2.80	0.1

Simulation constants	
Wet heat conductivity	0.386 W/(m·K)
Specific heat capacity	960.0 J/(kg·K)
Density	2600.0 kg/m³

Table 2: Simulation inputs and constants.

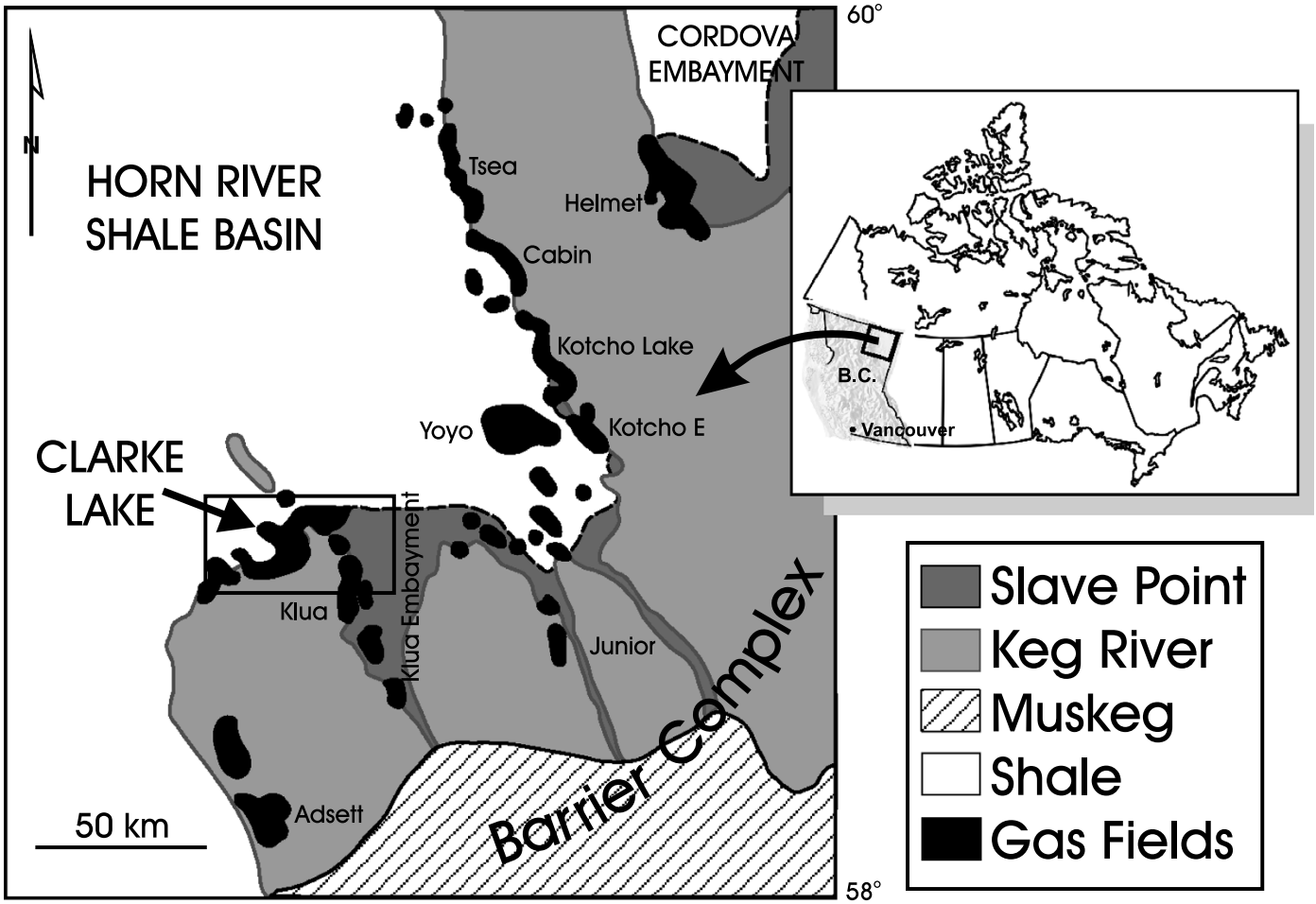

(Lonnee, 2006)

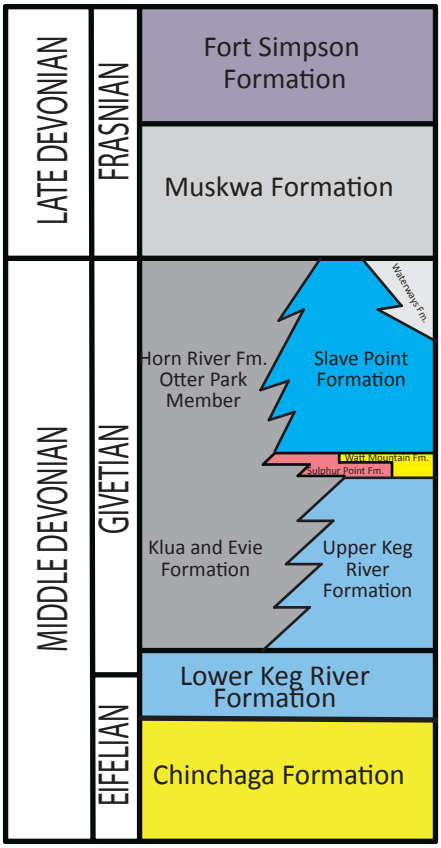

Figure 1: Location and stratigraphic column

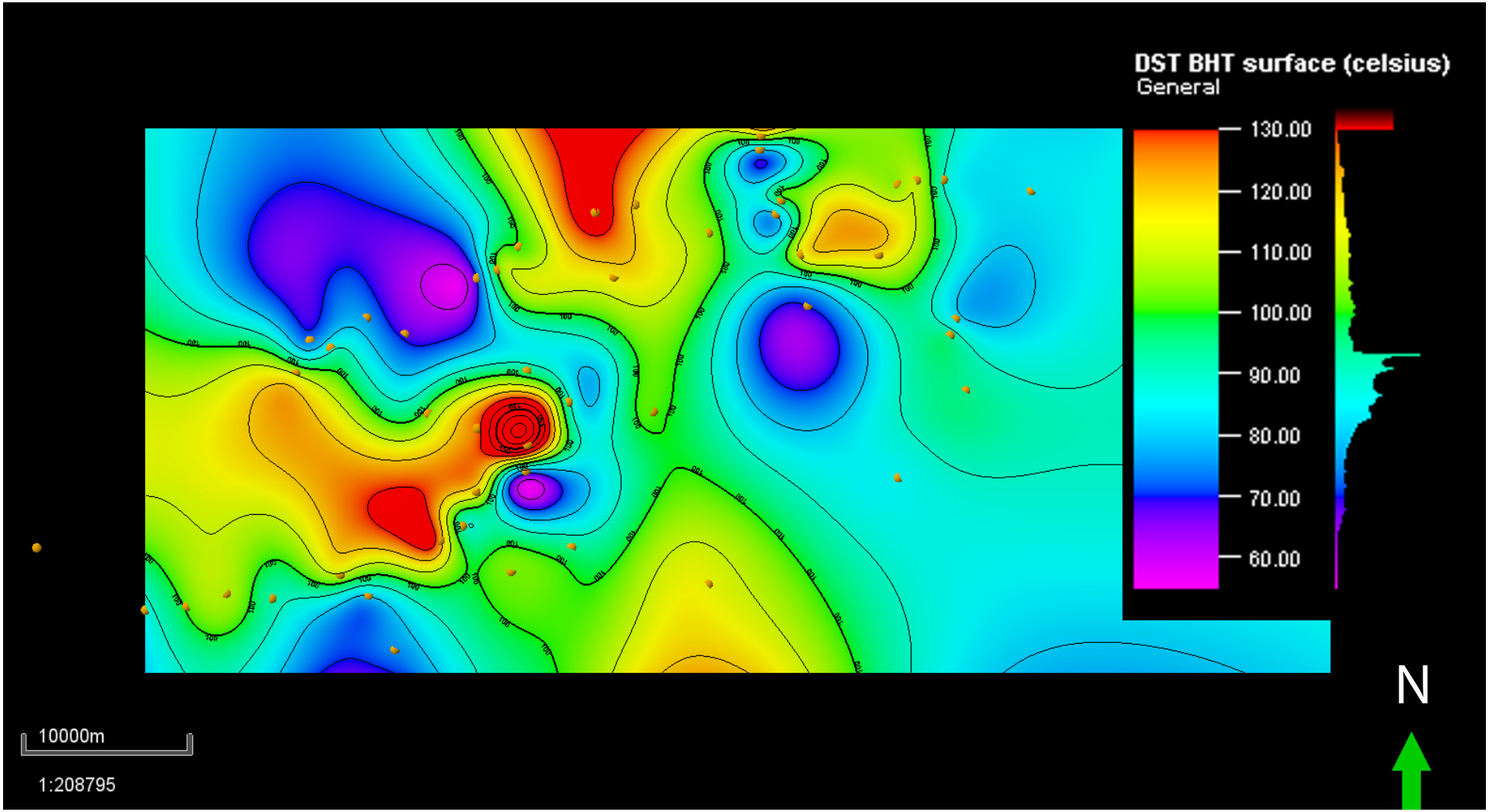

Figure 2: Reservoir temperature at Clake Lake field

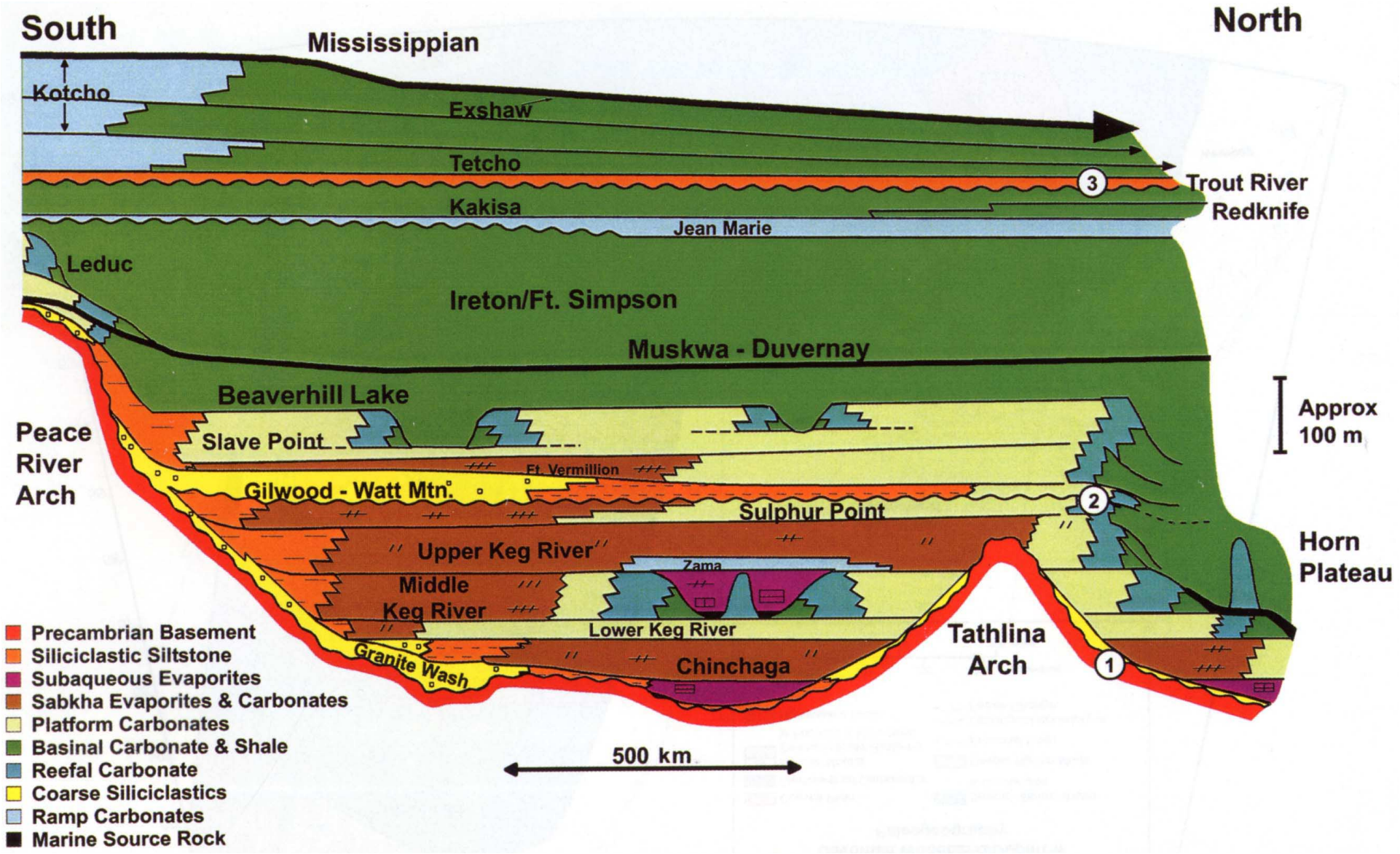

Figure 3: Devonian sequence stratigraphy

Major regional unconformities denoted by numbers 1, 2, 3 (Weissenberger, 2001).

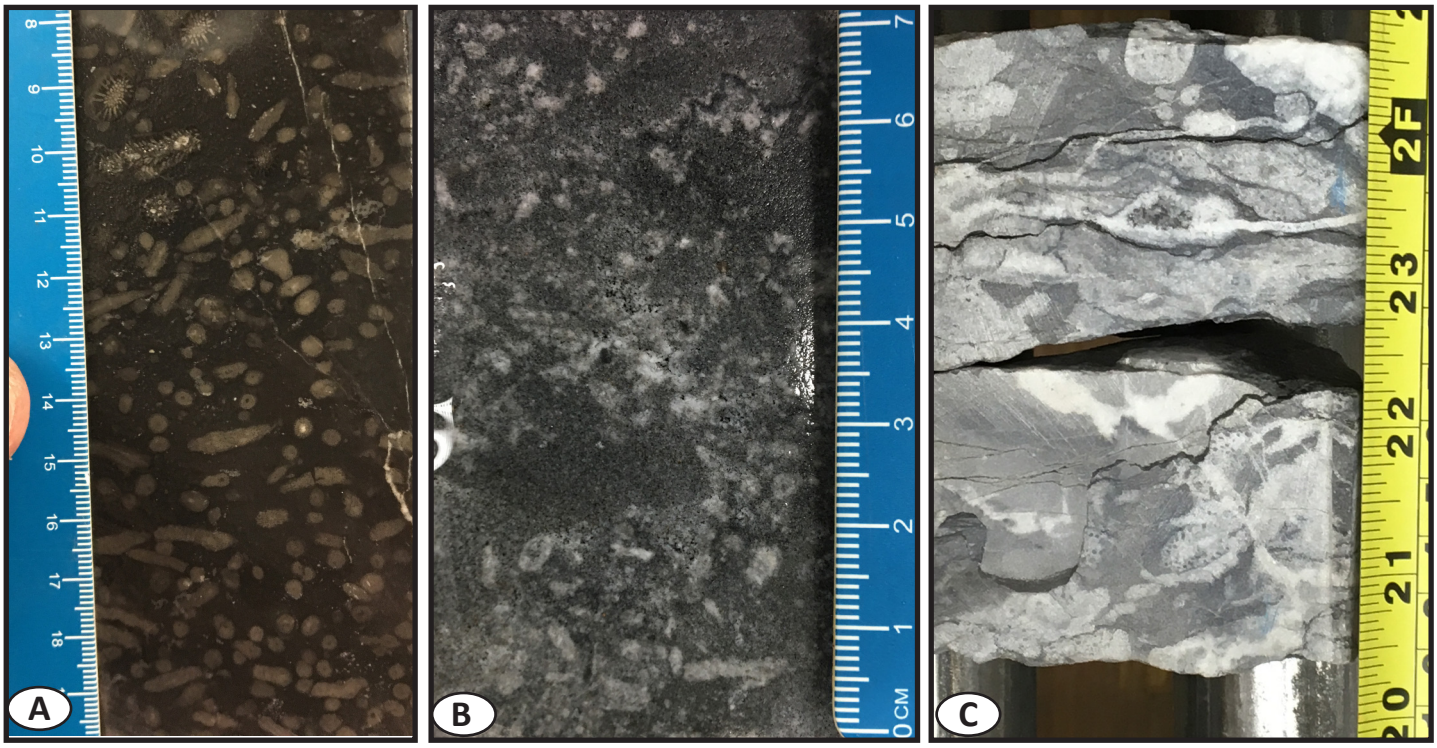

Figure 4: Facies 1A

Facies 1A displaying *Amphipora* and *Stachyodes* as well as coral fossils (A, 6427', CANLIN CLARKE C-056-L/094-J-09). Dolomitized facies 1A showing remnant fossils replaced by saddle dolomite within gray matrix dolomite (B, 6419', CANLIN CLARKE C- 050-K/094-J-09; C, 6561', CANLIN CLARKE C- 050-K/094-J-09).

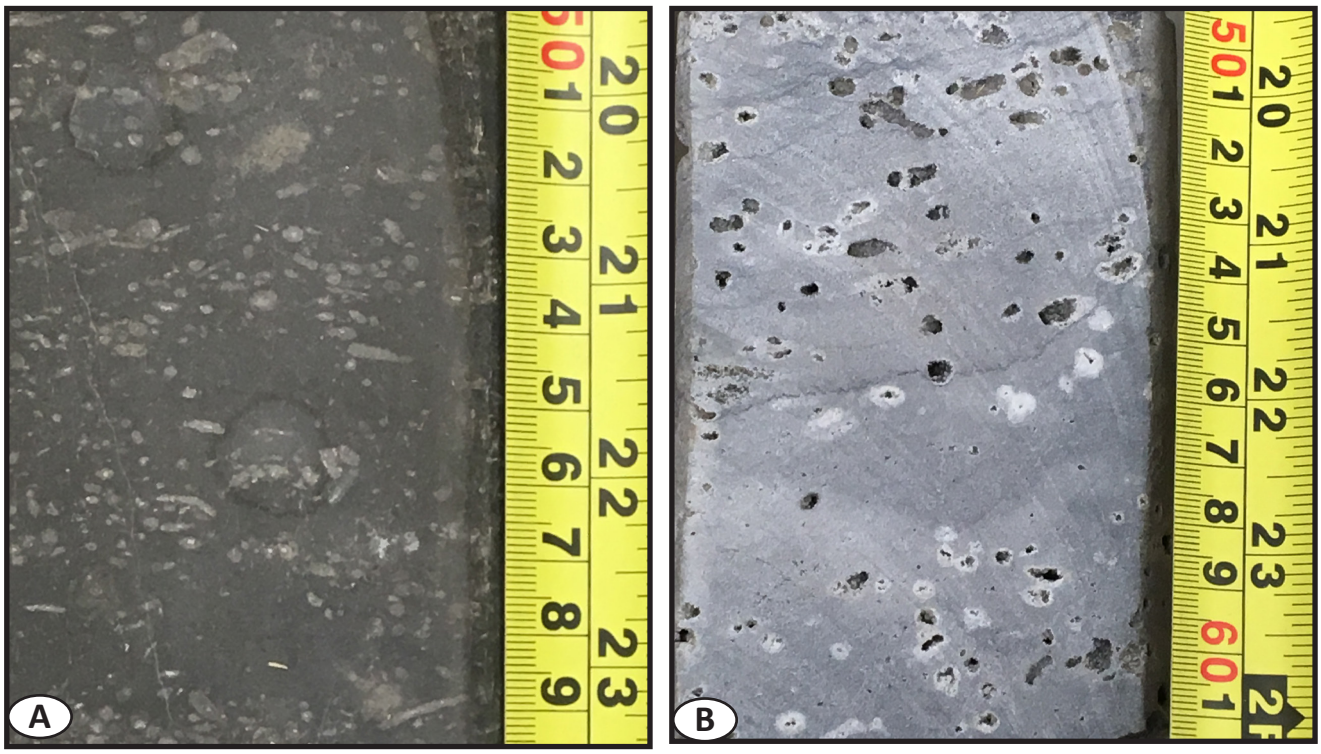

Figure 5: Facies 1B

Facies 1B displaying mm-scale *Amphipora* fossils as well as skeletal fragments (A, 6474.5', CANLIN CLARKE C-056-L/094-J-09). Dolomitized sections show mouldic porosity as well as GMD and partial to full infilling of mouldic pores by saddle dolomite (B, 6248.92', CANLIN CLARKE B- 072-L/094-J-09).

Figure 6: Facies 1C

Wavy laminated mudstone typical of facies 1C (A, 6440', GULF STATES IMP CLARKE LAKE C- 064-I/094-J-10). Contact between facies 1C and facies 1B with facies 1C showing no laminations and minor amounts of *Amphipora* fossils (B, 6423.3', GULF STATES IMP CLARKE LAKE C- 064-I/094-J-10). Dolomitized sections showing pervasive GMD, styolites and minor mouldic pores possibly from dissolution of *Amphipora* fossils (C, 6431', CANLIN CLARKE D- 072-G/094-J-10).

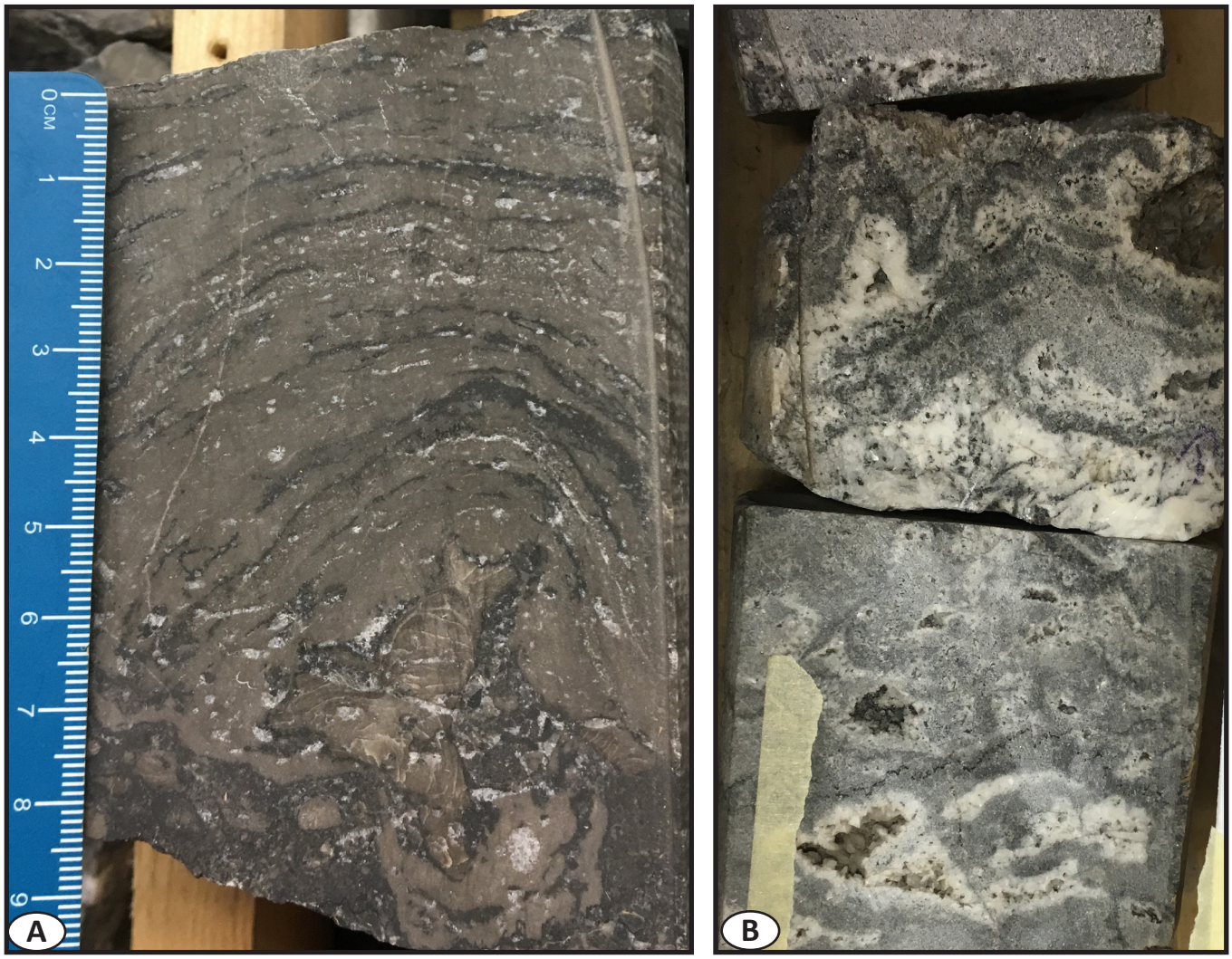

Figure 7: Facies 2A

Massive stromatoporoid boundstone of facies 2A displaying intraparticle pores that are completely filled by sparry calcite (A, 6235', CANLIN CLARKE B- 078-J/094-J-09). Dolomitized facies 2A in which stromatoporoid boundstone can still readily be seen through the diagenetic overprint (B, 6483.83', West National Imperial Clarke Lake - C-094-L).

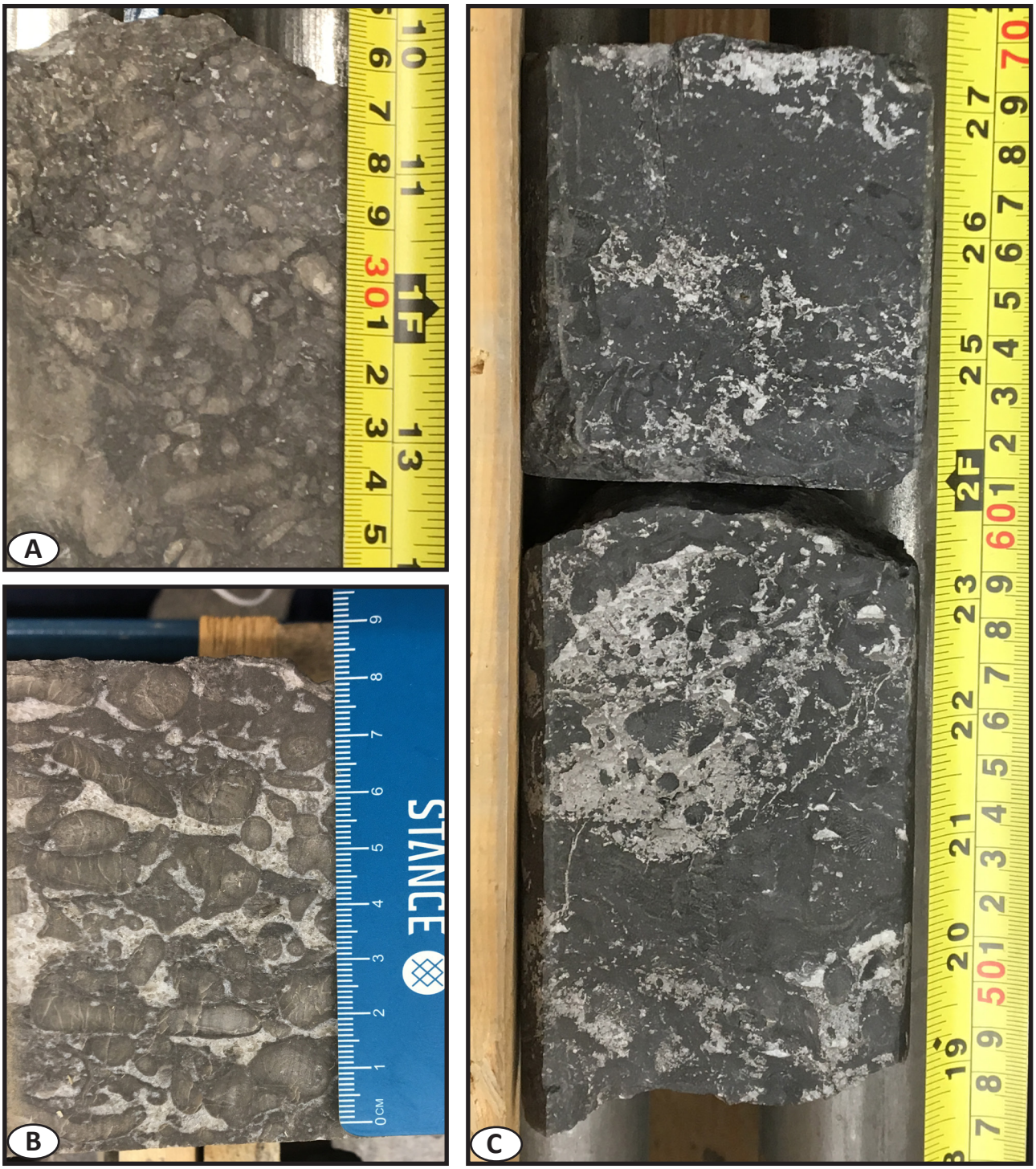

Figure 8: Facies 2B

Stachyodes Packestone of facies 2B displaying minor amounts of calcite cement and large formed fossils of *Stachyodes* (A, 6207.8', CANLIN CLARKE B- 078-J/094-J-09). Facies 2B with increased amounts of pore filling calcite (B, 6435', CANLIN CLARKE B- 078-J/094-J-09). Partially dolomitized and hydrothermally "cooked" facies 2B showing dolomite crystals partially replacing matrix (C, 6457.75', CANLIN CLARKE D- 091-L/094-J-09).

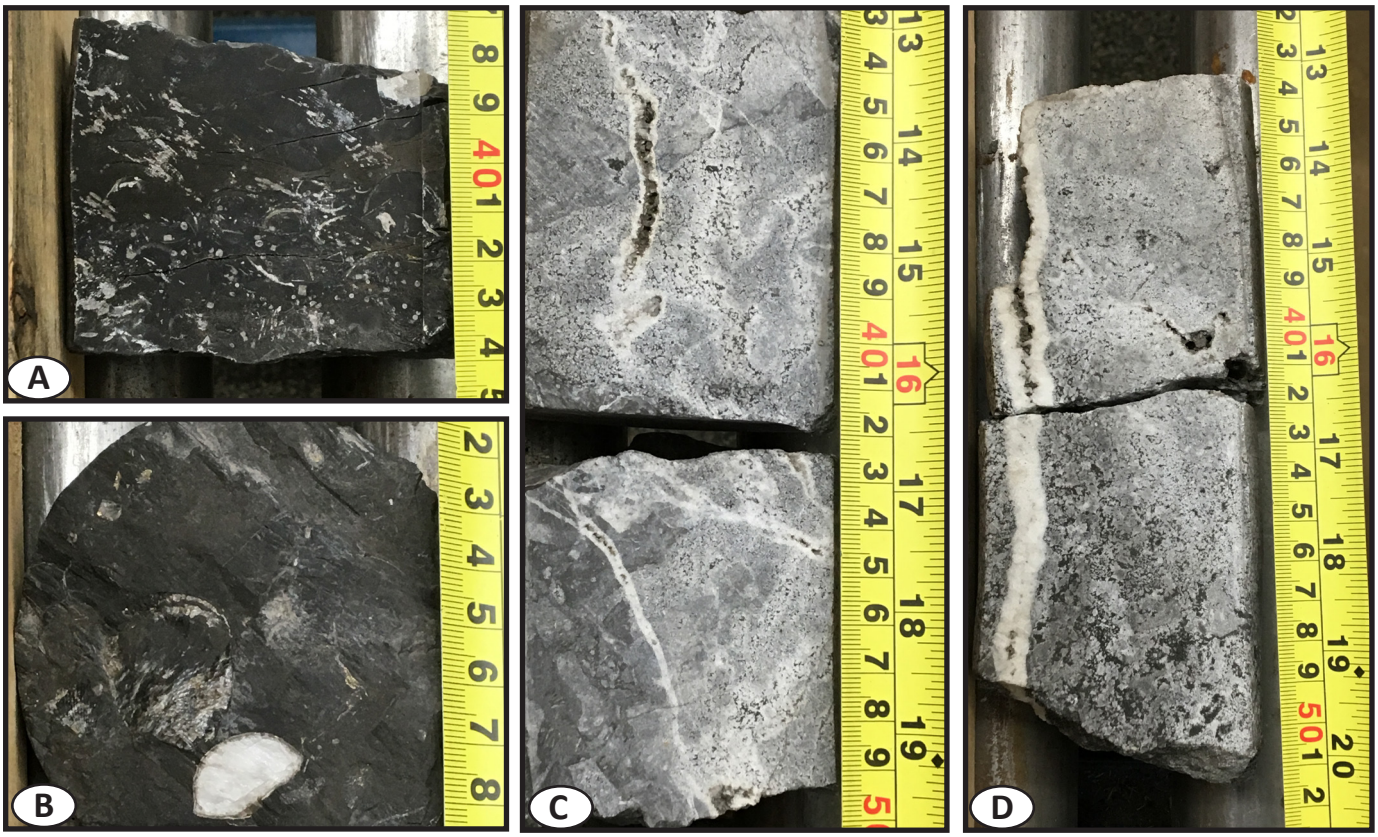

Figure 9: Facies 3A and 3B

Crinoid ossicles and brachiopod shell fragments of facies 3A partially replaced by dolomite (A, 6528.4', BA SHELL KLUA C- 070-E/094-J-09). Brachipod shells partially to fully replaced by calcite (B, 6388.3', BA SHELL KLUA C- 070-E/094-J-09). Facies 3A (C, 6317.1', CANLIN CLARKE B- 010-D/094-J-16) and facies 3B (D, 6207.8', CANLIN CLARKE B- 010-D/094-J-16) dolomitized and showing large sub-vertical veining that is partially to completely filled by white saddle dolomite.

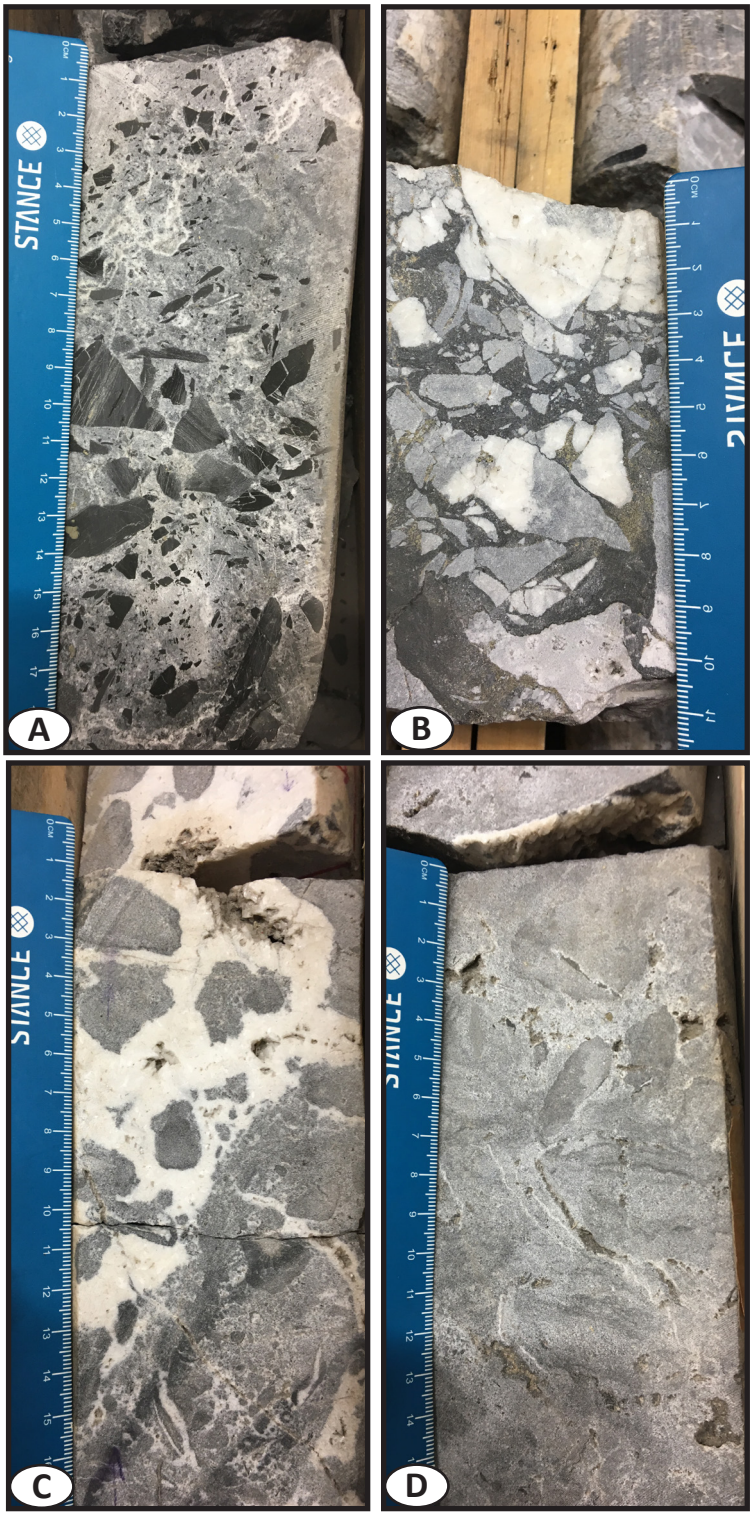

Figure 10: Facies Association 4

Various diagenetic textures. True breccia of facies 4A with angular mud clasts floating in gray matrix dolomite (A, 6768.92', CHEVRON MILO D- 079-F/094-J-10). Angular clasts floating in a dark matrix (possibly made of sulfides) with visible sulfide mineralization (B, 6790', CHEVRON MILO D- 079-F/094-J-10). Facies 4A breccia with less angular to rounded clasts floating in a saddle dolomite matrix (C, 6732.75', CANLIN ET AL CLARKE A- 065-G/094-J-10). Facies 4B showing an abundance of gray matrix dolomite with possible relict clasts still visible (D, 6695', CANLIN ET AL CLARKE A- 065-G/094-J-10).

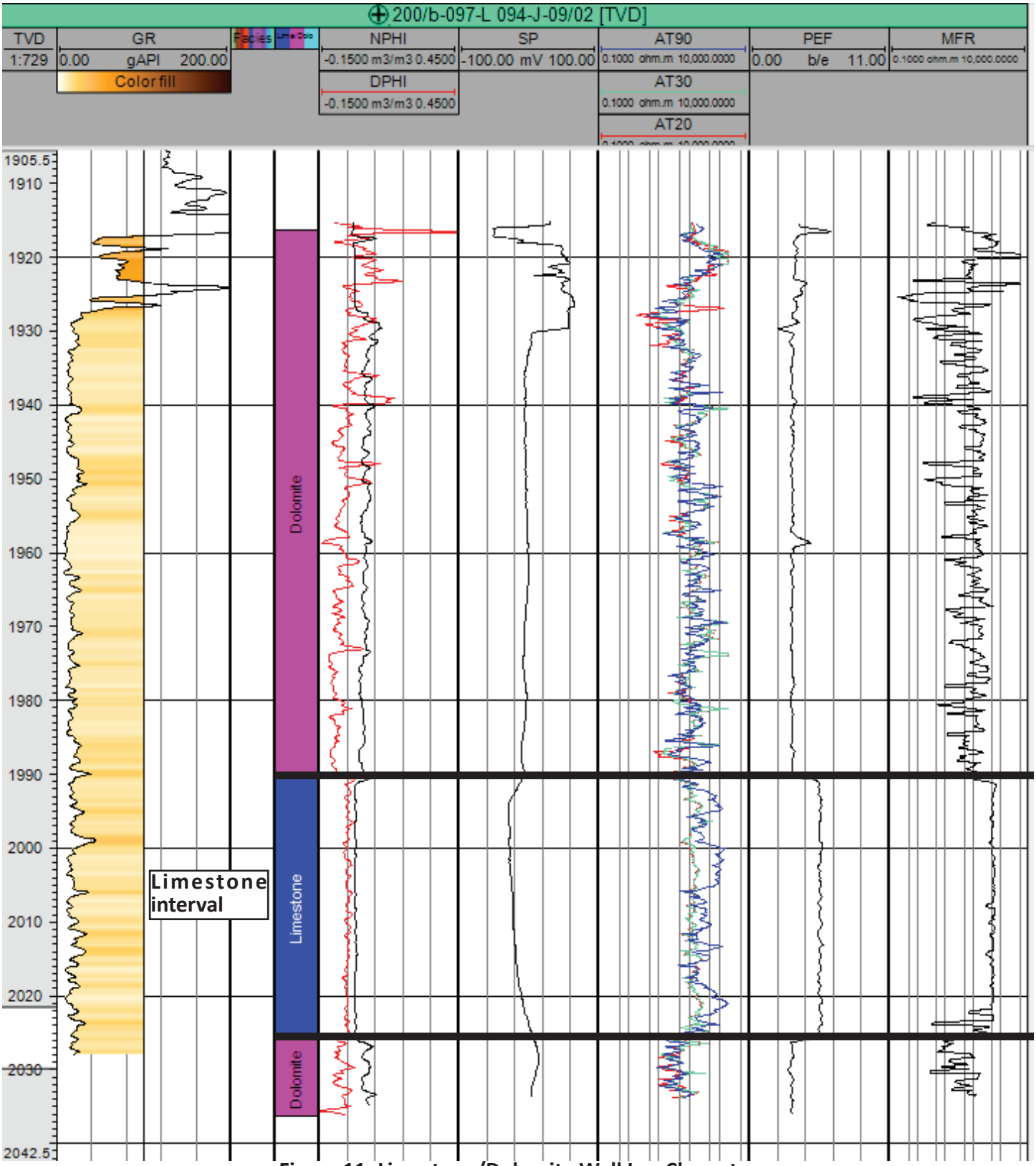

Figure 11: Limestone/Dolomite Well Log Character

Well section showing relative differences in neutron porosity, density porosity, SP, resistivity, and photoelectric log signatures between limestone (~1990m - ~2025m) and dolomite intervals.

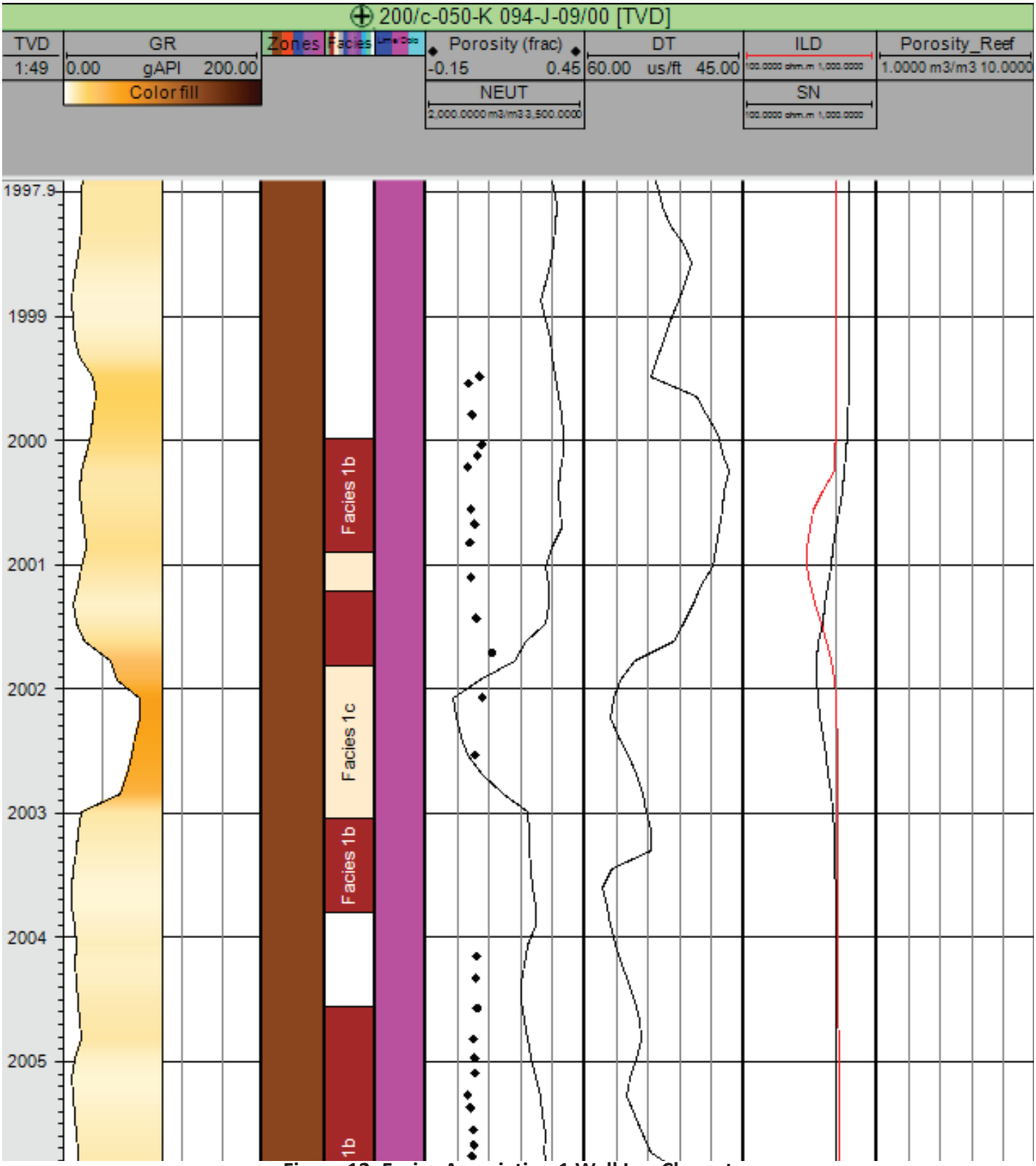

Figure 12: Facies Association 1 Well Log Character

Well section showing facies 1C is by a high gamma ray log response, decrease in porosity/neutron counts and an increase in sonic two-way travel time within the interval 2001.82m to 2003m. Facies 1B shows low gamma ray log response, an increase in porosity/neutron counts and a decrease in sonic two-way travel time.

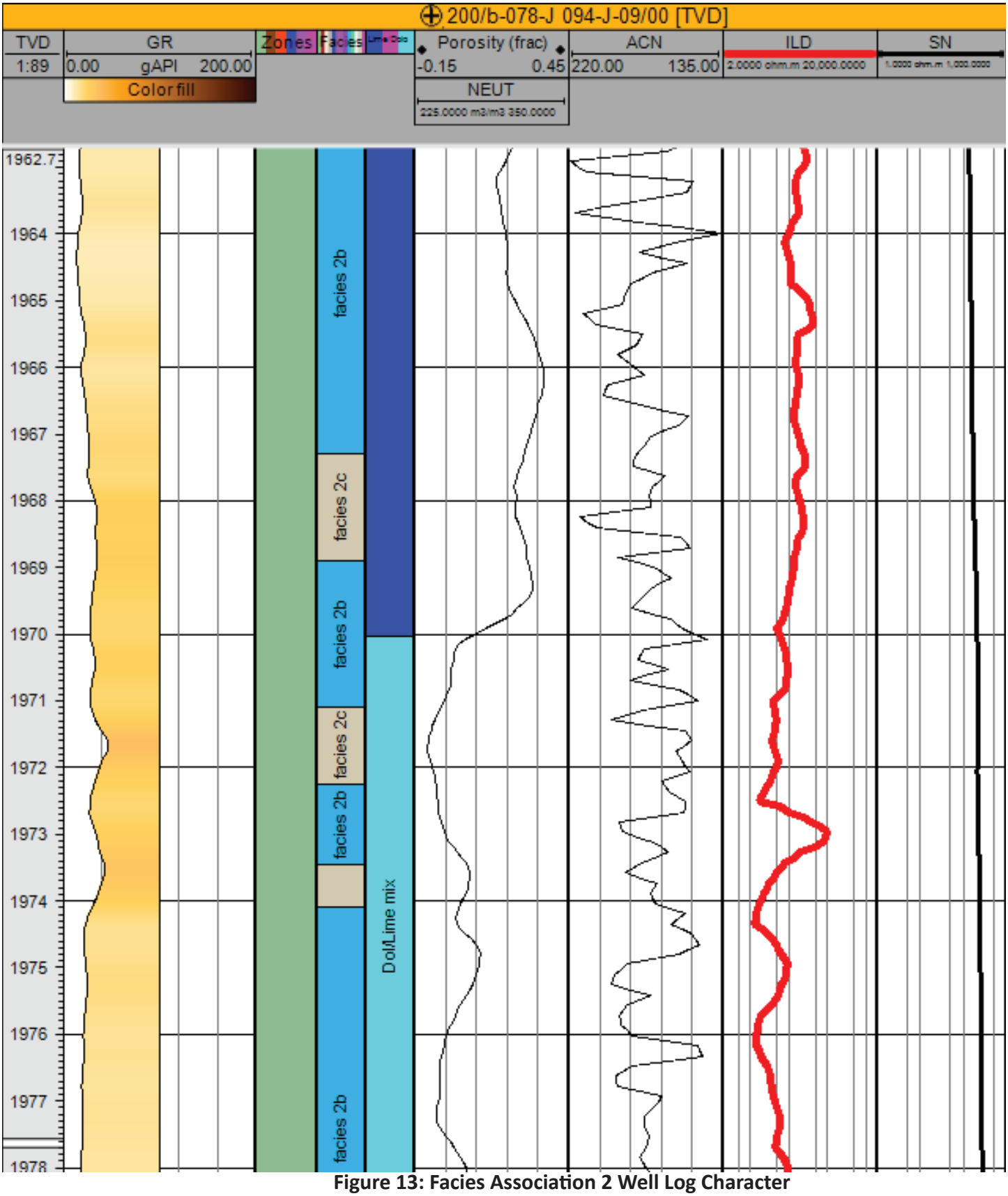

Figure 13: Facies Association 2 Well Log Character

Well Section showing facies 2B with a relatively lower gamma ray response compared to wackestones of facies 2C. This is shown in the interval of ~1967.5m to 1978m. The section shows a shoaling upward sequence where packstone intervals of facies 2B and intervals of facies 2C grade into a coarser grainstone/packstone section at 1962.7m to 1967.5m

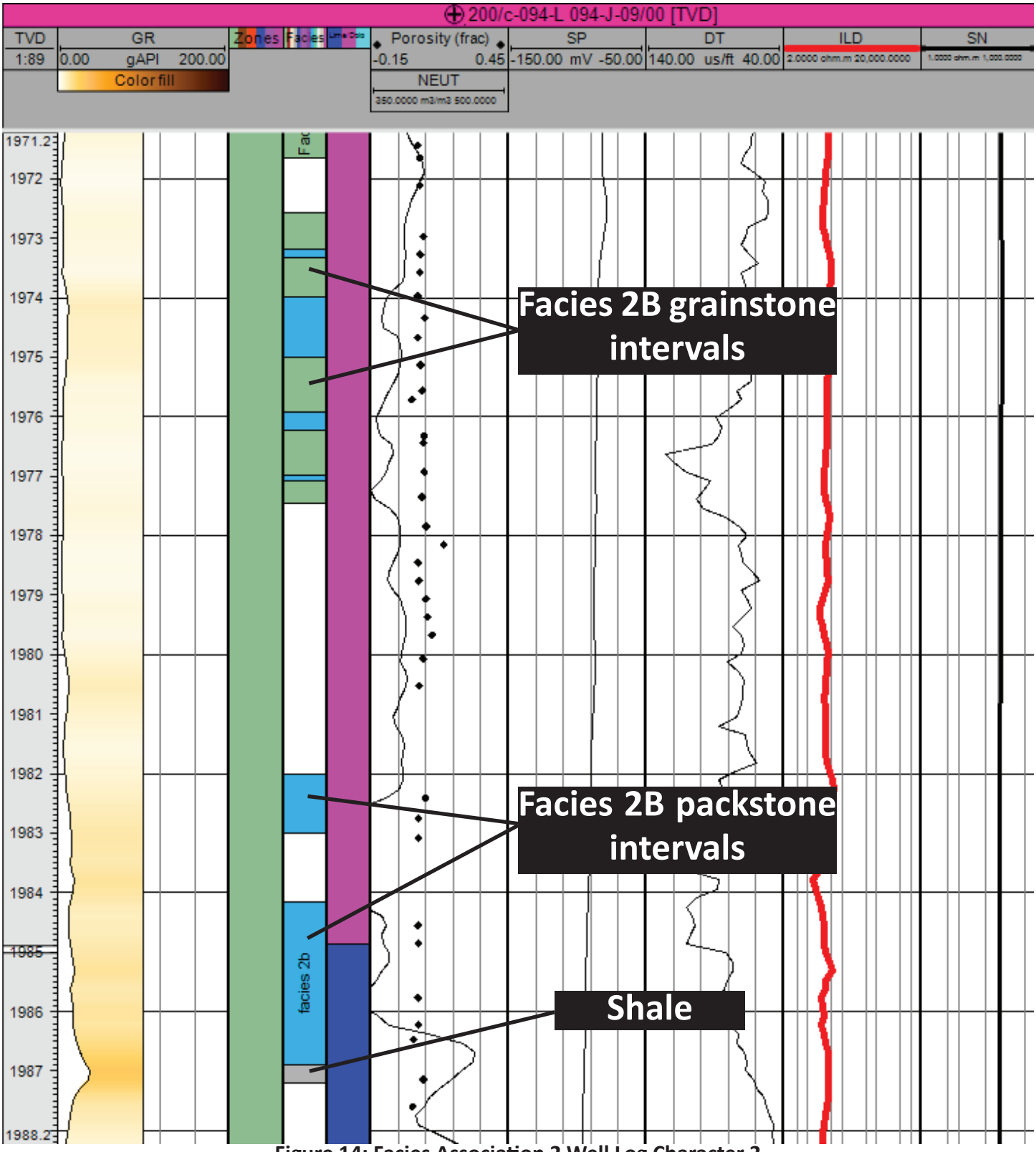

Figure 14: Facies Association 2 Well Log Character 2

Well section shows a coarser interval of Facies Association 2. Shale seen in core shows up on the gamma ray log at 1987m. Thinner intervals of facies 2B packstones cause slight decreases in porosity/neutron counts shown from 1974m to 1977.5m, whereas intervals of facies 2B grainstone show increases in porosity/neutron counts.

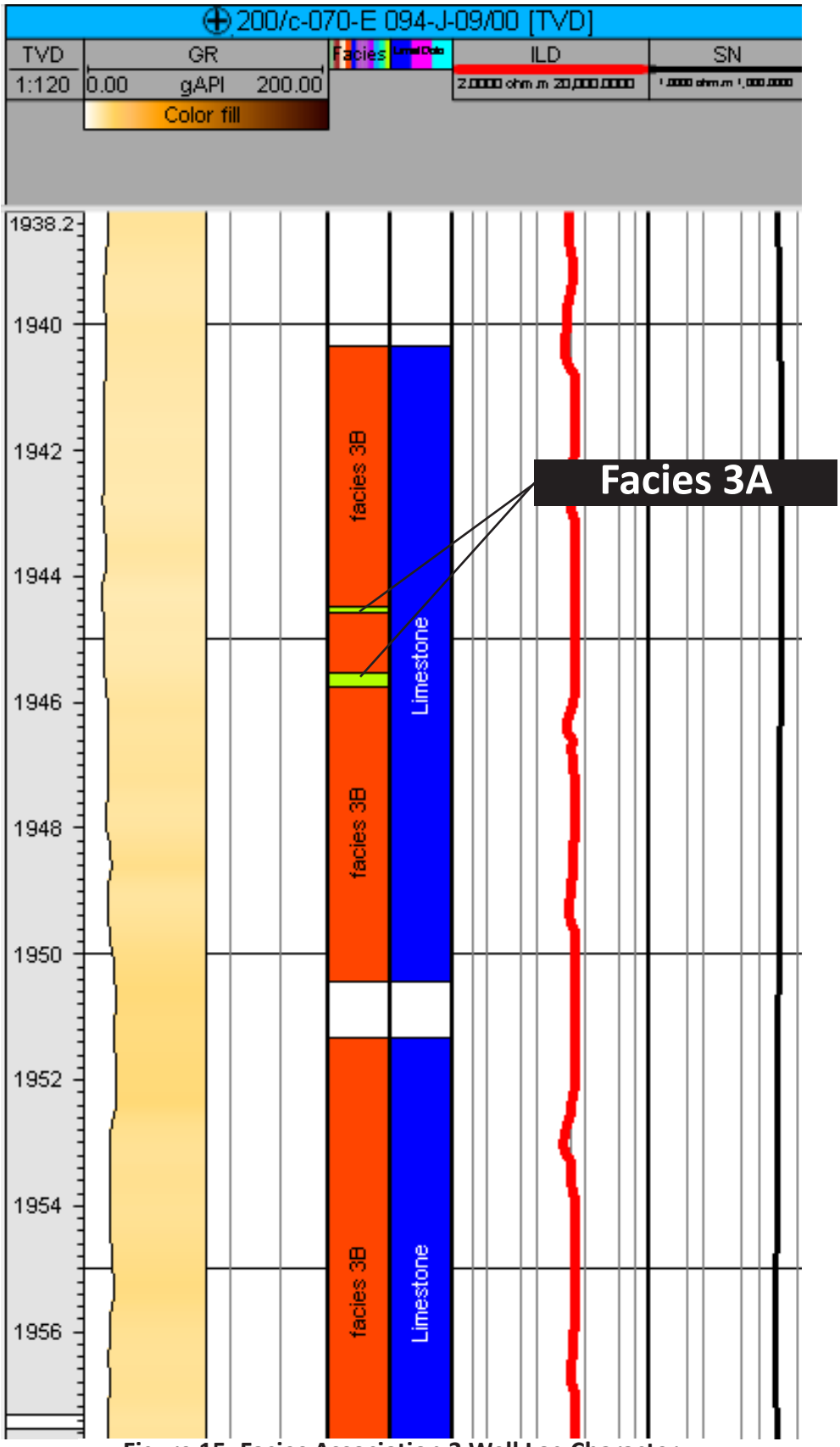

Figure 15: Facies Association 3 Well Log Character

This well section displays Facies 3A and 3B showing an overall decrease in gamma ray log signature attributed to the increased amounts of mud.

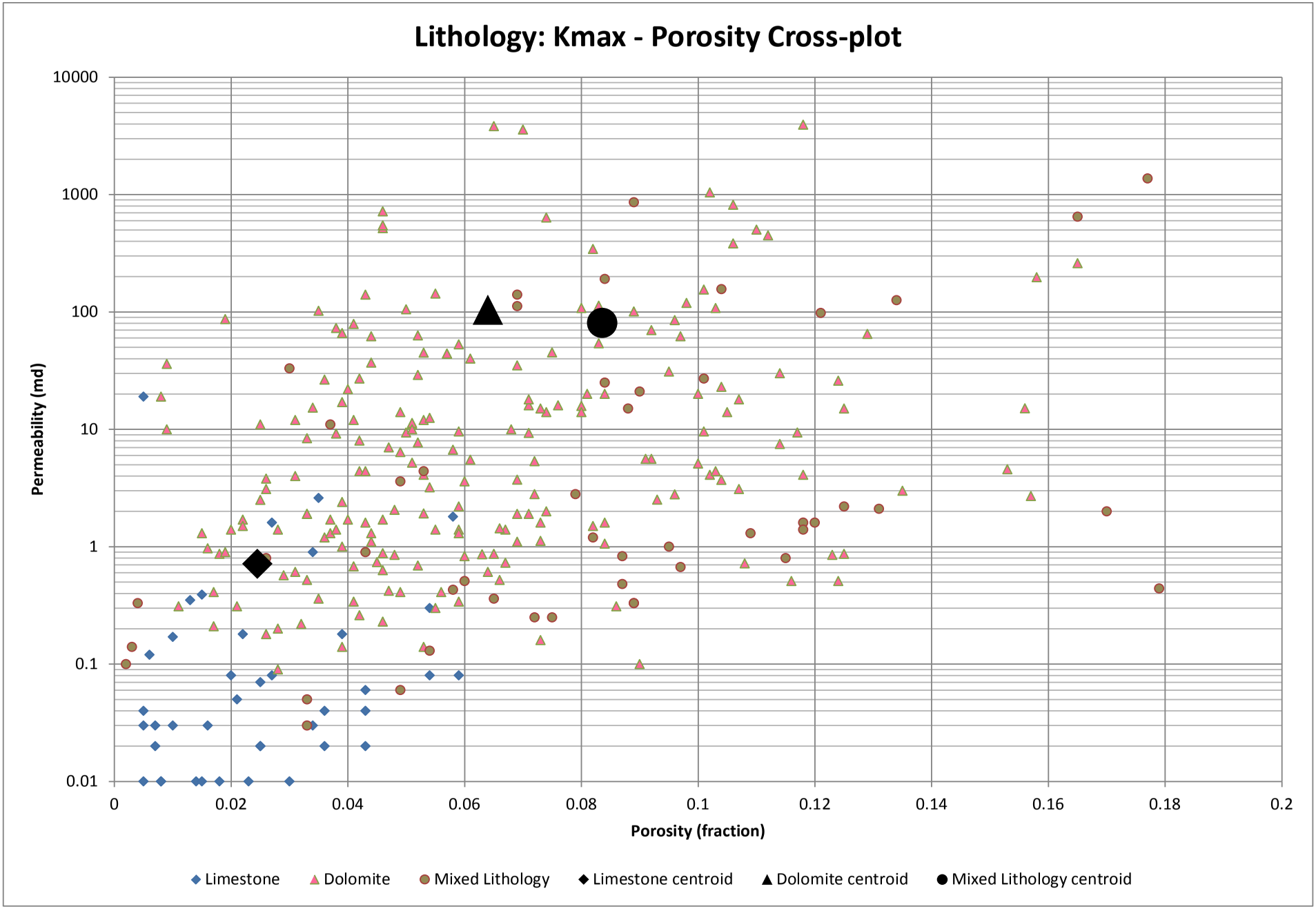

Figure 16: Kmax vs Porosity by Dolomite/Limestone

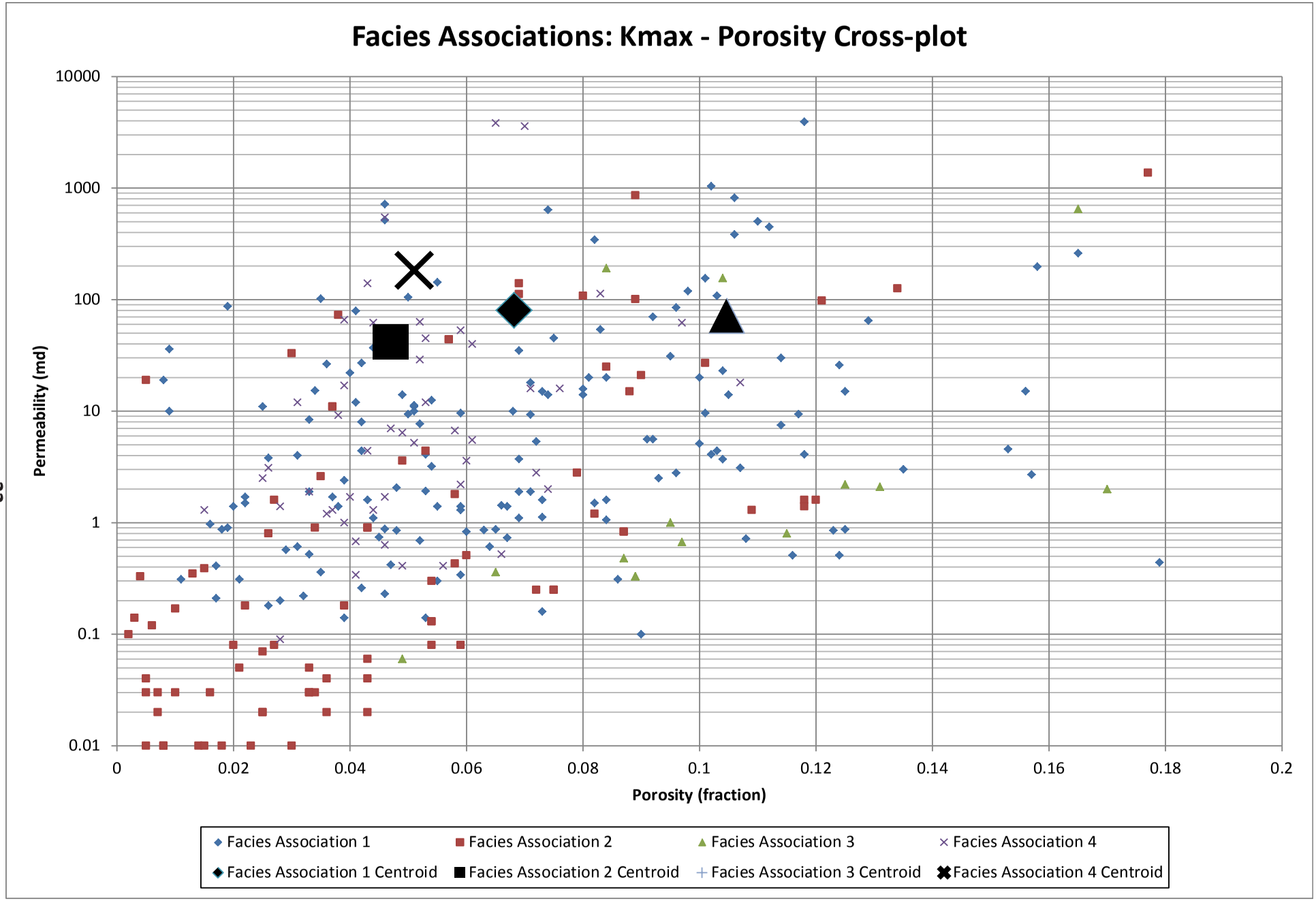

Figure 17: Kmax vs Porosity by Facies Association

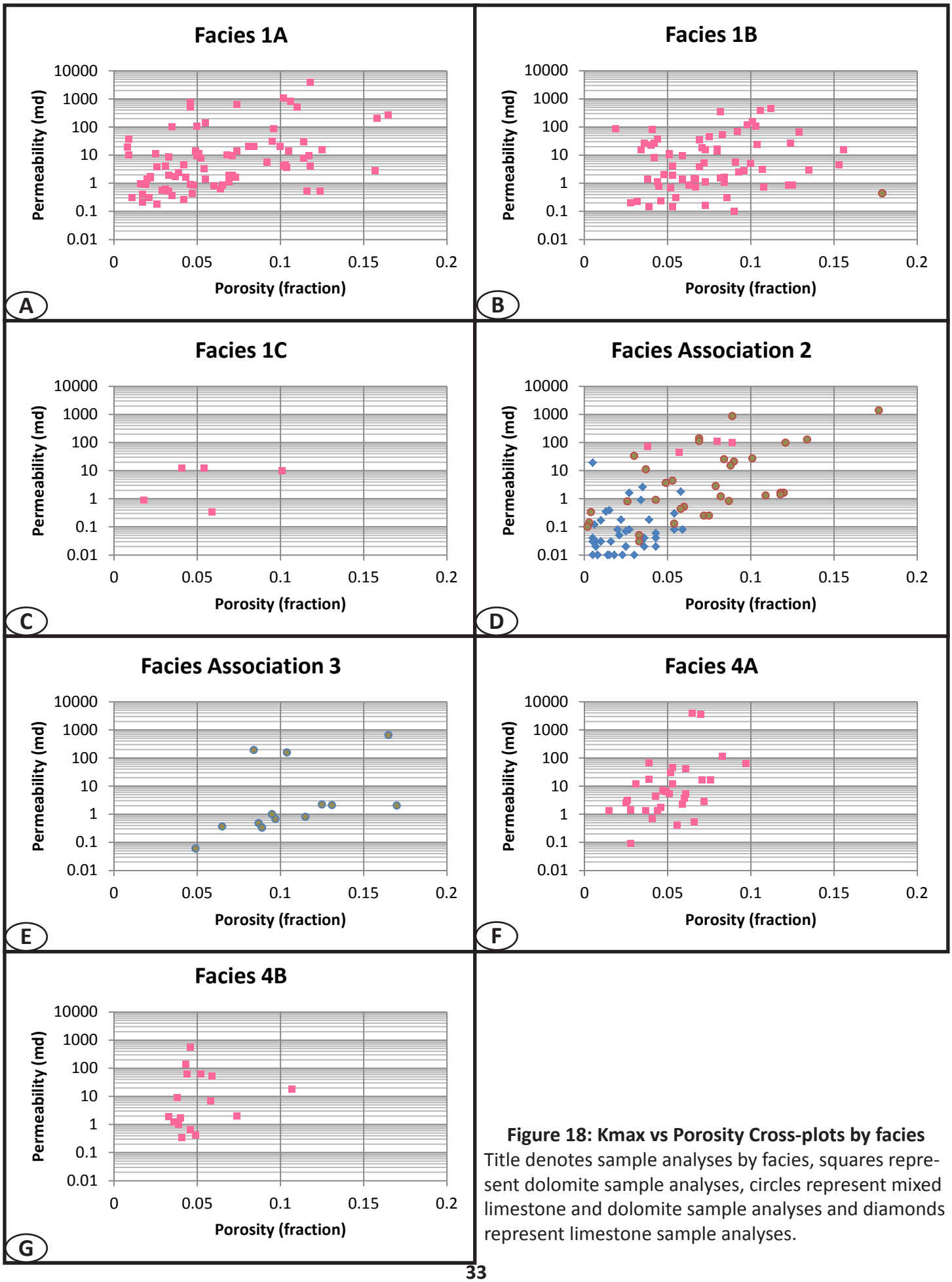

Figure 18: Kmax vs Porosity Cross-plots by facies
Title denotes sample analyses by facies, squares represent dolomite sample analyses, circles represent mixed limestone and dolomite sample analyses and diamonds represent limestone sample analyses.

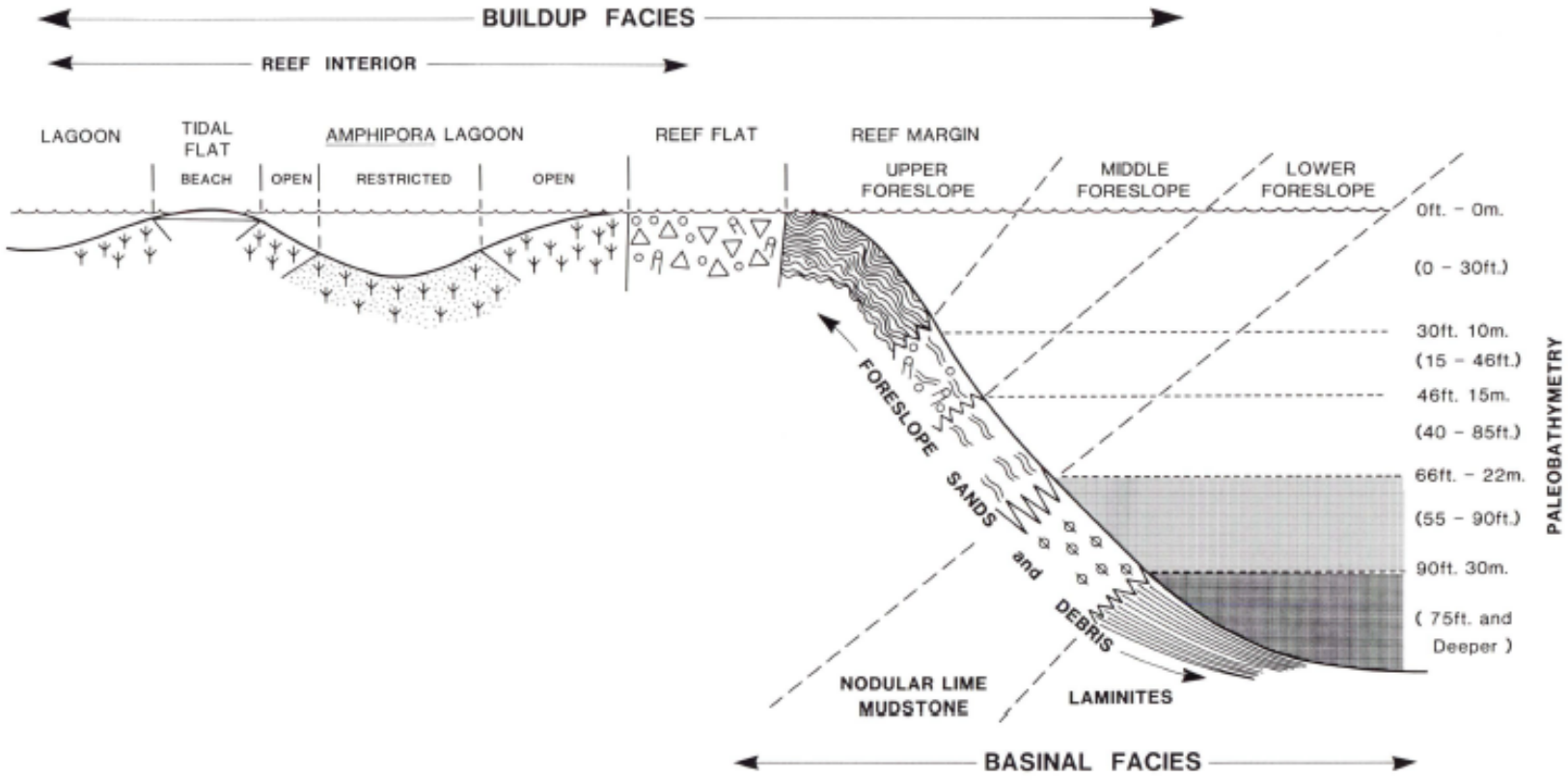

Figure 3. Paleobathymetric profile of Swan Hills reef facies.

Figure 19: Depositional Model (Wendte, 1992)

Depositional model for the Swan Hills Formation at Judy Creek field, proposed by Wendte (1992).

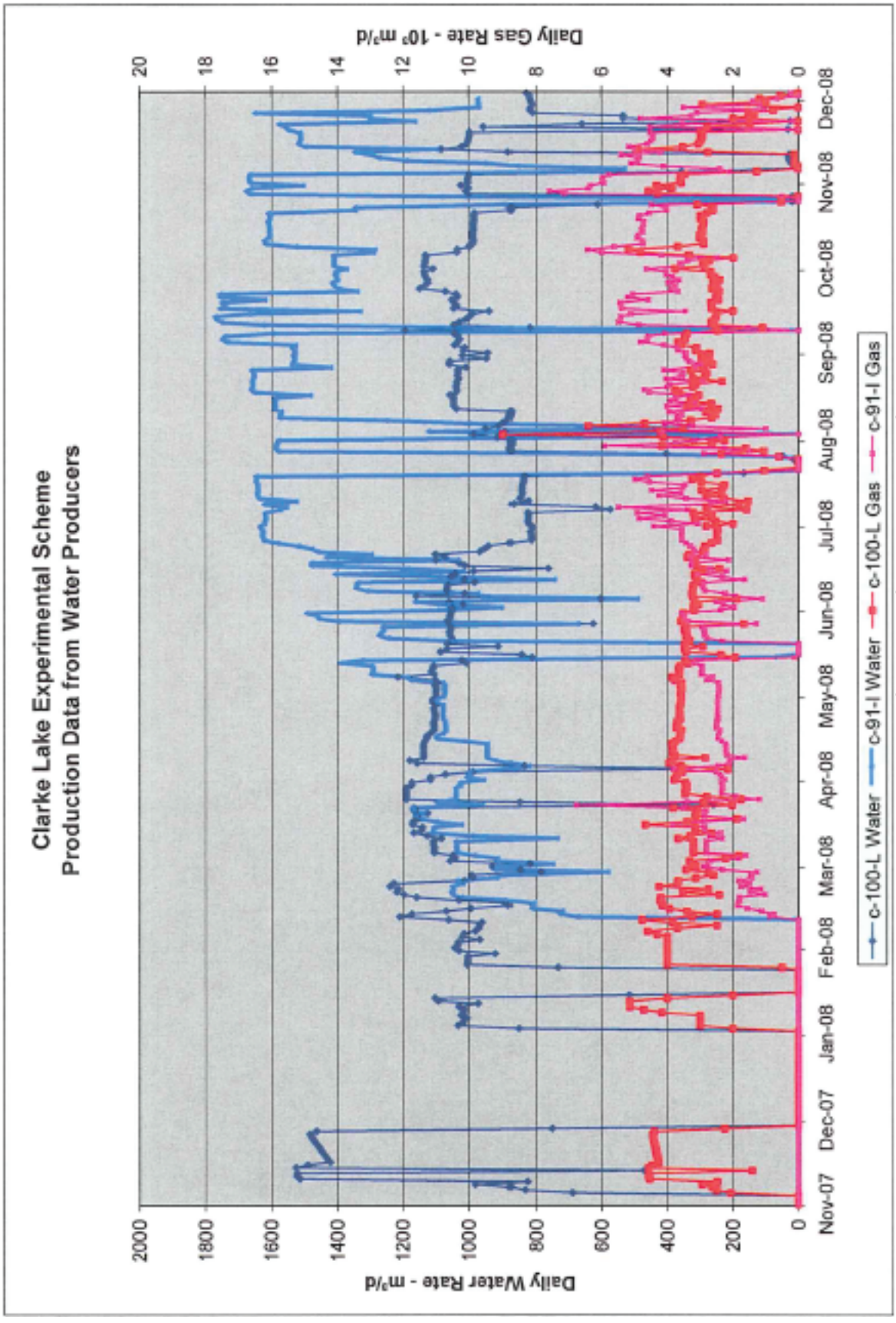

Figure 20: Co-produced fluid data from Clarke Lake field

Co-produced fluid rates of production wells taken from the Petro-Canada Experimental Scheme Annual Report #4.

Doublet Model - Facies 1A - Max High Reservoir Pressure

Time = 1500 seconds

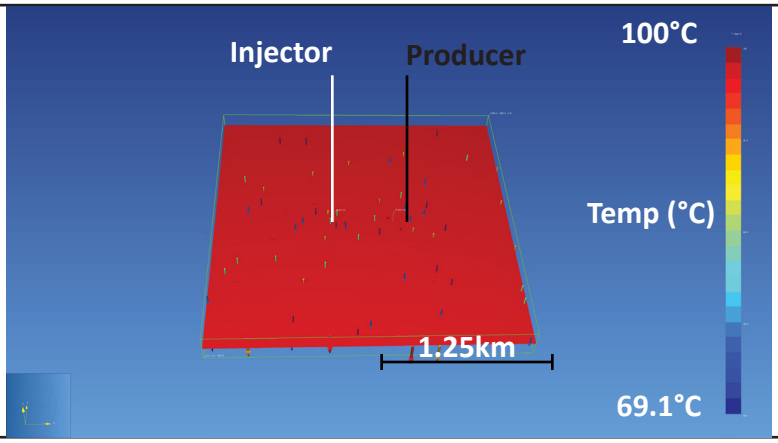

Time = ~76 days

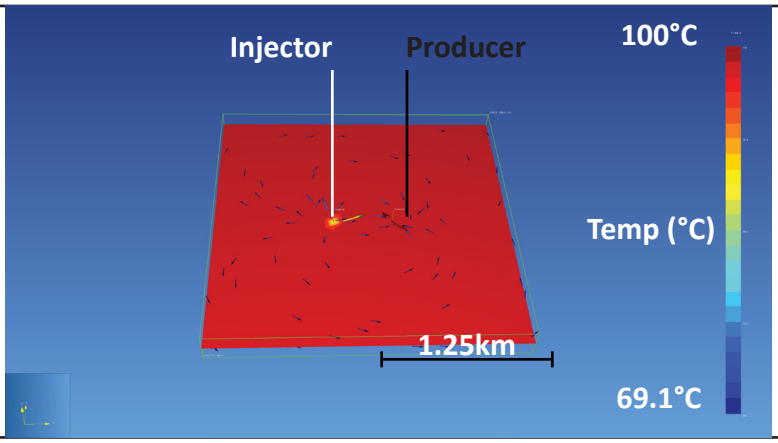

Time = ~5 years

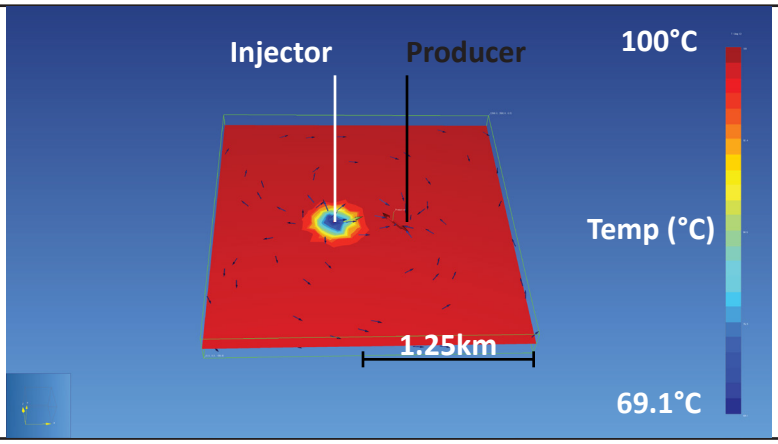

Time = 25 years

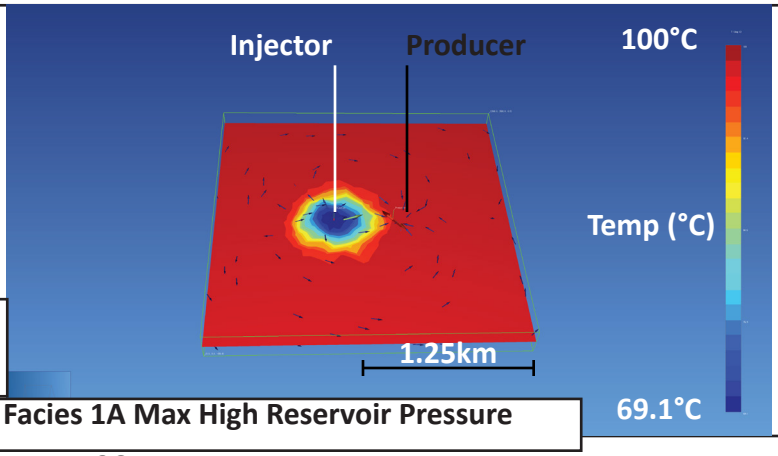

Temperature change through four timesteps in a simulation taken at high reservoir pressure using maximum Facies 1A values of permeability and porosity.

Figure 21: Doublet Temperature Model - Facies 1A Max High Reservoir Pressure

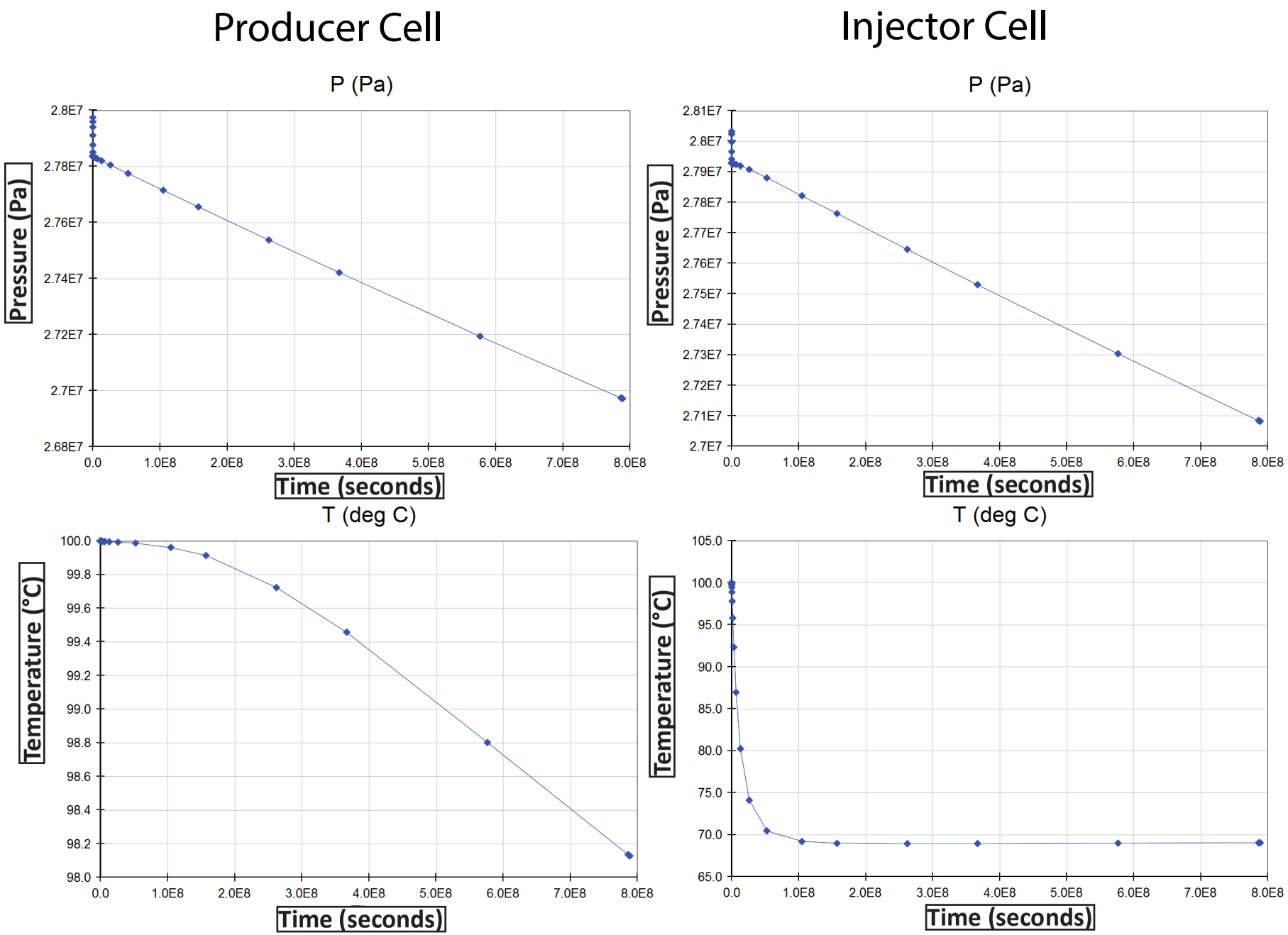

Figure 22: Producer and Injector Cell Graphs - Facies 1A Max High Reservoir Pressure

Temperature and pressure values as a function of time at the production and injection simulation cells for the simulation based on high reservoir pressure using cells populated with maximum porosity and permeability values for Facies 1A.

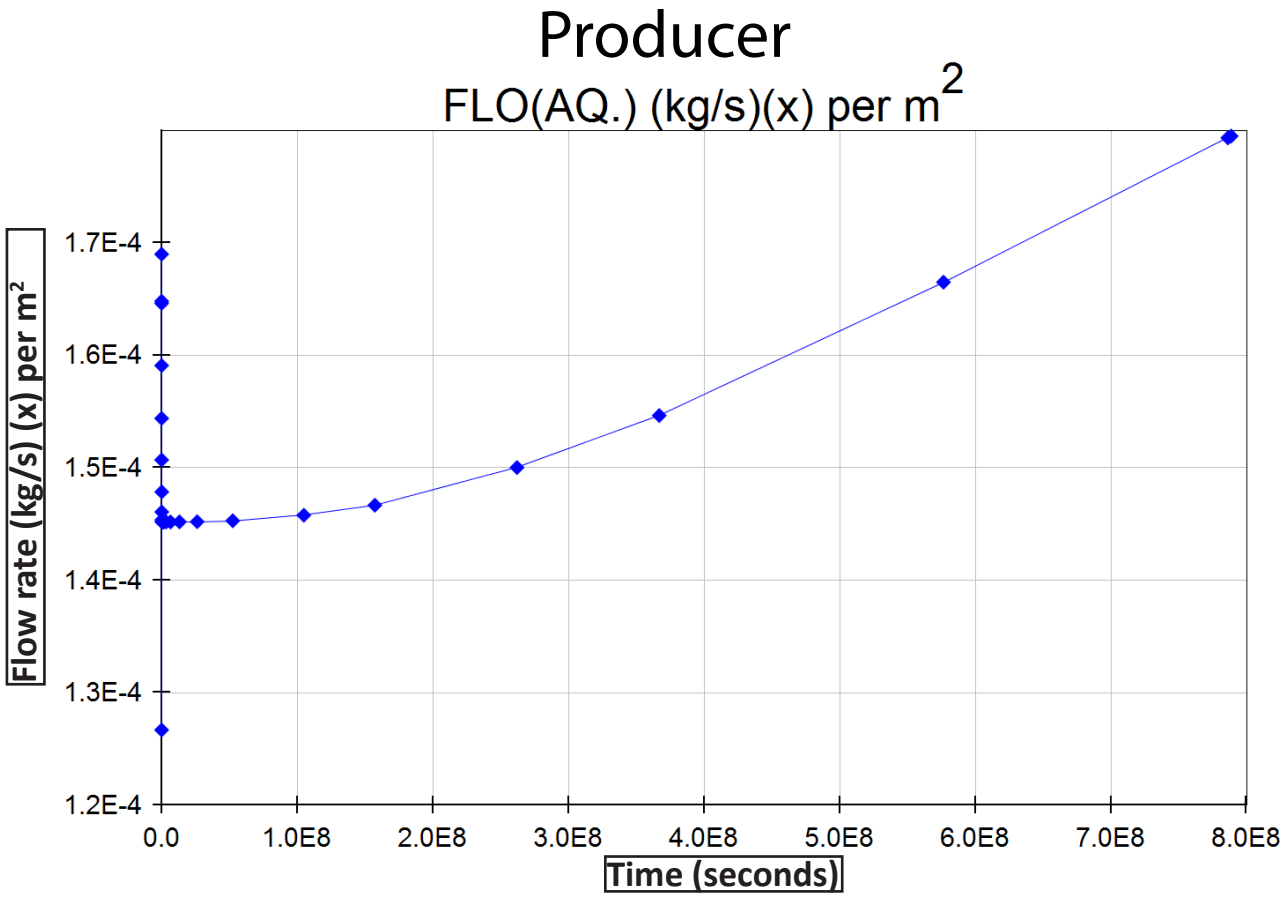

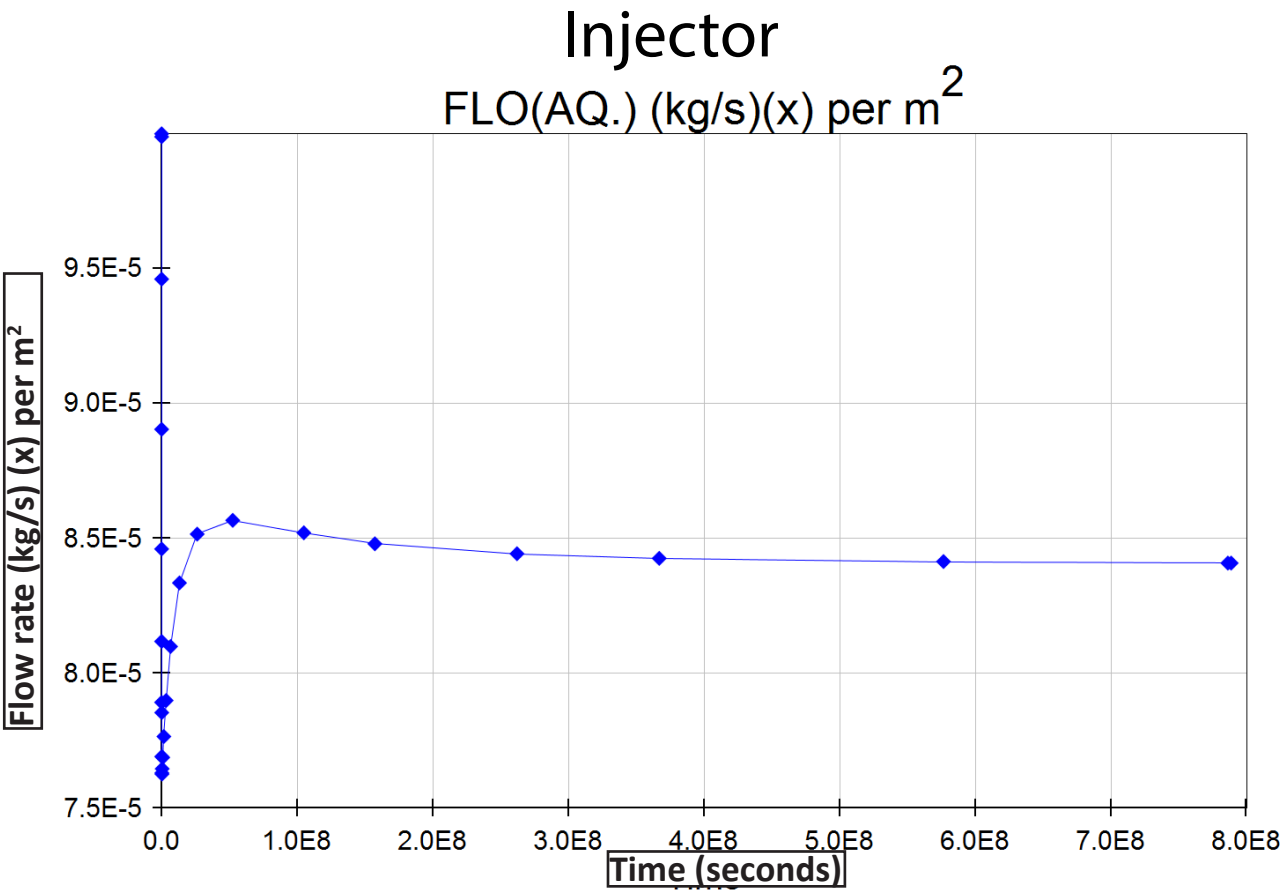

Figure 23: Producer and Injector Cell Graphs - FLO (Kg/s)(x) per m²

Flow rate in kg/s in the x-direction per meter squared as a function of time at the production and injection simulation cells for the high reservoir pressure simulation using maximum values of porosity and permeability for Facies 1A.

Doublet Pressure Model - Facies 1A - Minimum High Reservoir Pressure

Time = 1500 seconds

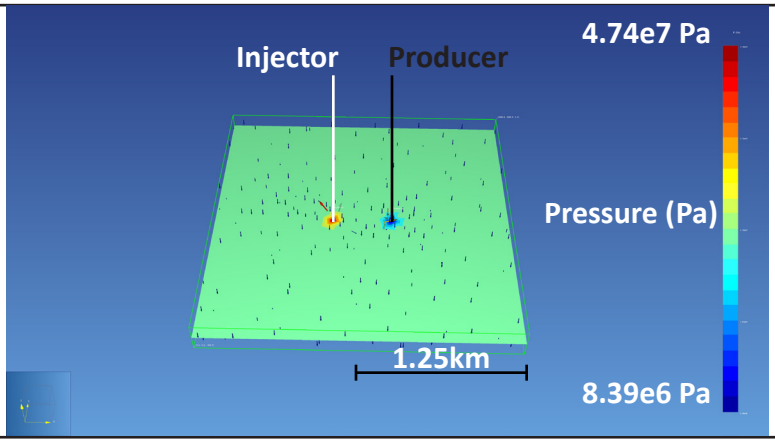

Time = 8606 seconds

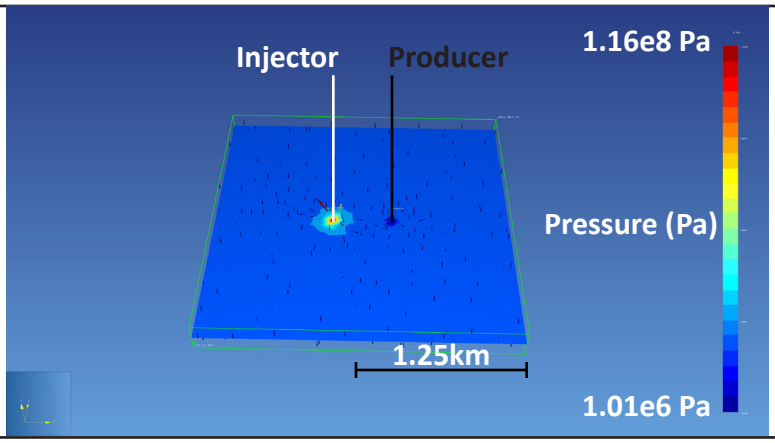

Time = ~7.7 hours

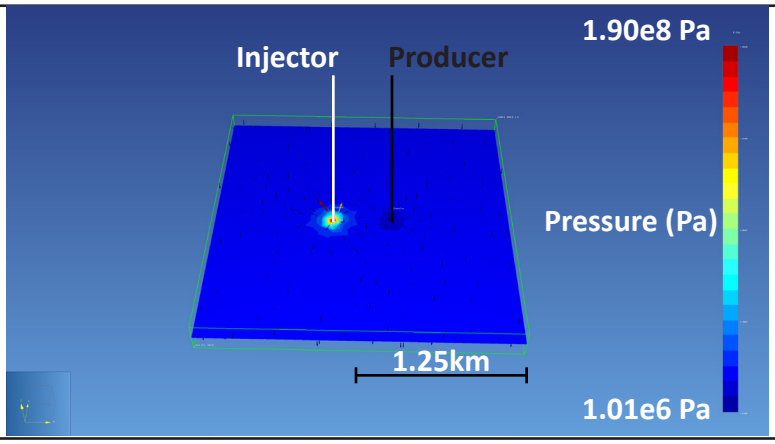

Time = ~48 hours

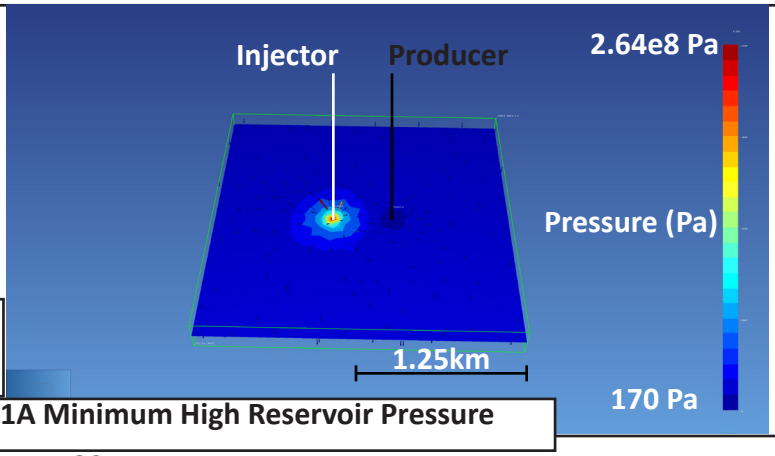

Pressure change through four timesteps in a simulation taken at high reservoir pressure using minimum Facies 1A values of permeability and porosity.

Figure 24: Doublet Pressure Model - Facies 1A Minimum High Reservoir Pressure

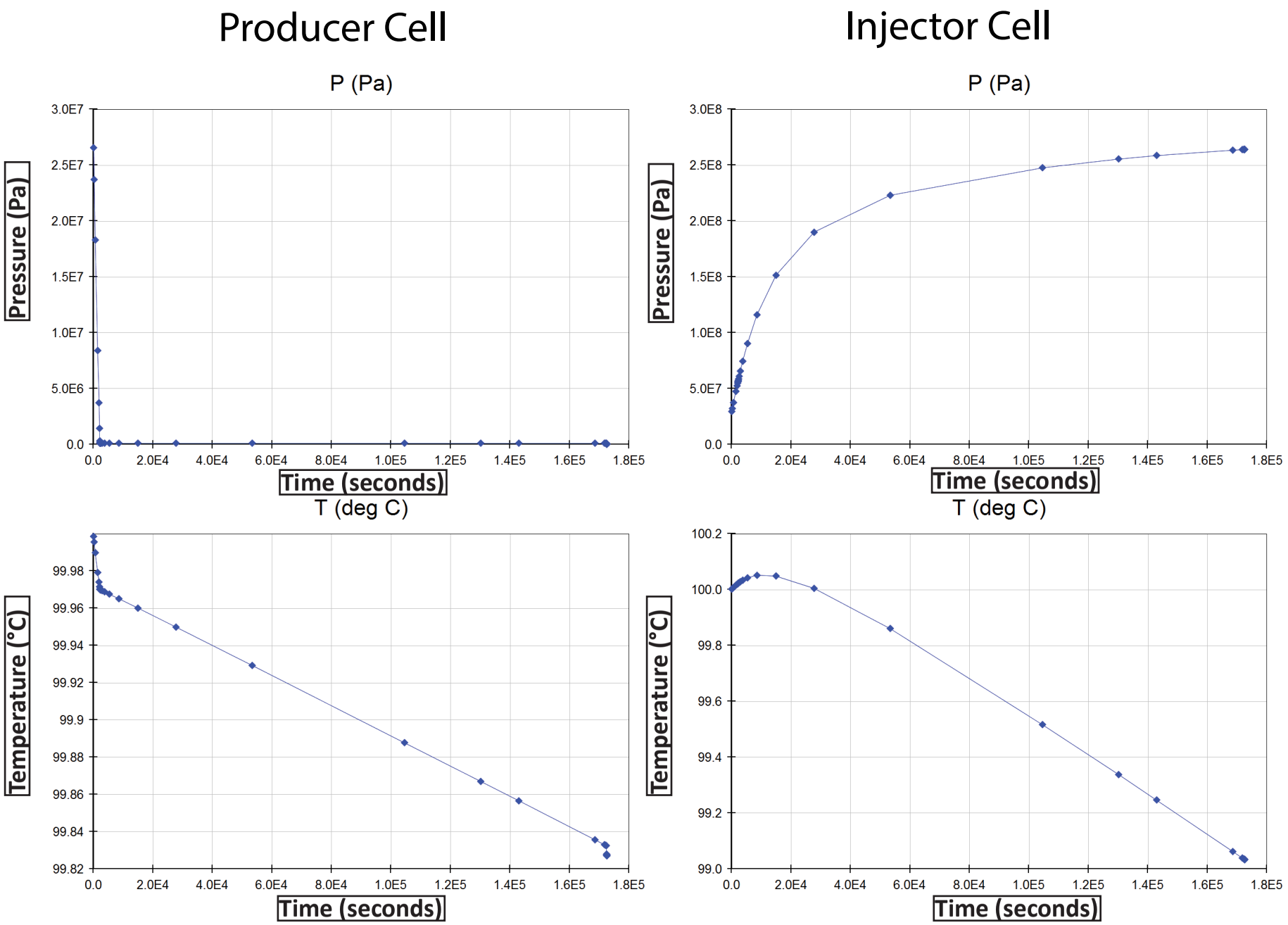

Figure 25: Producer and Injector Cell Graphs - Facies 1A Minimum High Reservoir Pressure

Temperature and pressure values as a function of time at the production and injection simulation cells for the simulation based on high reservoir pressure using cells populated with minimum porosity and permeability values for Facies 1A.

200kg/s Temperature Model - Facies 1A - High Reservoir Pressure

Time = 1500 seconds

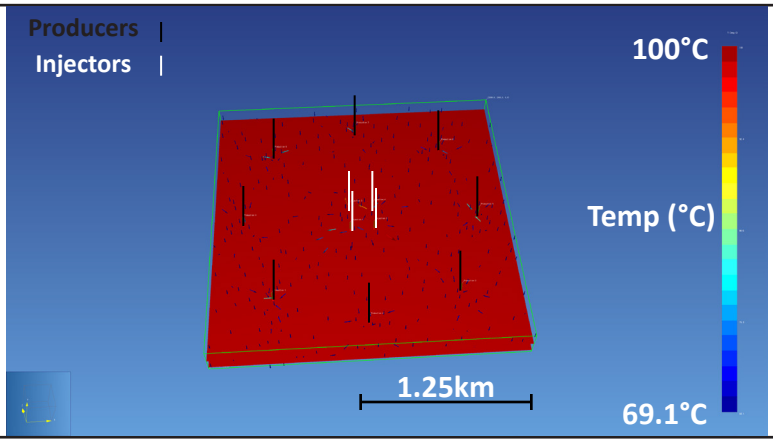

Time = ~76 days

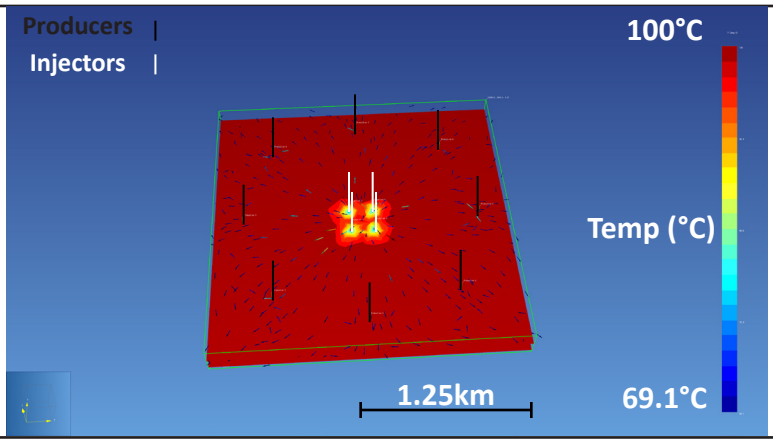

Time = ~5 years

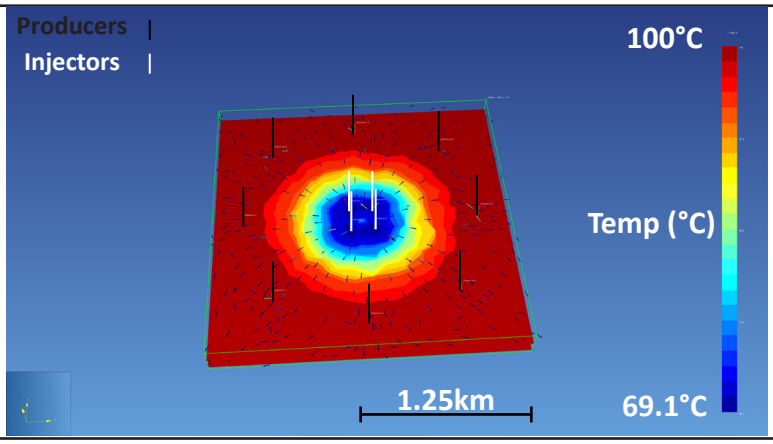

Time = 25 years

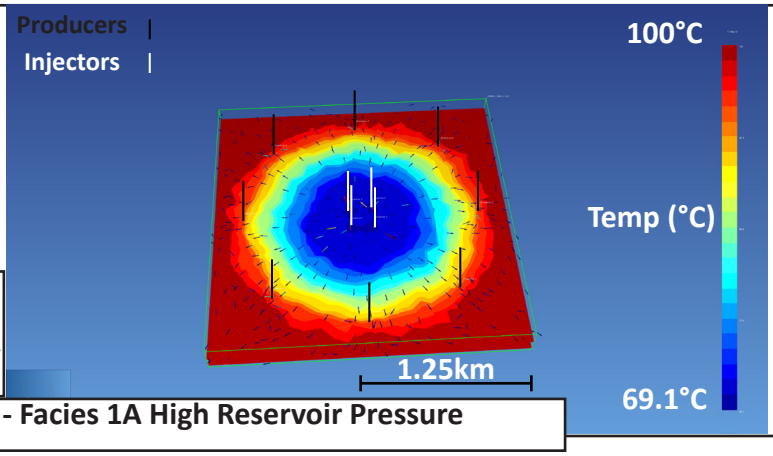

Temperature change through four timesteps in a simulation taken at high reservoir pressure using four injector and eight producer wells and mean porosity and permeability of Facies 1A

Figure 26: 200kg/s Temperature Model - Facies 1A High Reservoir Pressure

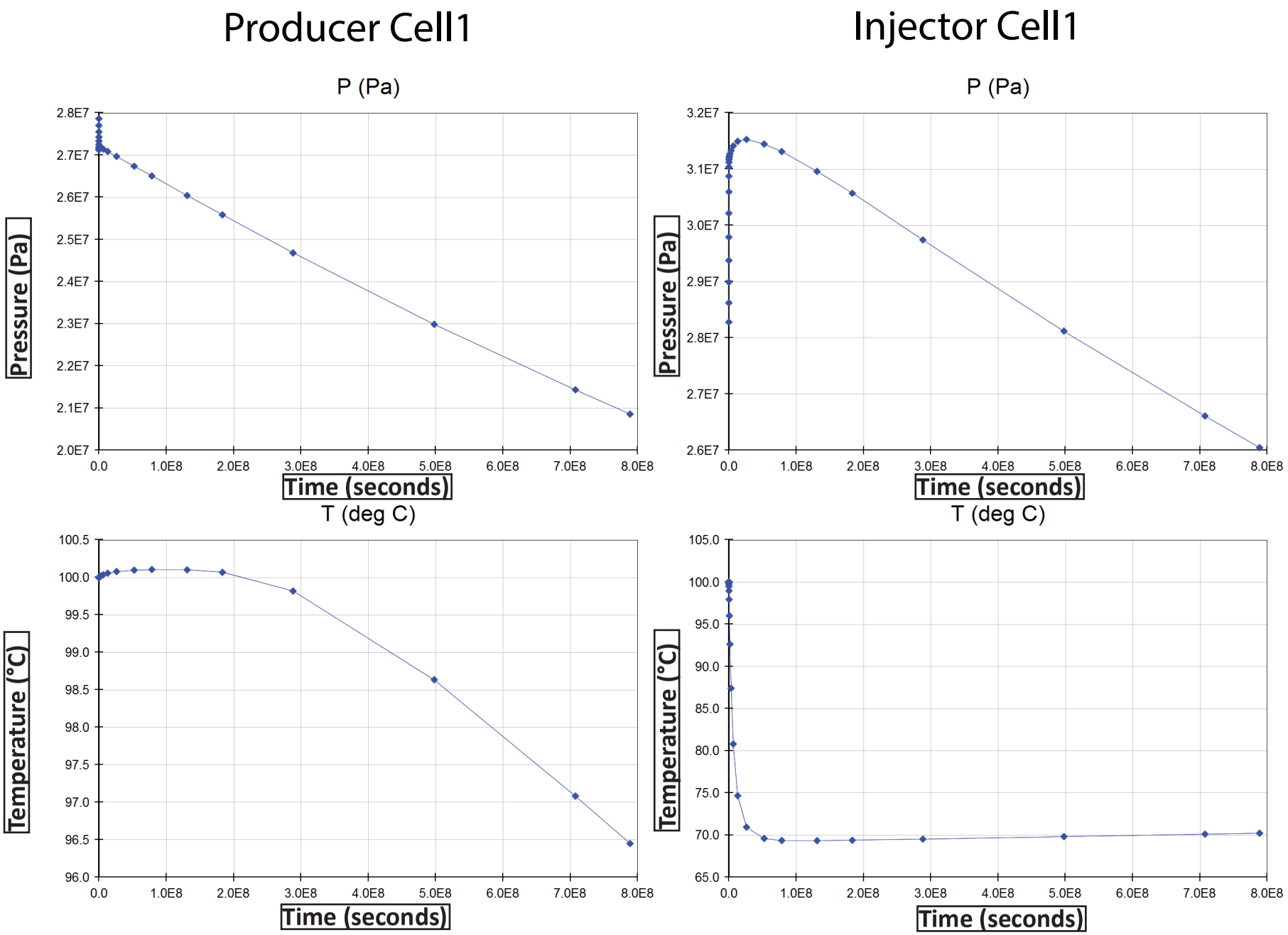

Figure 27: Producer and Injector Cell Graphs - Facies 1A 200kg/s High Reservoir Pressure

Temperature and pressure values as a function of time at a singular production and injection simulation cell for the simulation based on an eight producer and four injector configuation at high reservoir pressure using cells populated with mean porosity and permeability values for Facies 1A.

Appendix A

Doublet Model - Facies 1A - Max Low Reservoir Pressure

Time = 1500 seconds

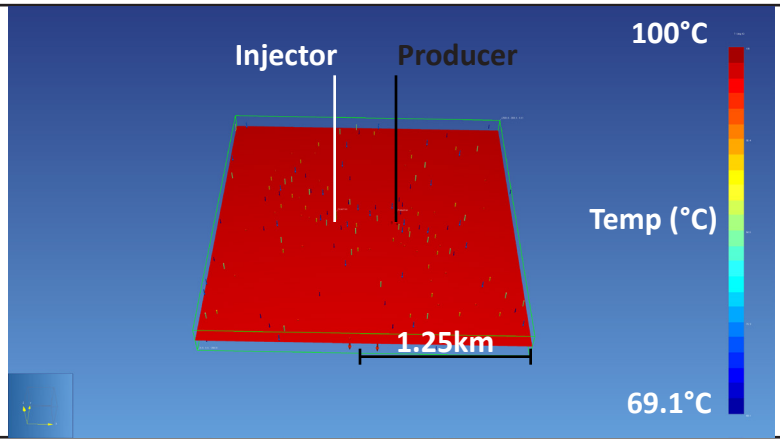

Time = ~76 days

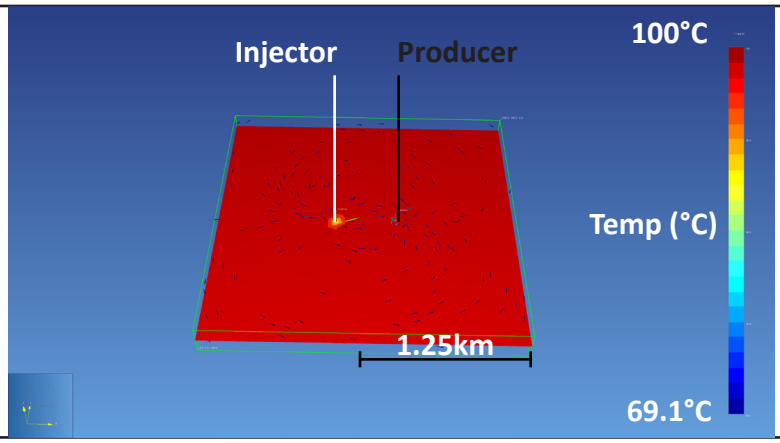

Time = ~5 years

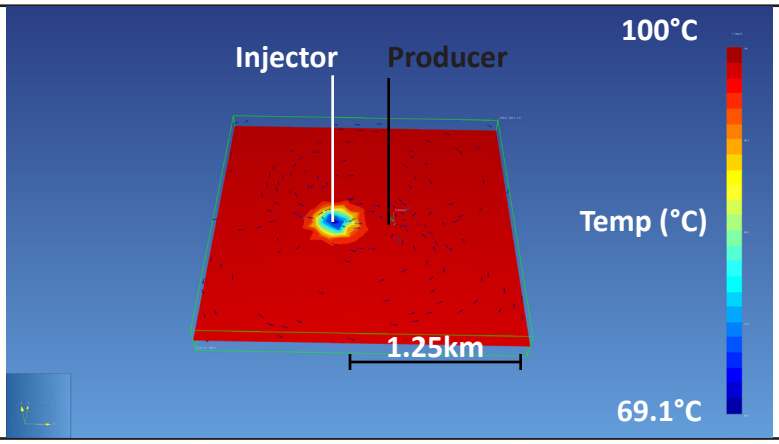

Time = 25 years

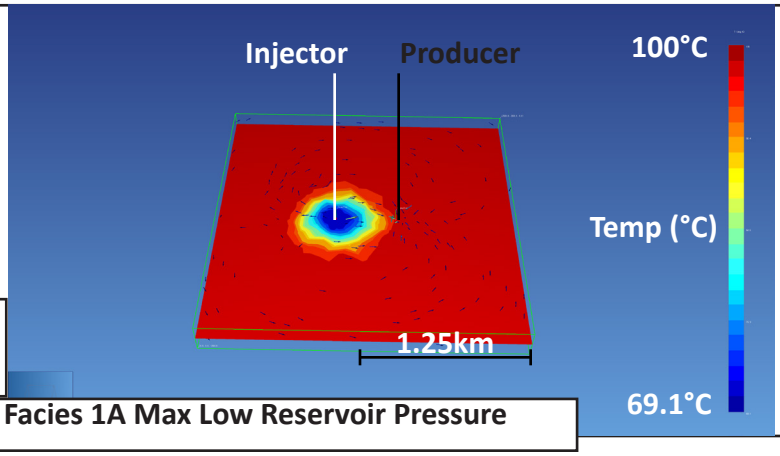

Temperature change through four timesteps in a simulation taken at low reservoir pressure using max Facies 1A values for porosity and permeability.

Figure A1: Doublet Temperature Model - Facies 1A Max Low Reservoir Pressure

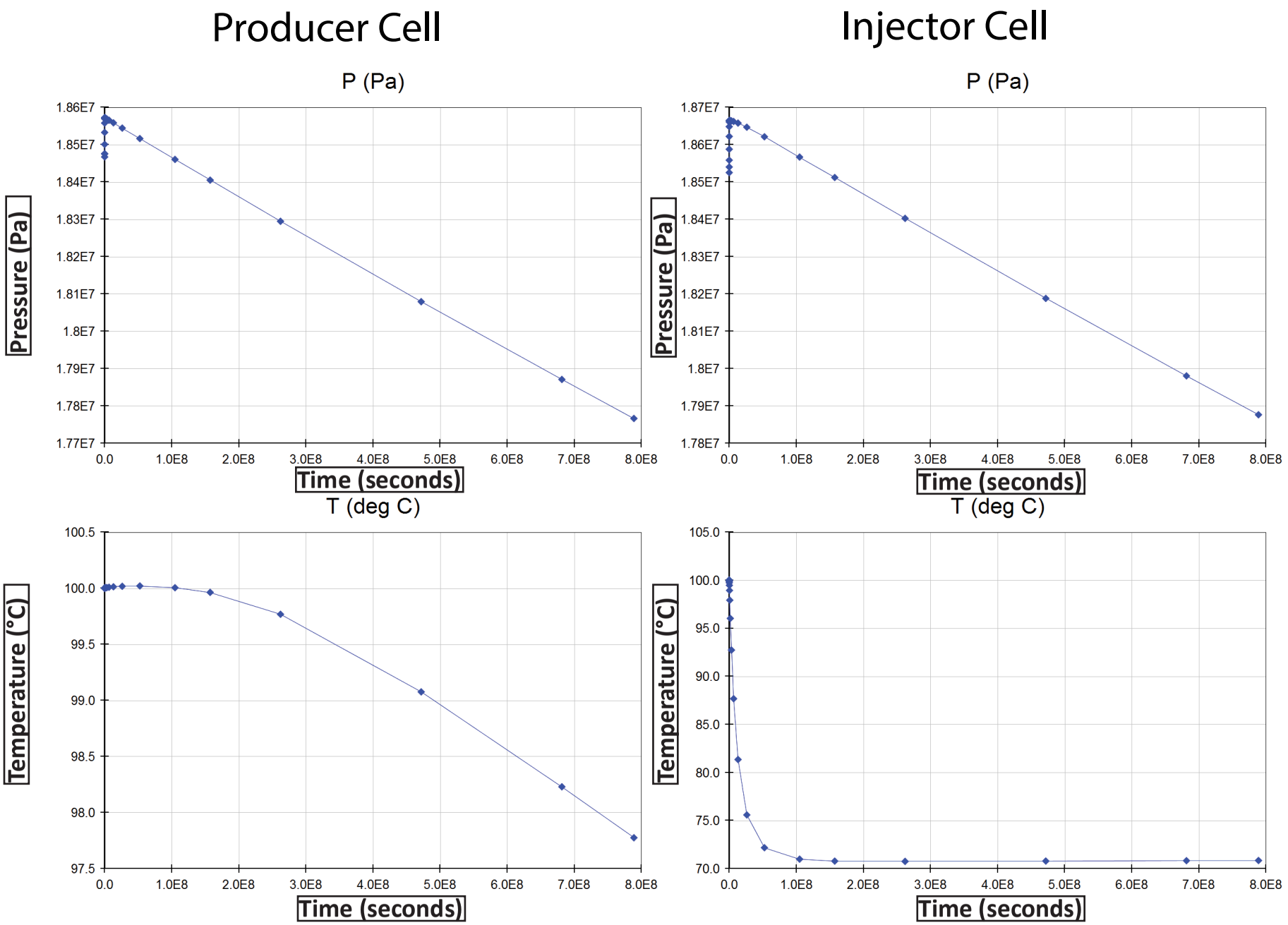

Figure A2: Producer and Injector Cell Graphs - Facies 1A Max Low Reservoir Pressure

Temperature and pressure values as a function of time at the production and injection simulation cells for the simulation based on low reservoir pressure using cells populated with maximum porosity and permeability values for Facies 1A.

Doublet Model - Facies 1A - Mean High Reservoir Pressure

Time = 1500 seconds

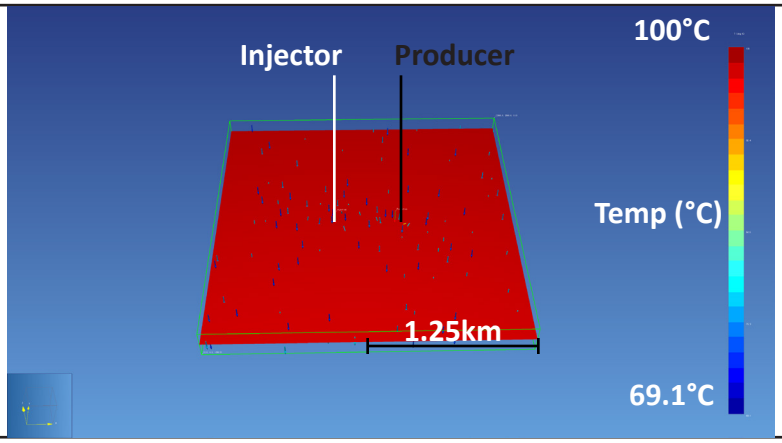

Time = ~76 days

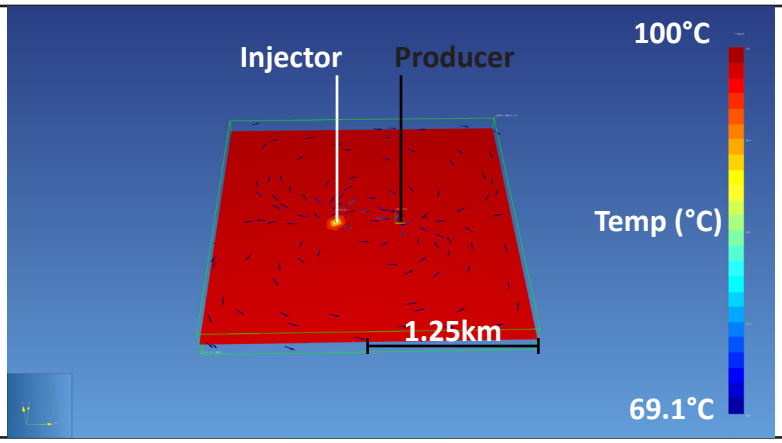

Time = ~5 years

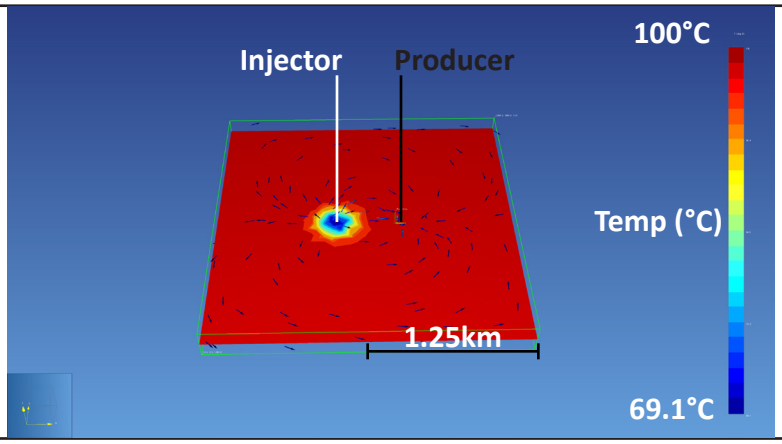

Time = 25 years

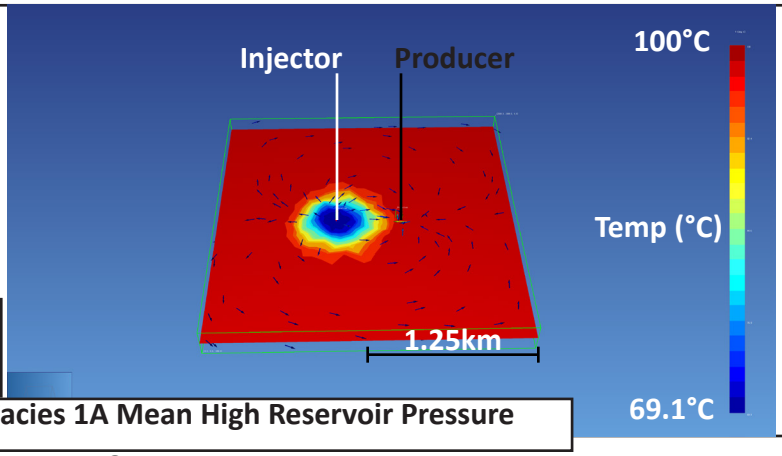

Temperature change through four timesteps in a simulation taken at high reservoir pressure using mean Facies 1A values for porosity and permeability.

Figure A3: Doublet Temperature Model - Facies 1A Mean High Reservoir Pressure

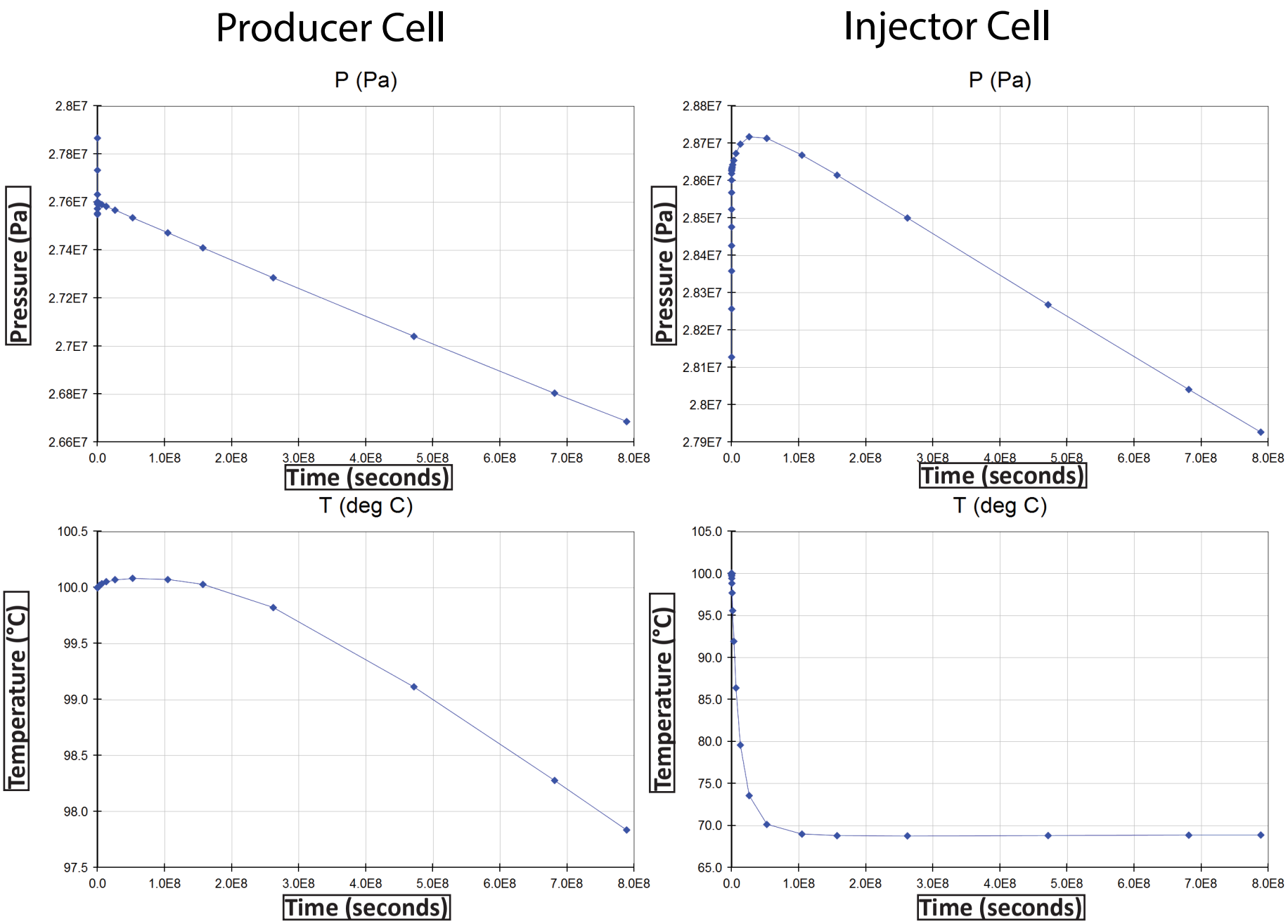

Figure A4: Producer and Injector Cell Graphs - Facies 1A Mean High Reservoir Pressure

Temperature and pressure values as a function of time at the production and injection simulation cells for the simulation based on high reservoir pressure using cells populated with mean porosity and permeability values for Facies 1A.

Doublet Model - Facies 1A - Mean Low Reservoir Pressure

Time = 1500 seconds

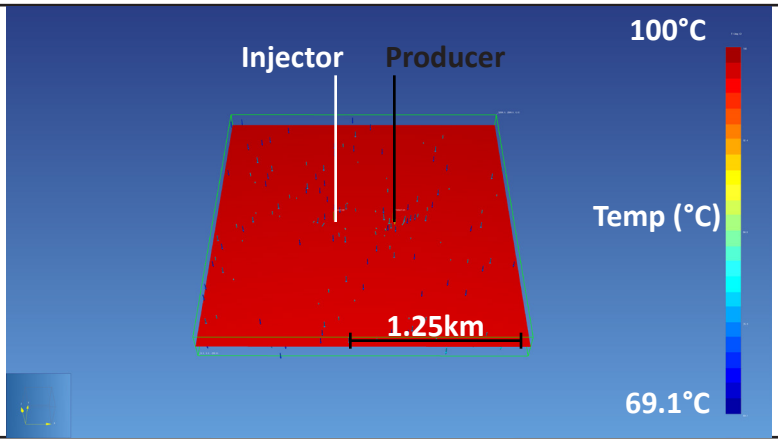

Time = ~76 days

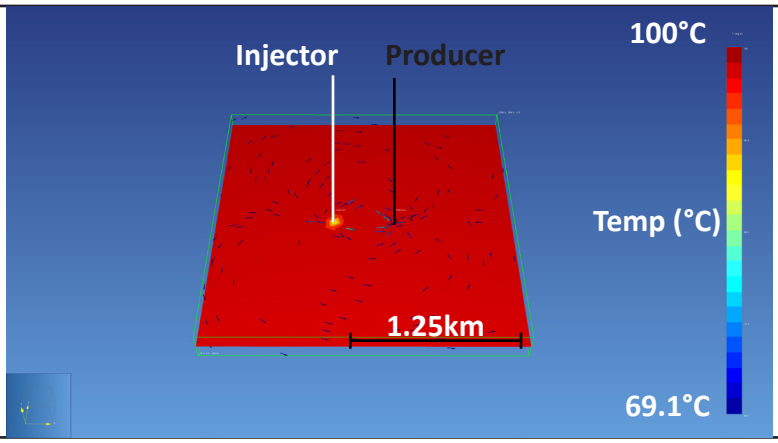

Time = ~5 years

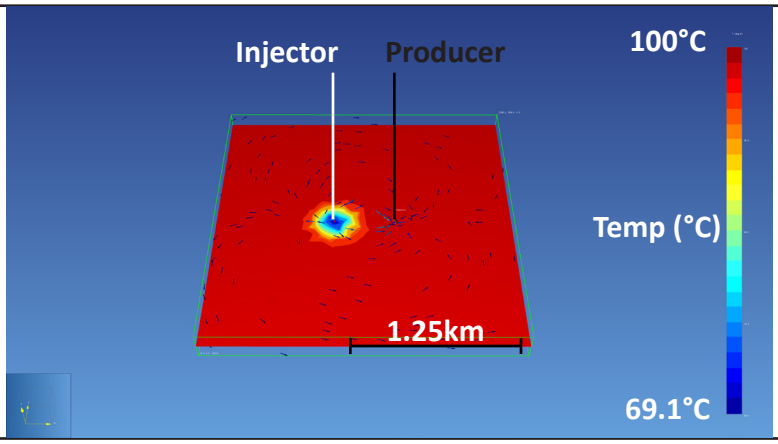

Time = 25 years

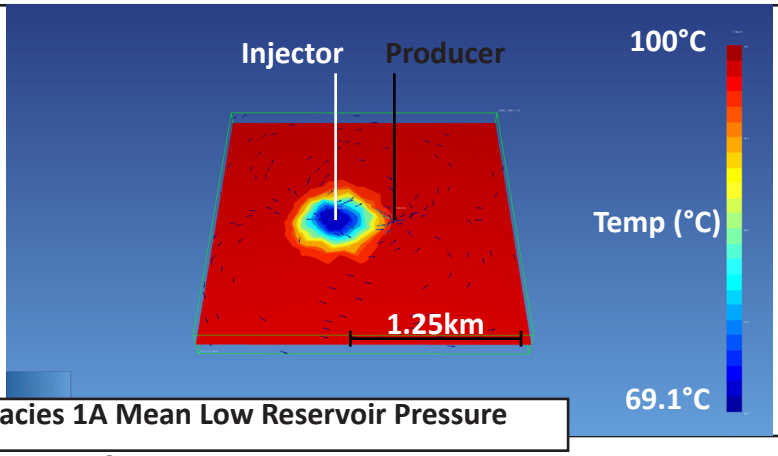

Temperature change through four timesteps in a simulation taken at low reservoir pressure using mean Facies 1A values for porosity and permeability.

Figure A5: Doublet Temperature Model - Facies 1A Mean Low Reservoir Pressure

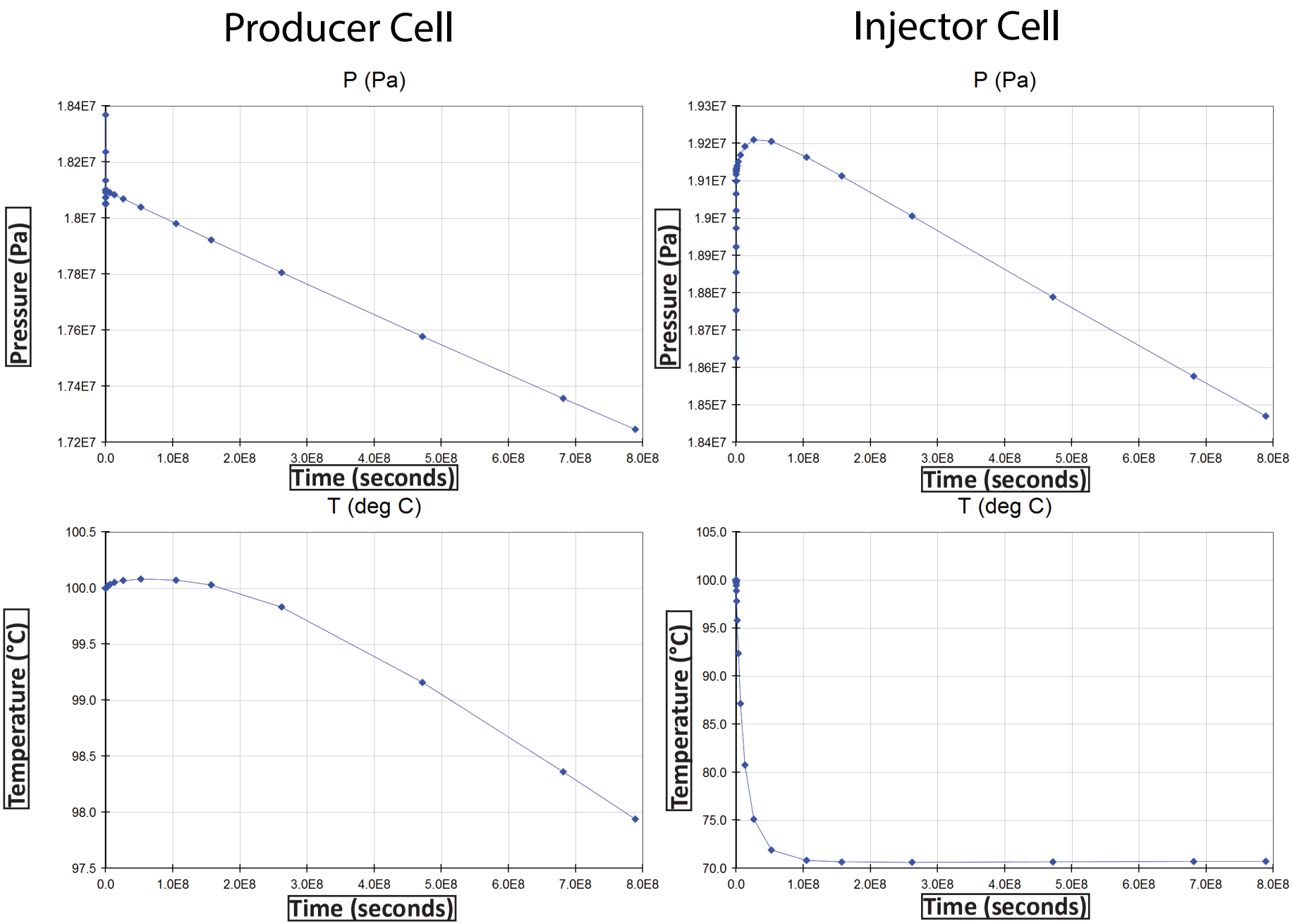

Figure A6: Producer and Injector Cell Graphs - Facies 1A Mean Low Reservoir Pressure

Temperature and pressure values as a function of time at the production and injection simulation cells for the simulation based on low reservoir pressure using cells populated with mean porosity and permeability values for Facies 1A.

Doublet Model - Facies 1A - Median High Reservoir Pressure

Time = 1500 seconds

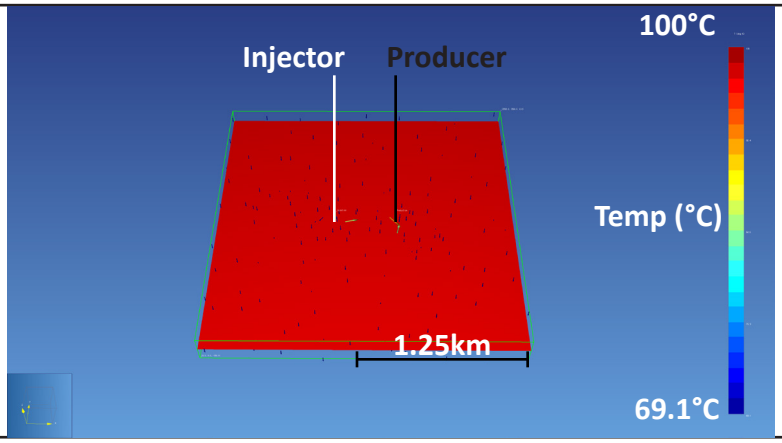

Time = ~76 days

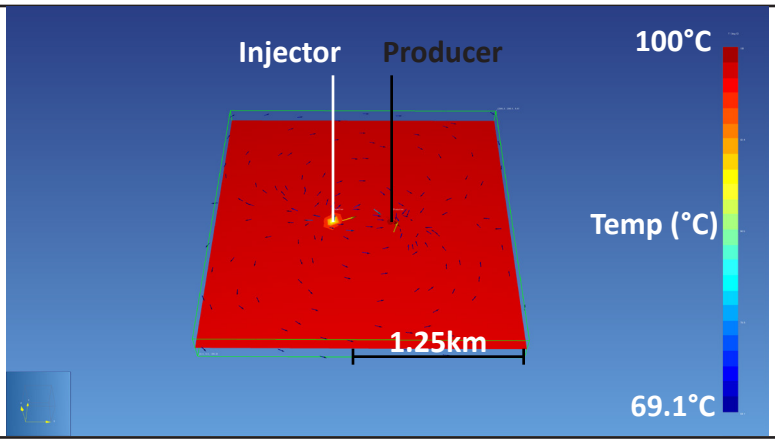

Time = ~5 years

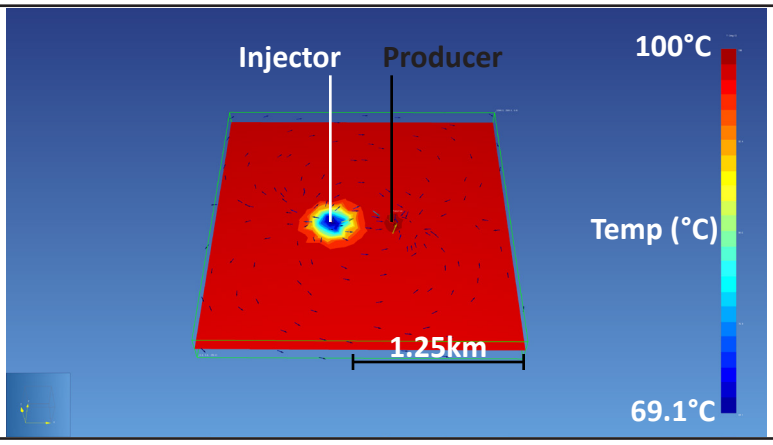

Time = 25 years

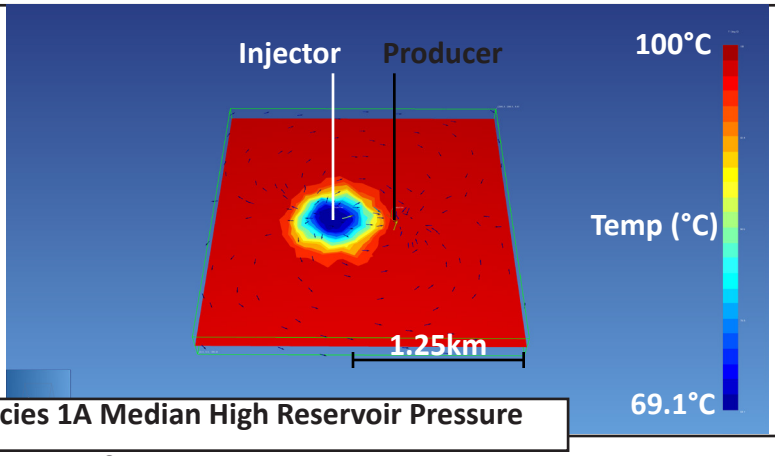

Temperature change through four timesteps in a simulation taken at high reservoir pressure using median Facies 1A values for porosity and permeability.

Figure A7: Doublet Temperature Model - Facies 1A Median High Reservoir Pressure

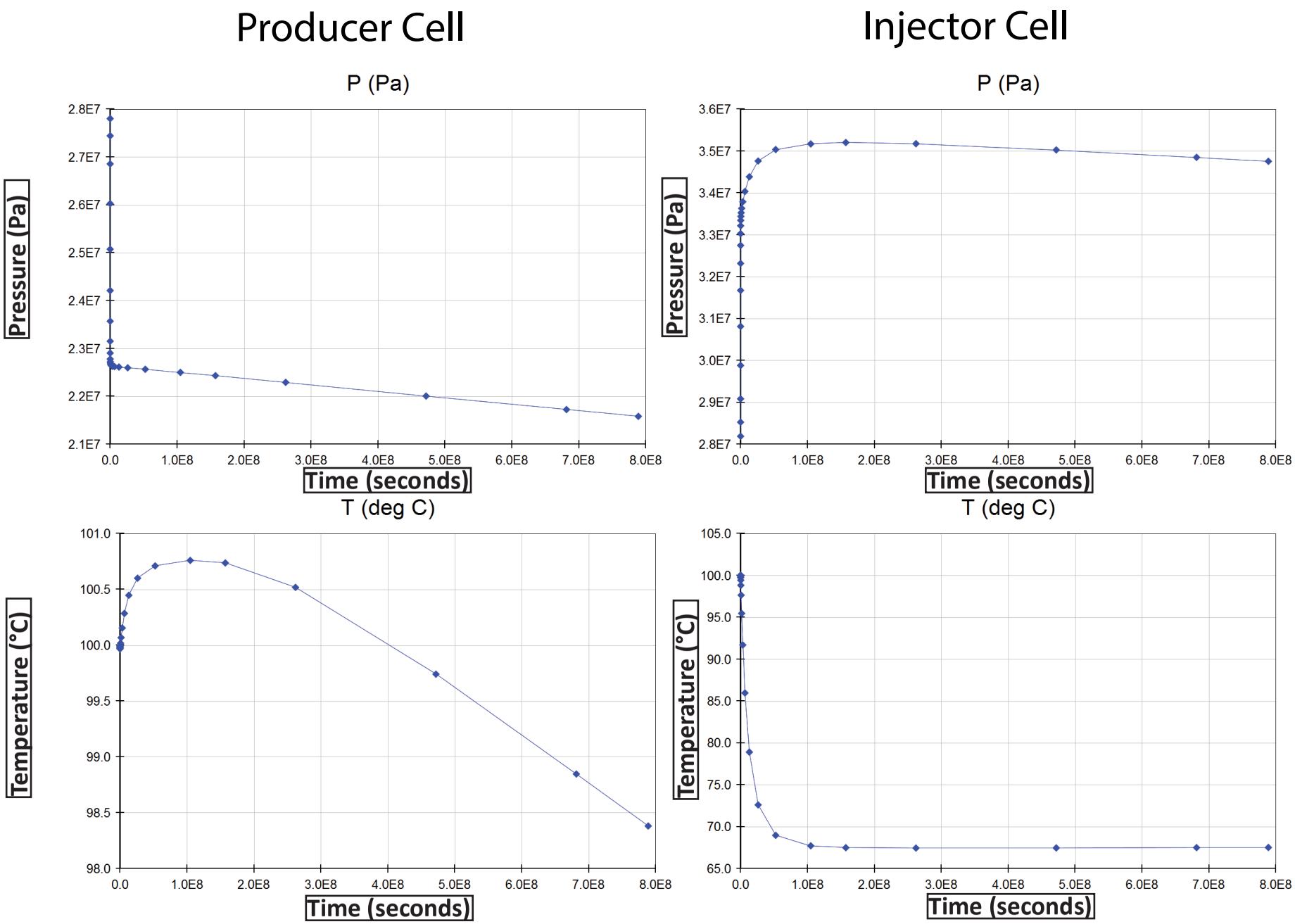

Figure A8: Producer and Injector Cell Graphs - Facies 1A Median High Reservoir Pressure

Temperature and pressure values as a function of time at the production and injection simulation cells for the simulation based on high reservoir pressure using cells populated with median porosity and permeability values for Facies 1A.

Doublet Model - Facies 1A - Median Low Reservoir Pressure

Time = 1500 seconds

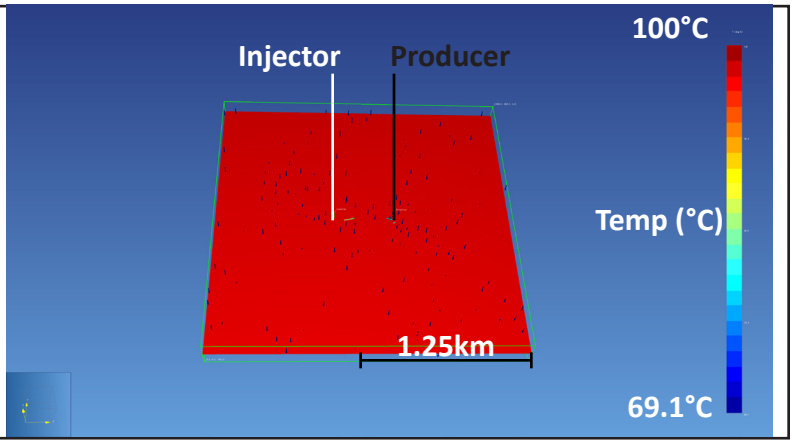

Time = ~76 days

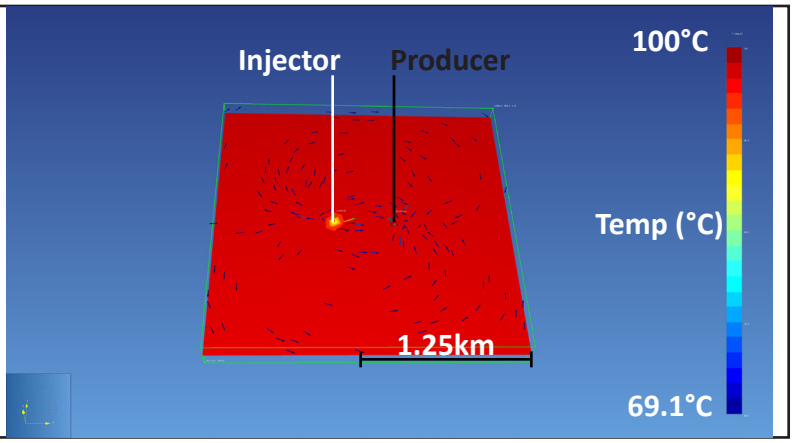

Time = ~5 years

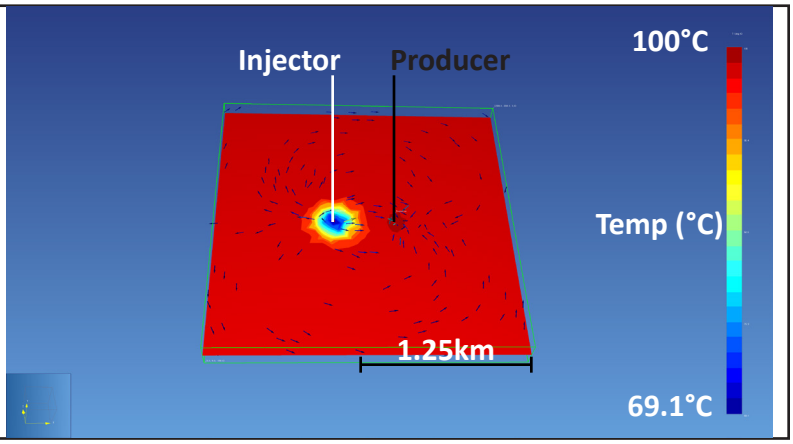

Time = 25 years

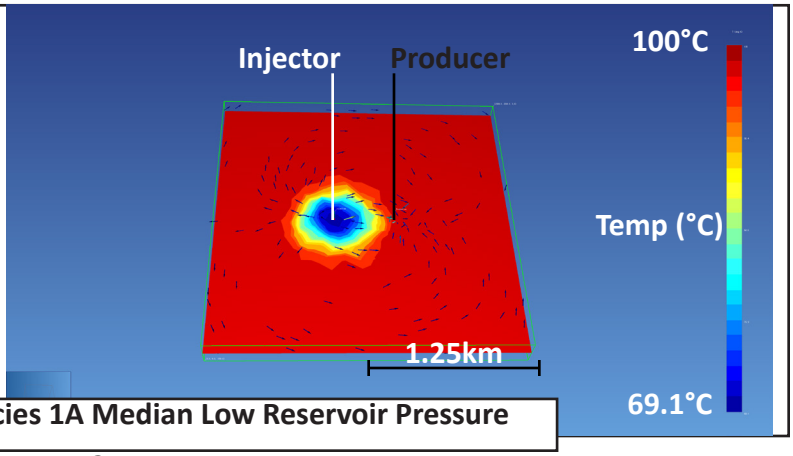

Temperature change through four timesteps in a simulation taken at low reservoir pressure using median Facies 1A values for porosity and permeability.

Figure A9: Doublet Temperature Model - Facies 1A Median Low Reservoir Pressure

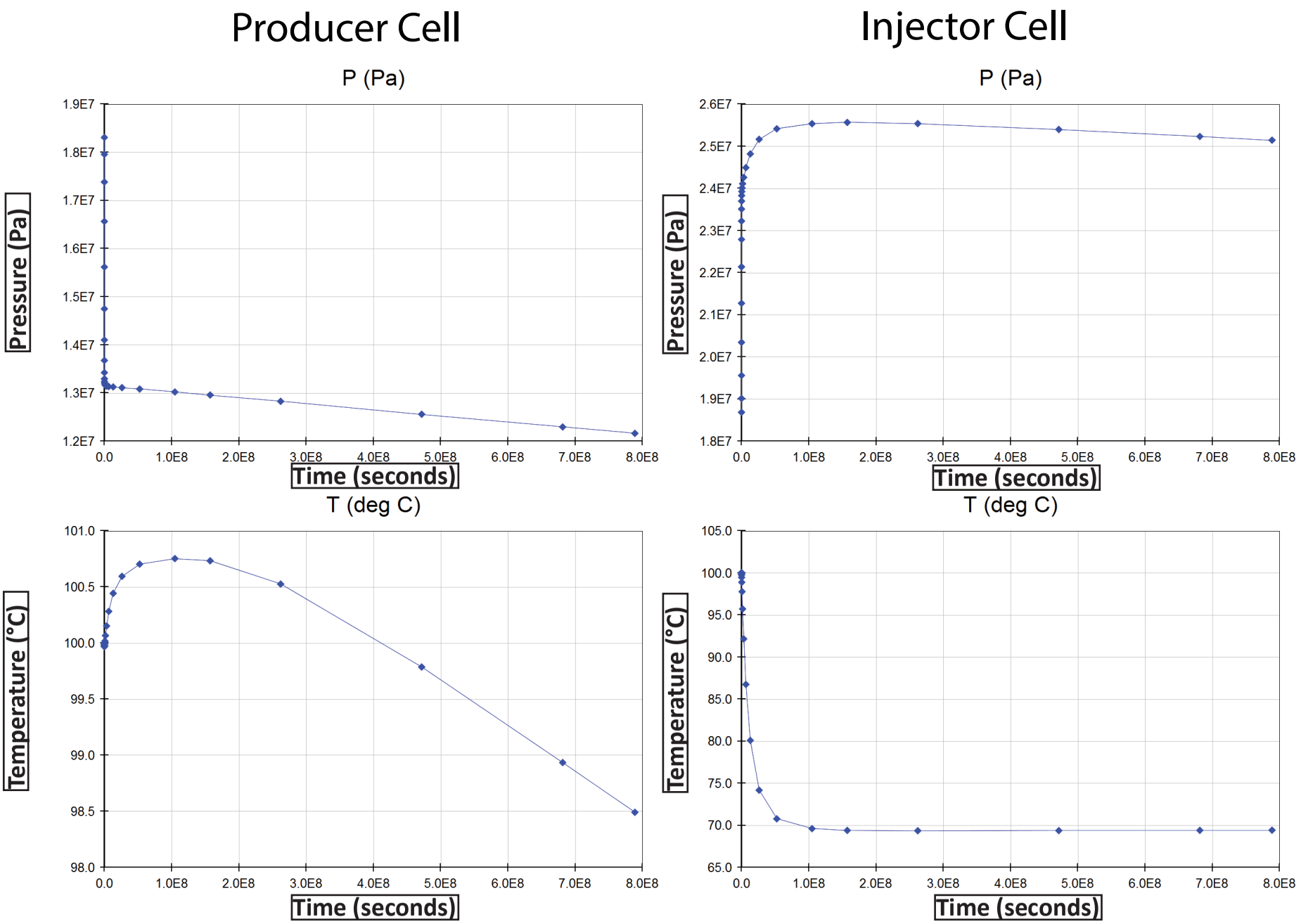

Figure A10: Producer and Injector Cell Graphs - Facies 1A Median Low Reservoir Pressure

Temperature and pressure values as a function of time at the production and injection simulation cells for the simulation based on low reservoir pressure using cells populated with median porosity and permeability values for Facies 1A.

Doublet Pressure Model - Facies 1A - Minimum Low Reservoir Pressure

Time = 1518 seconds

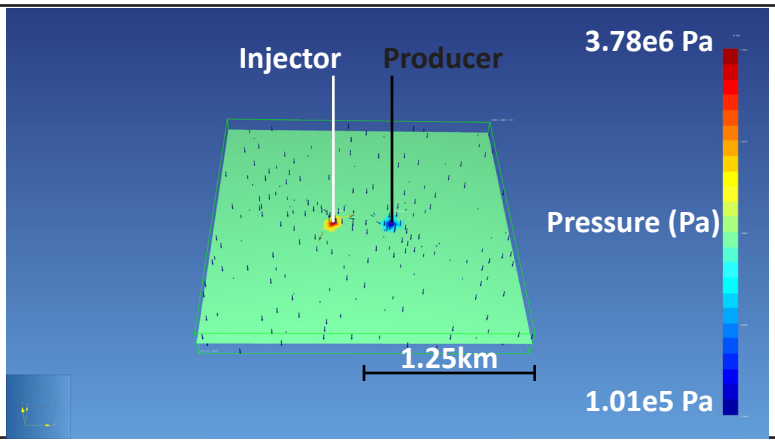

Time = 7818 seconds

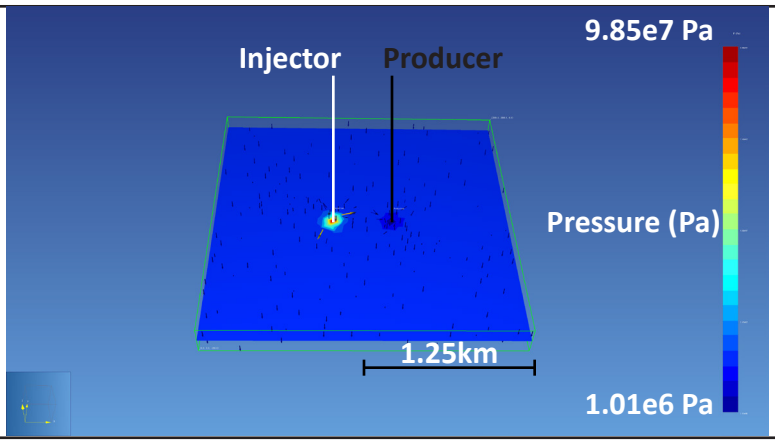

Time = ~29 hours

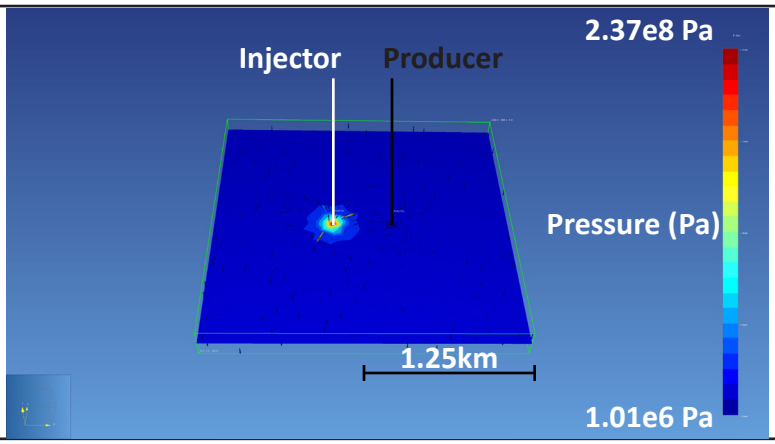

Time = ~45 hours

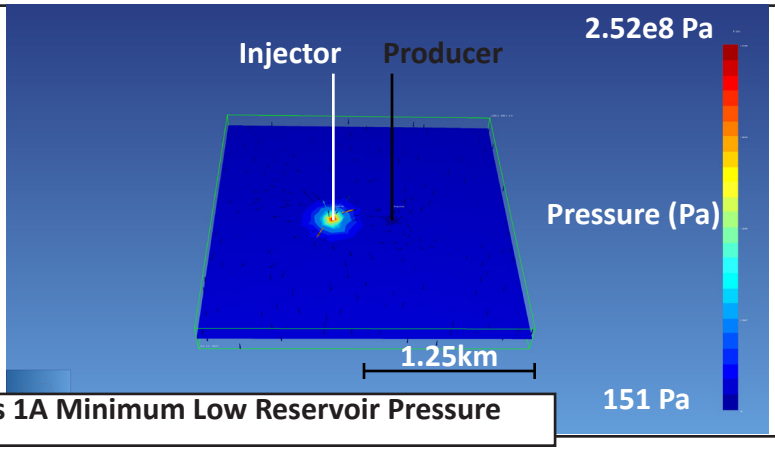

Pressure change through four timesteps in a simulation taken at low reservoir pressure using minimum Facies 1A values for porosity and permeability.

Figure A11: Doublet Pressure Model - Facies 1A Minimum Low Reservoir Pressure

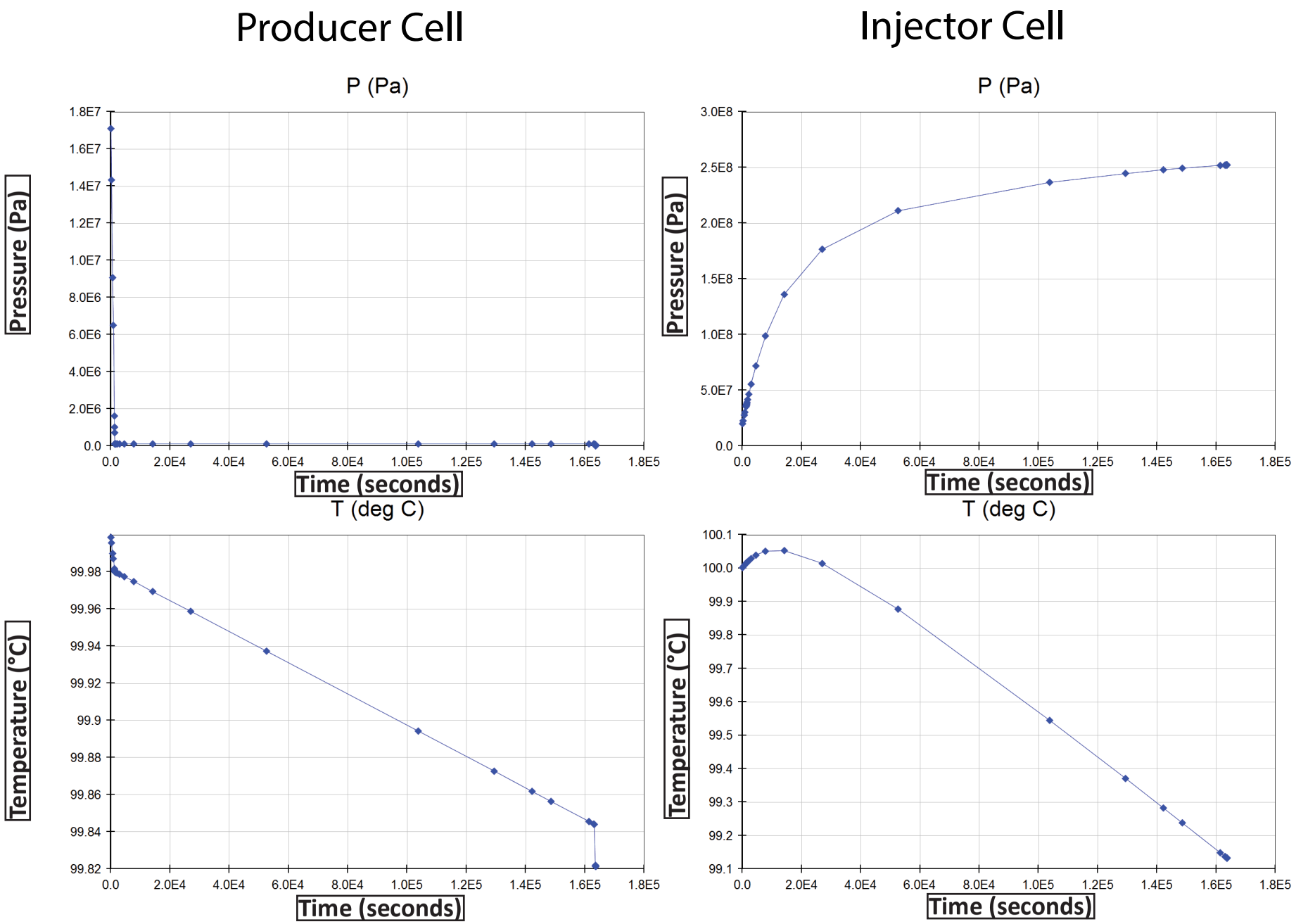

Figure A12: Producer and Injector Cell Graphs - Facies 1A Minimum Low Reservoir Pressure

Temperature and pressure values as a function of time at the production and injection simulation cells for the simulation based on low reservoir pressure using cells populated with minimum porosity and permeability values for Facies 1A.

Doublet Pressure Model - Facies 1A - Q1 High Reservoir Pressure

Time = 1500 seconds

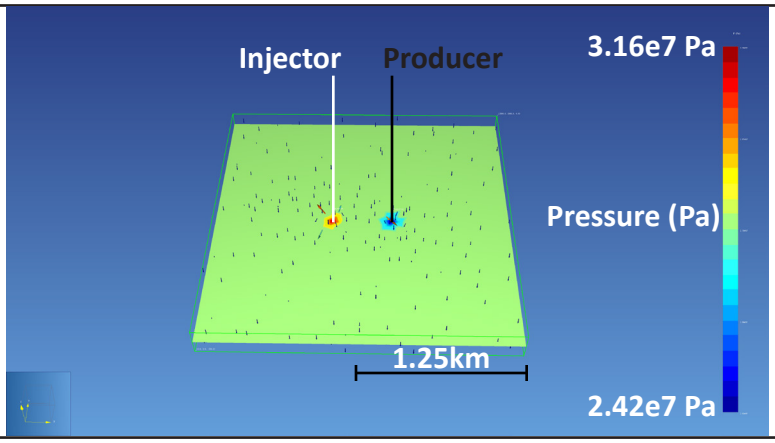

Time = ~83 days

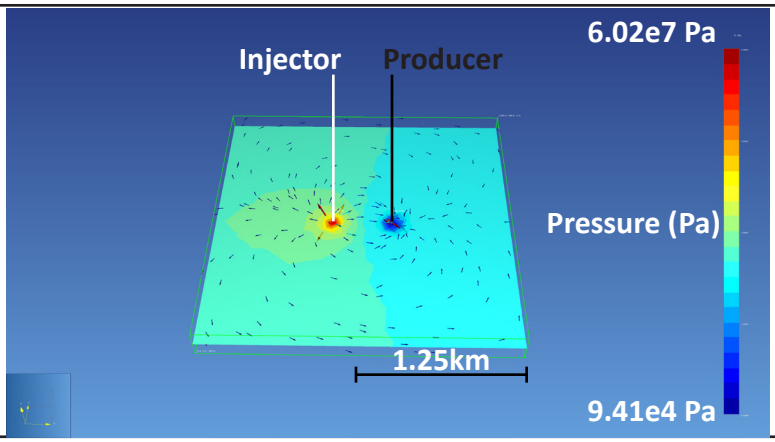

Time = ~158 days

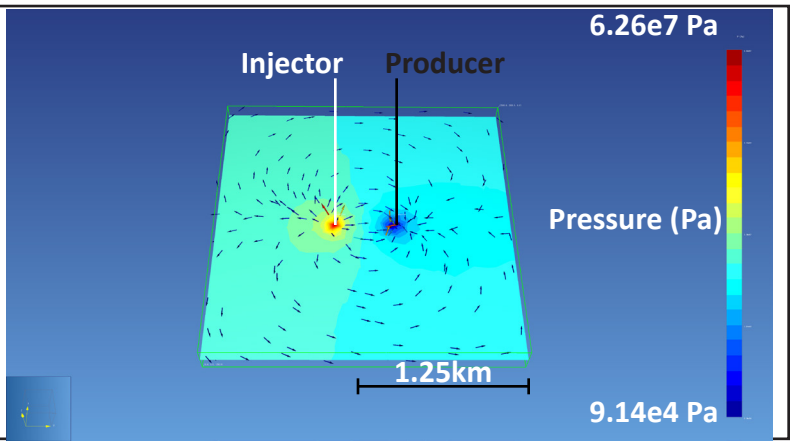

Time = ~265 days

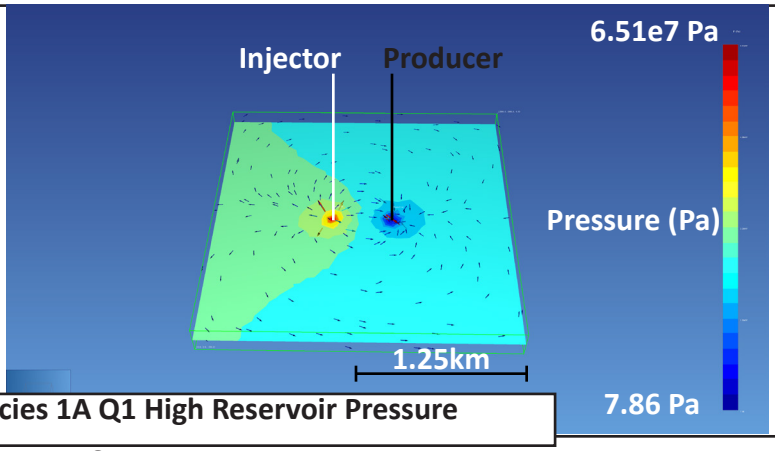

Pressure change through four timesteps in a simulation taken at high reservoir pressure using Q1 Facies 1A values for porosity and permeability.

Figure A13: Doublet Pressure Model - Facies 1A Q1 High Reservoir Pressure

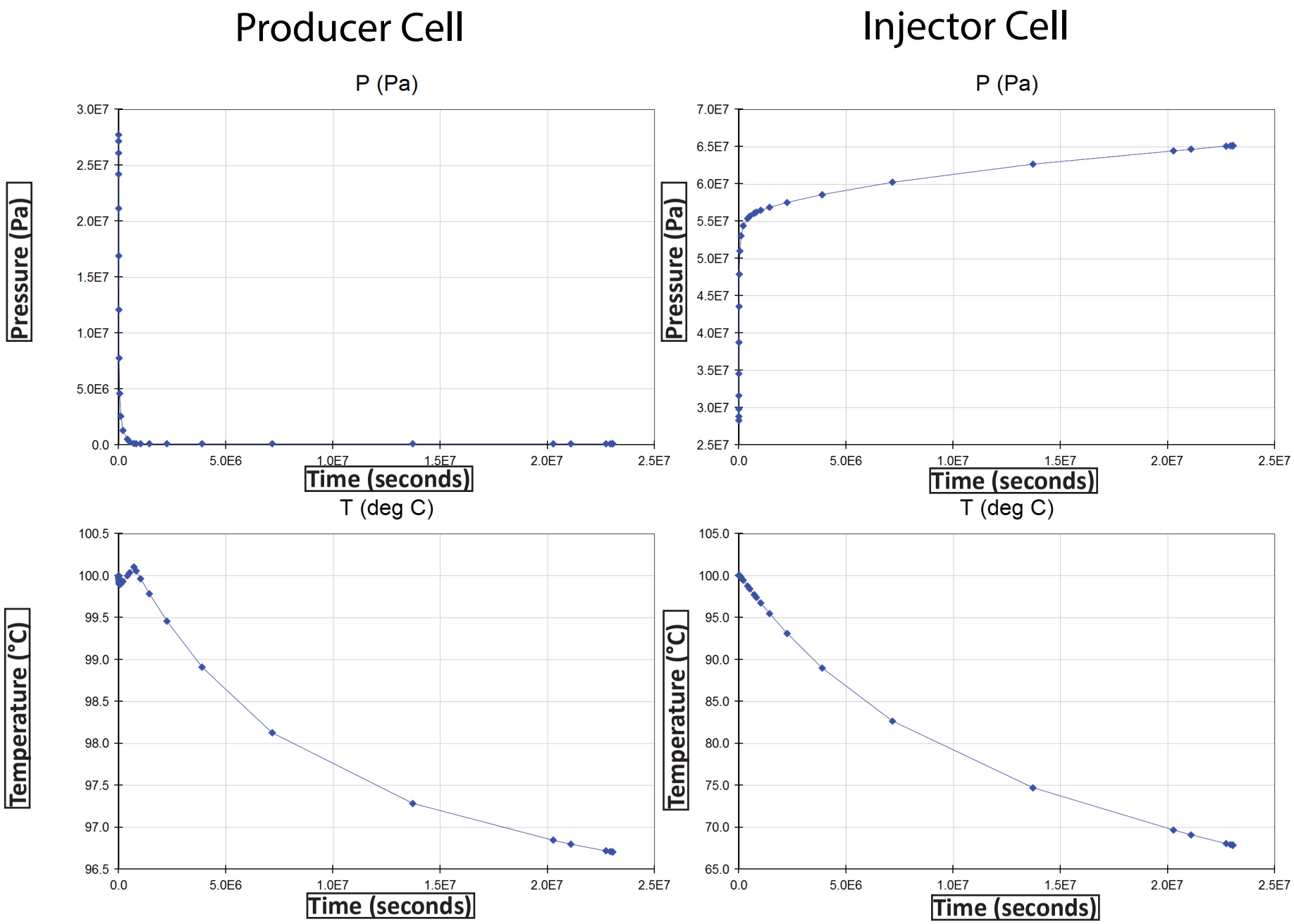

Figure A14: Producer and Injector Cell Graphs - Facies 1A Q1 High Reservoir Pressure

Temperature and pressure values as a function of time at the production and injection simulation cells for the simulation based on high reservoir pressure using cells populated with Q1 porosity and permeability values for Facies 1A.

Doublet Pressure Model - Facies 1A - Q1 Low Reservoir Pressure

Time = 1500 seconds

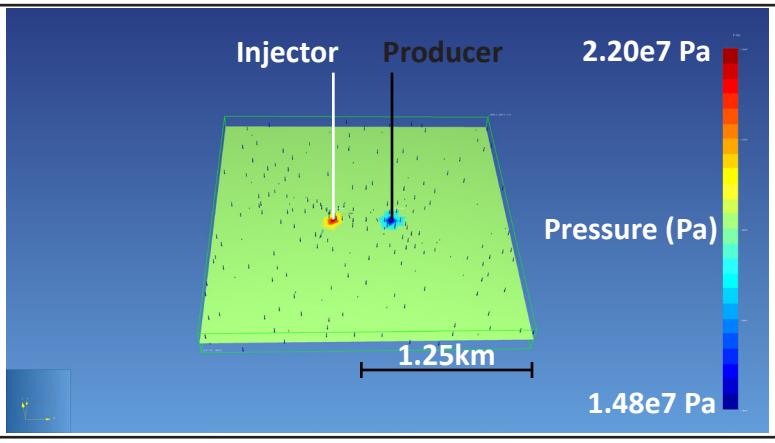

Time = 1270 seconds

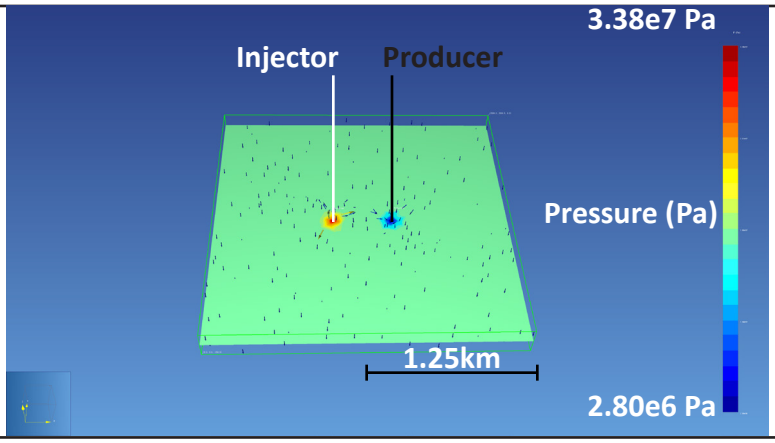

Time = ~2.6 days

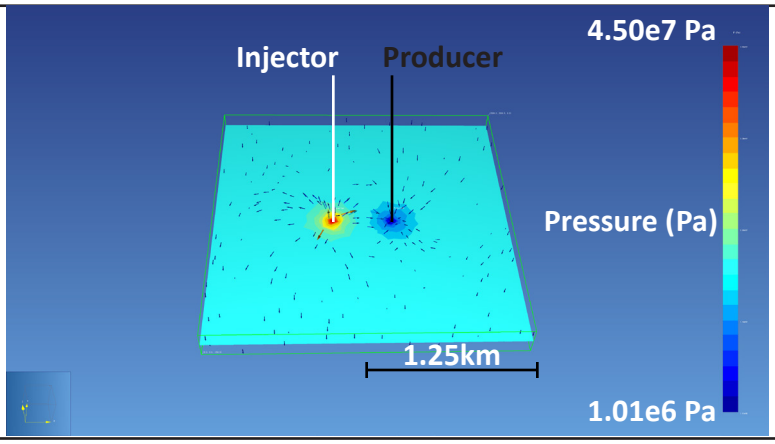

Time = ~26 days

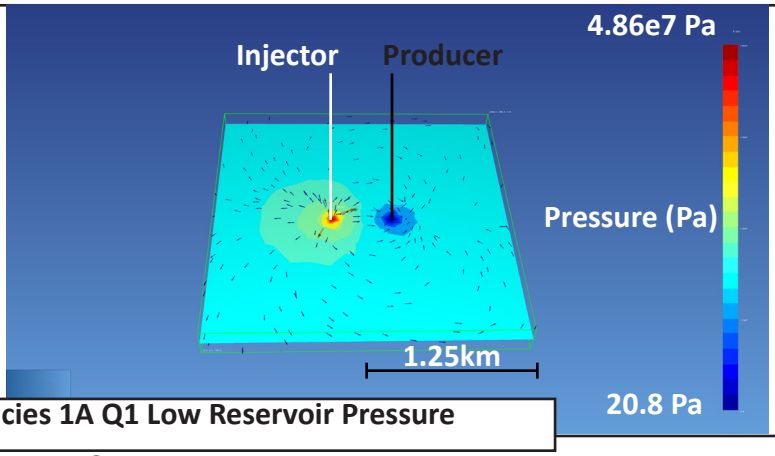

Pressure change through four timesteps in a simulation taken at low reservoir pressure using Q1 Facies 1A values for porosity and permeability.

Figure A15: Doublet Pressure Model - Facies 1A Q1 Low Reservoir Pressure

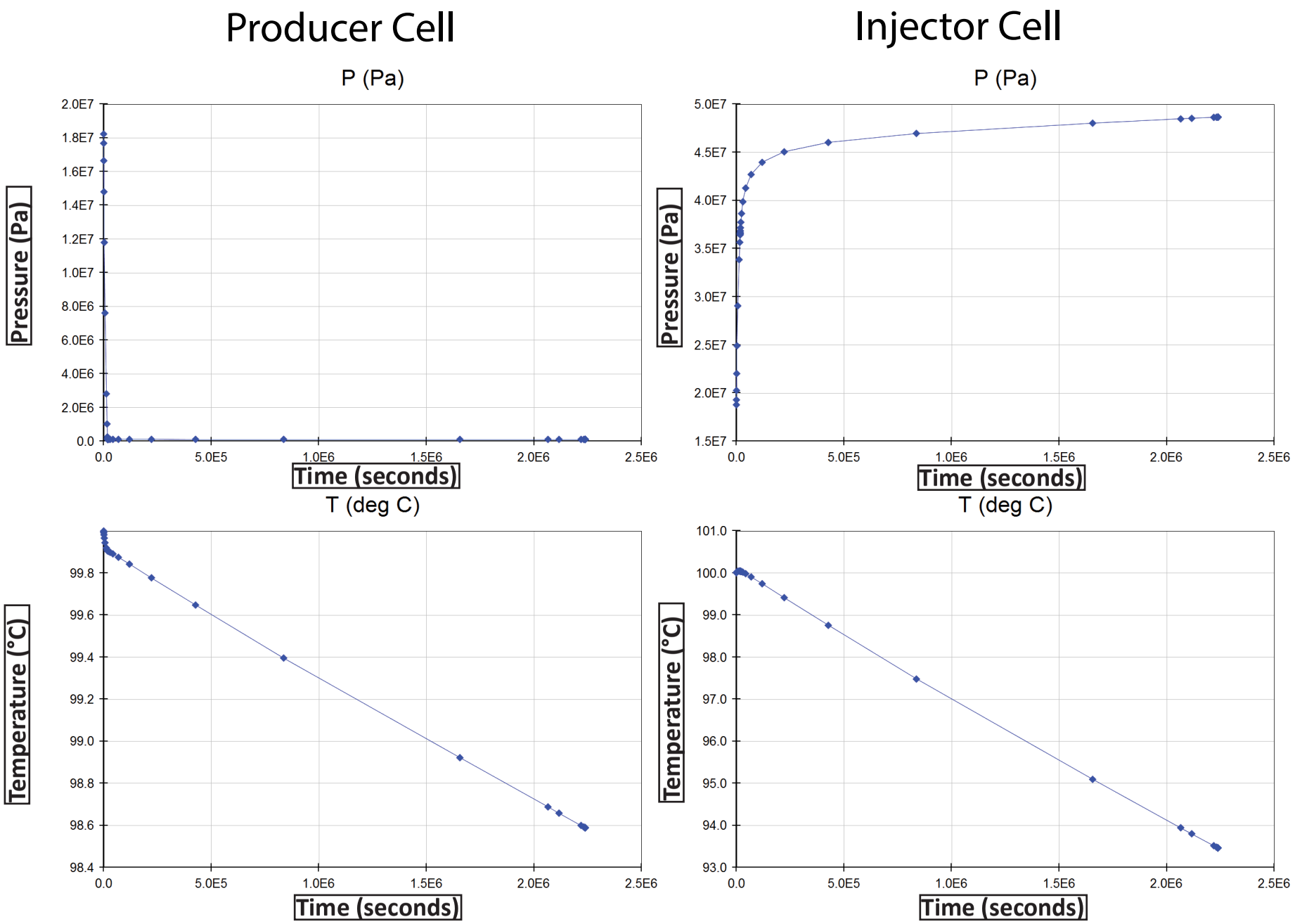

Figure A16: Producer and Injector Cell Graphs - Facies 1A Q1 Low Reservoir Pressure

Temperature and pressure values as a function of time at the production and injection simulation cells for the simulation based on low reservoir pressure using cells populated with Q1 porosity and permeability values for Facies 1A.

Doublet Temperature Model - Facies 1A - Q3 High Reservoir Pressure

Time = 1500 seconds

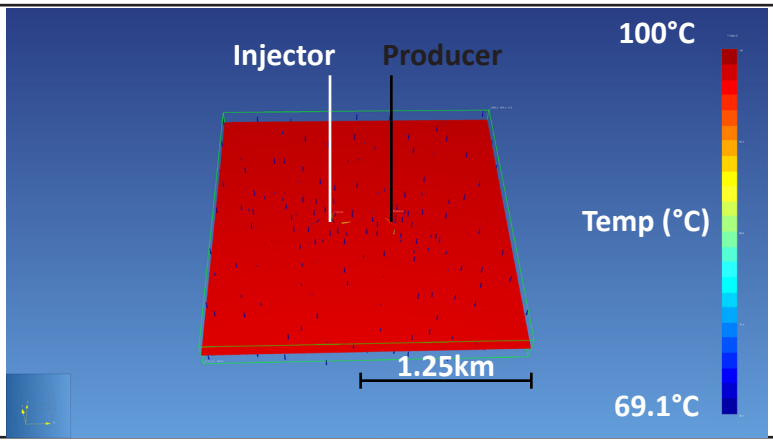

Time = ~76 days

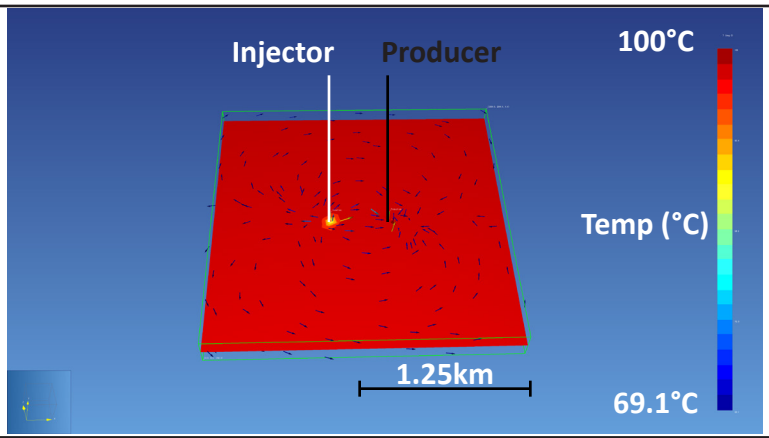

Time = ~5 years

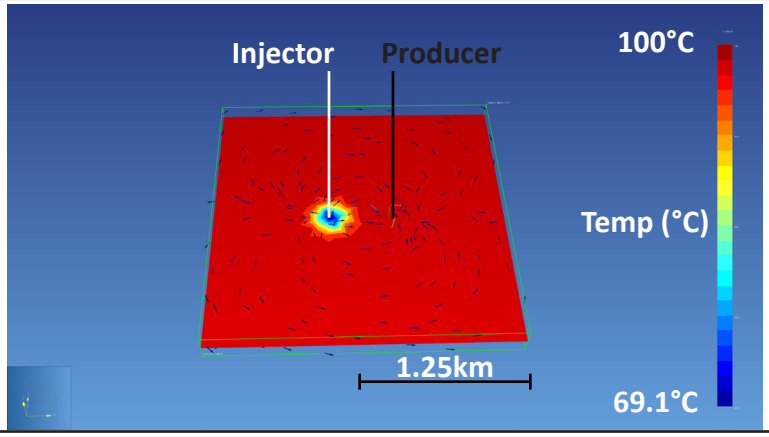

Time = 25 years

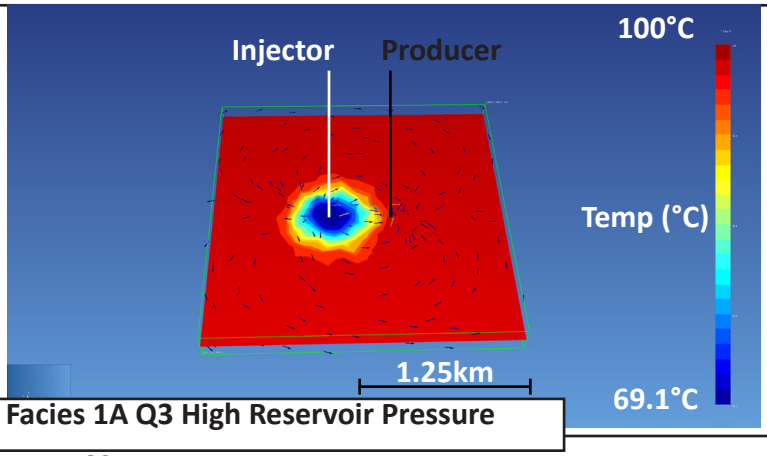

Temperature change through four timesteps in a simulation taken at high reservoir pressure using Q3 Facies 1A values for porosity and permeability.

Figure A17: Doublet Temperature Model - Facies 1A Q3 High Reservoir Pressure

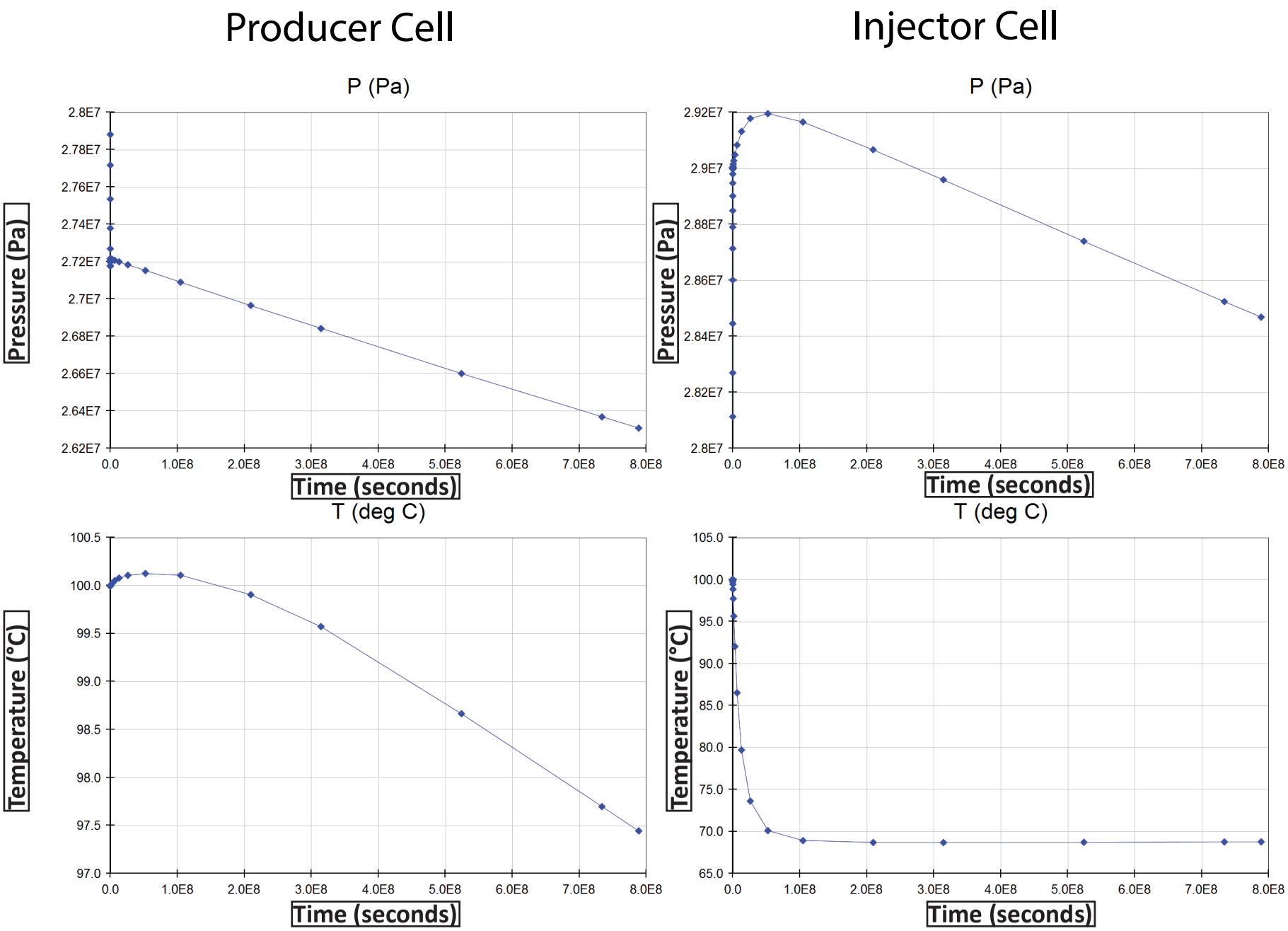

Figure A18: Producer and Injector Cell Graphs - Facies 1A Q3 High Reservoir Pressure

Temperature and pressure values as a function of time at the production and injection simulation cells for the simulation based on high reservoir pressure using cells populated with Q3 porosity and permeability values for Facies 1A.

Doublet Temperature Model - Facies 1A - Q3 Low Reservoir Pressure

Time = 1500 seconds

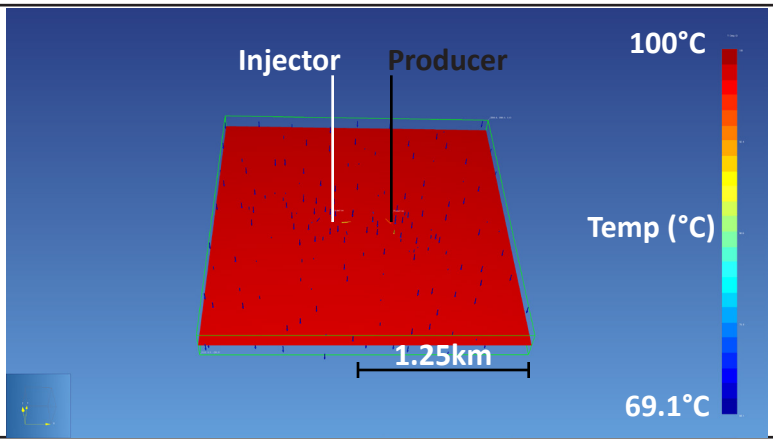

Time = ~76 days

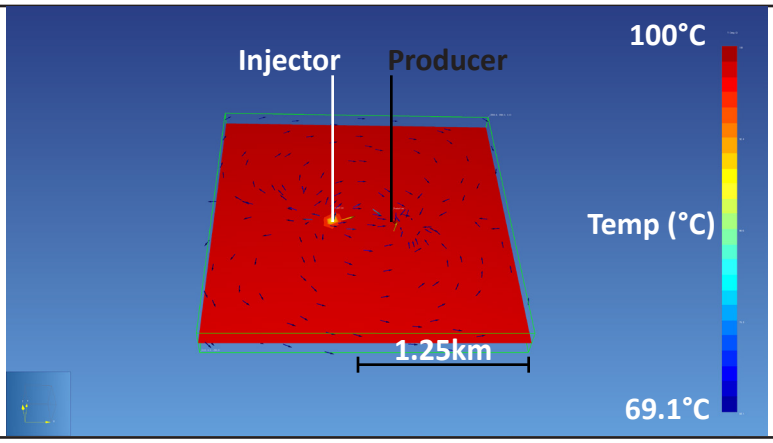

Time = ~5 years

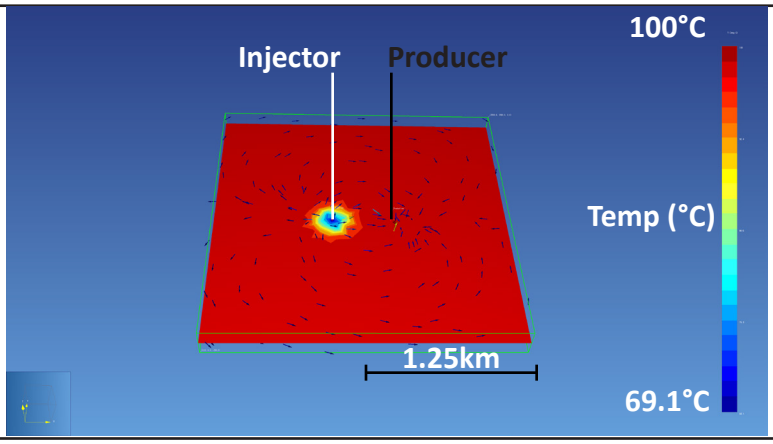

Time = 25 years

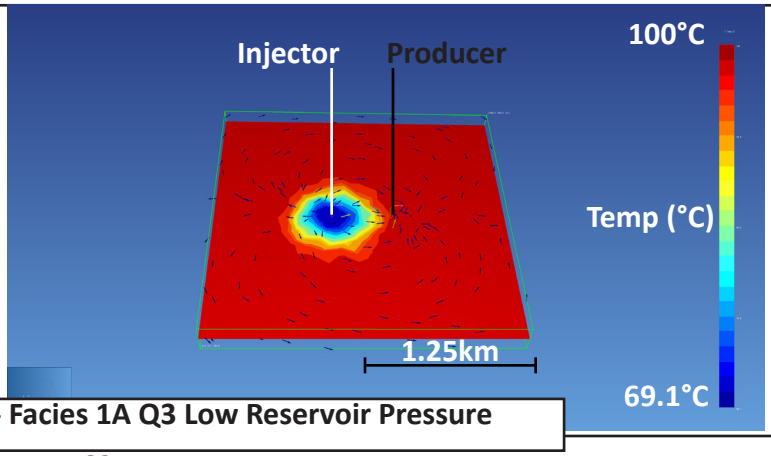

Temperature change through four timesteps in a simulation taken at low reservoir pressure using Q3 Facies 1A values for porosity and permeability.

Figure A19: Doublet Temperature Model - Facies 1A Q3 Low Reservoir Pressure

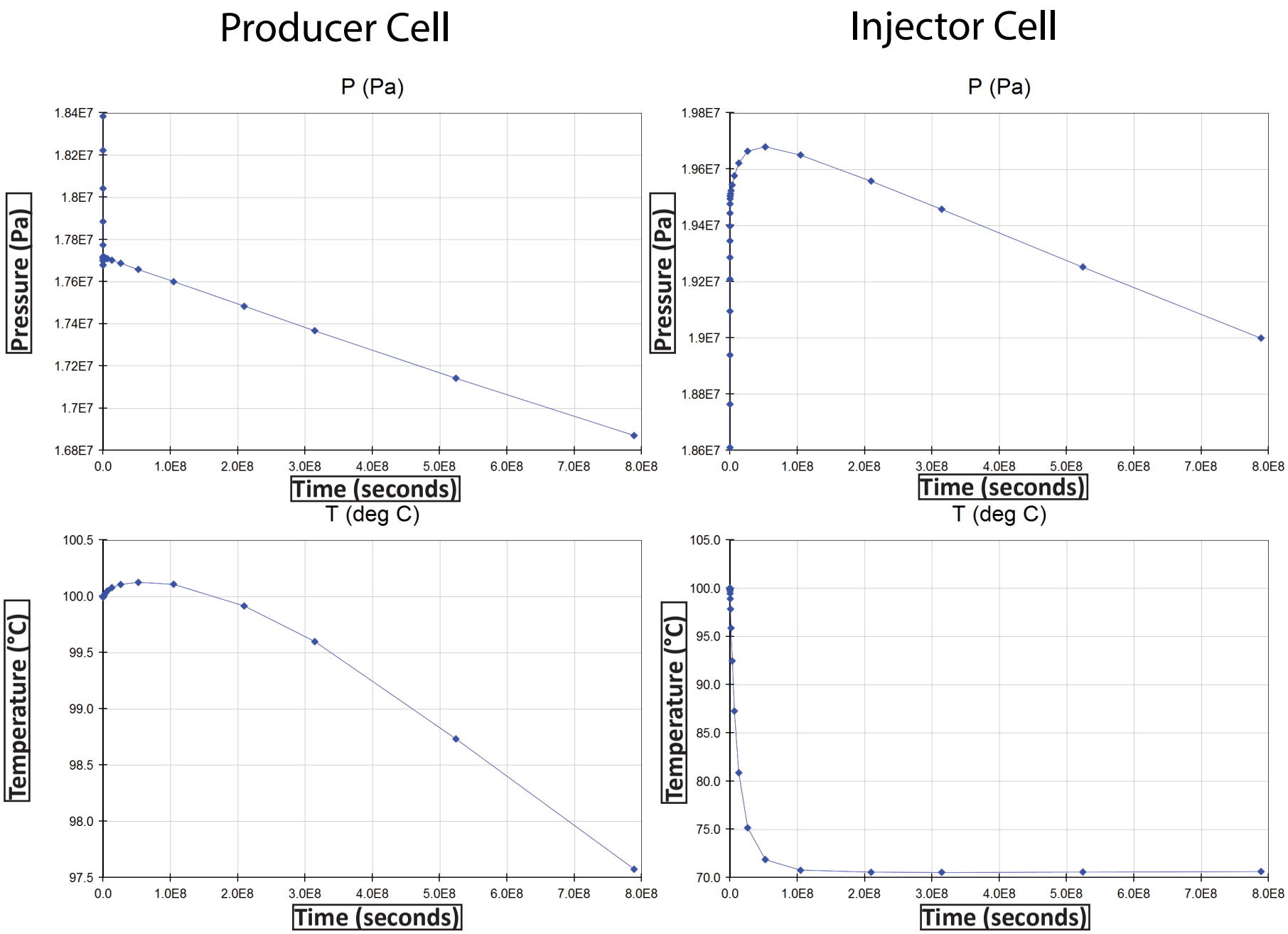

Figure A20: Producer and Injector Cell Graphs - Facies 1A Q3 Low Reservoir Pressure

Temperature and pressure values as a function of time at the production and injection simulation cells for the simulation based on low reservoir pressure using cells populated with Q3 porosity and permeability values for Facies 1A.

200kg/s Temperature Model - Facies 1A - Low Reservoir Pressure

Time = 1500 seconds

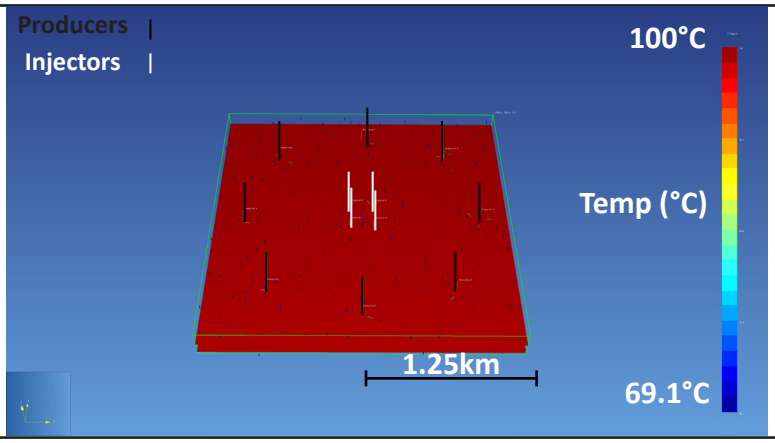

Time = ~76 days

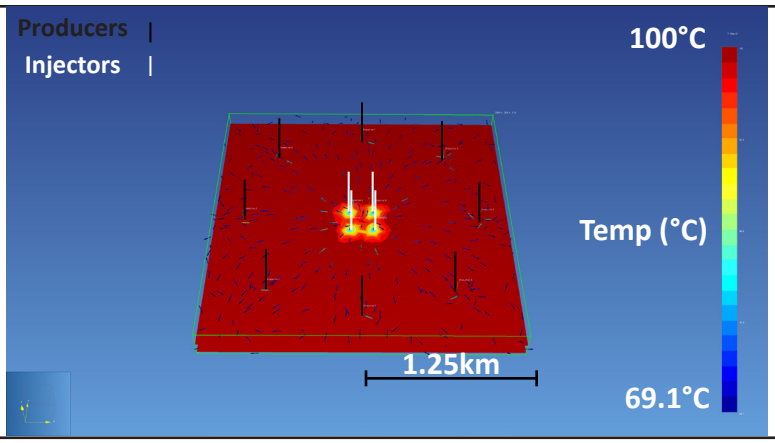

Time = ~5 years

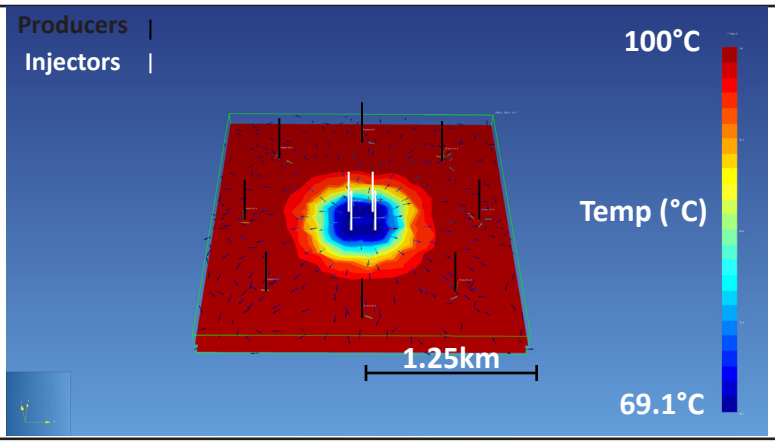

Time = 25 years

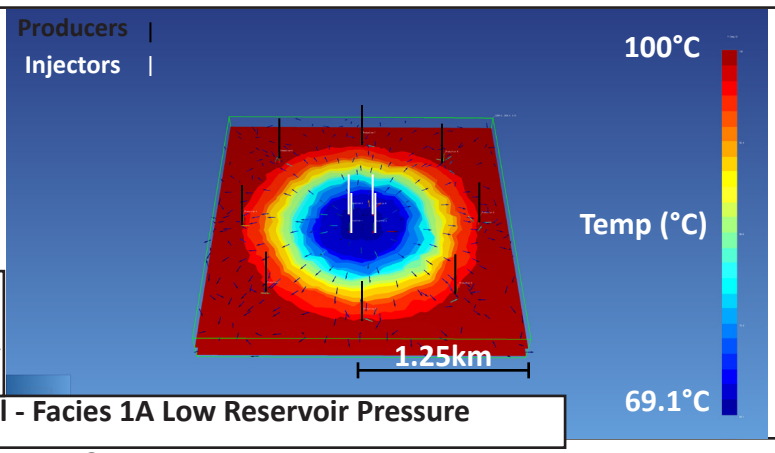

Temperature change through four timesteps in the simulation taken at low reservoir pressure using four injector and eight producer wells and mean porosity and permeability of Facies 1A.

Figure A21: 200kg/s Temperature Model - Facies 1A Low Reservoir Pressure

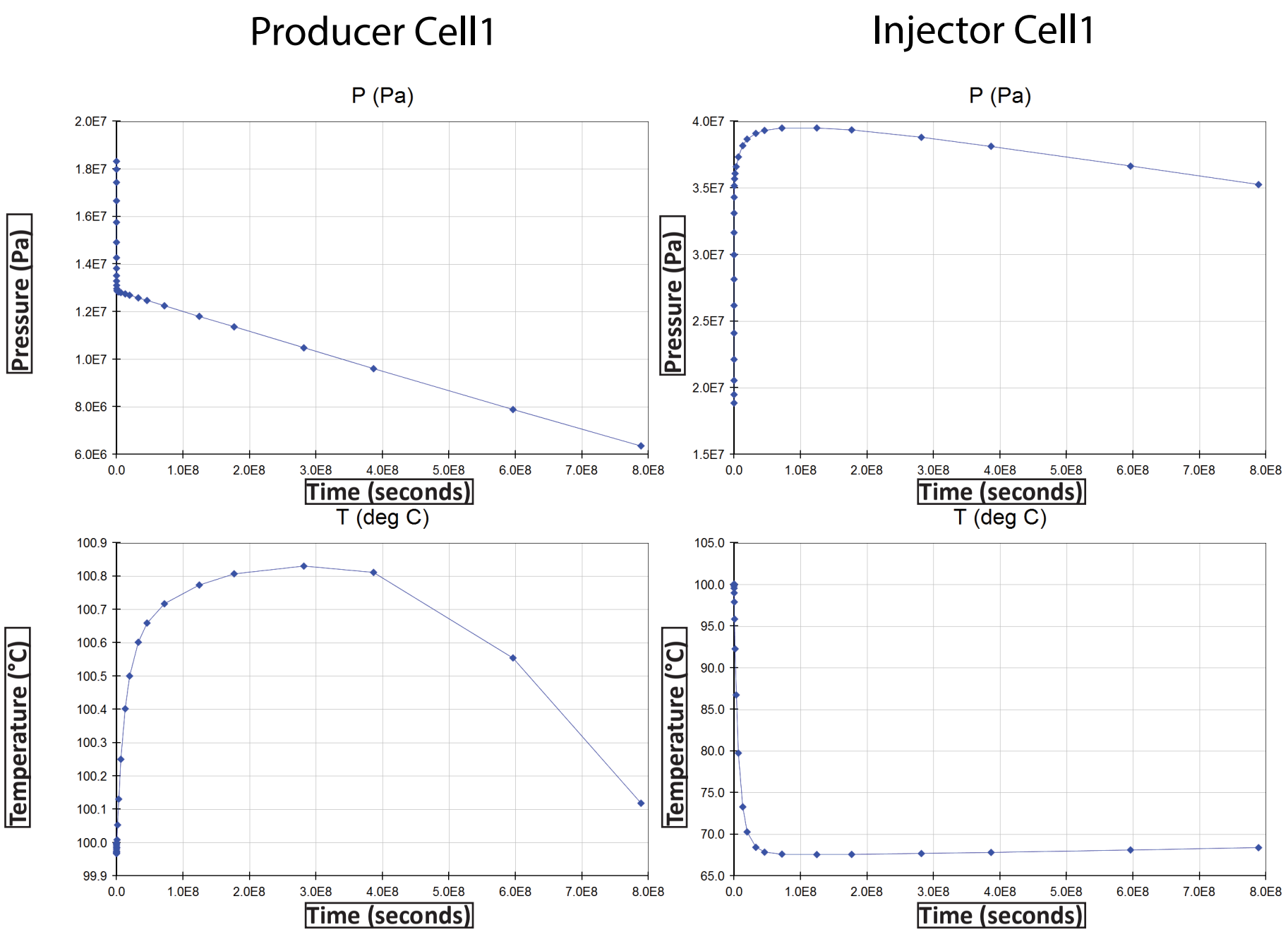

Figure A22: Producer and Injector Cell Graphs - Facies 1A 200kg/s Low Reservoir Pressure

Temperature and pressure values as a function of time at a singular production and injection simulation cell for the simulation based on an eight producer and four injector configuation at low reservoir pressure using cells populated with mean porosity and permeability values for Facies 1A.

Appendix B

CANLIN ET AL CLARKE A- 065-G/094-J-10

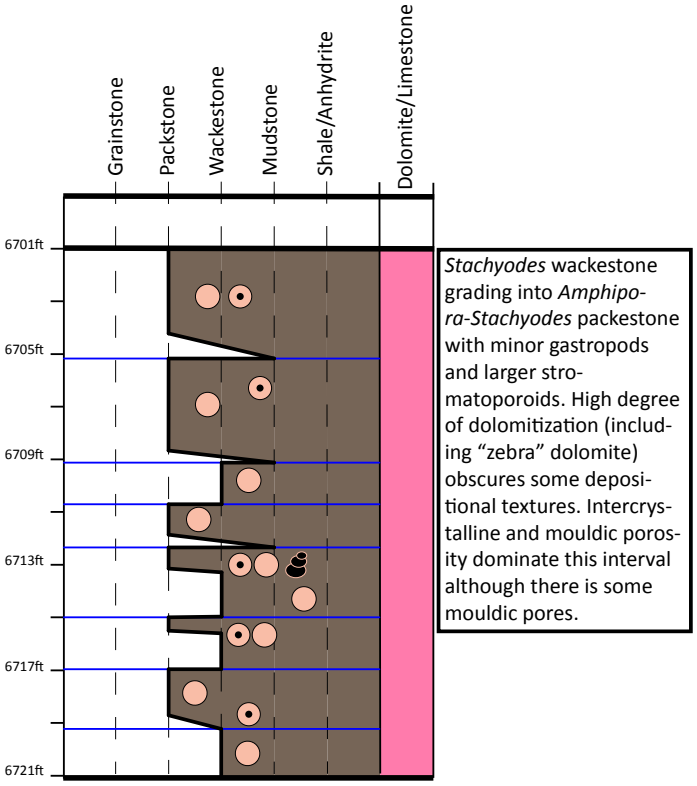

Stachyodes wackestone grading into *Amphipora-Stachyodes* packestone with minor gastropods and larger stromatoporoids. High degree of dolomitization (including "zebra" dolomite) obscures some depositional textures. Intercrystalline and mouldic porosity dominate this interval although there is some mouldic pores.

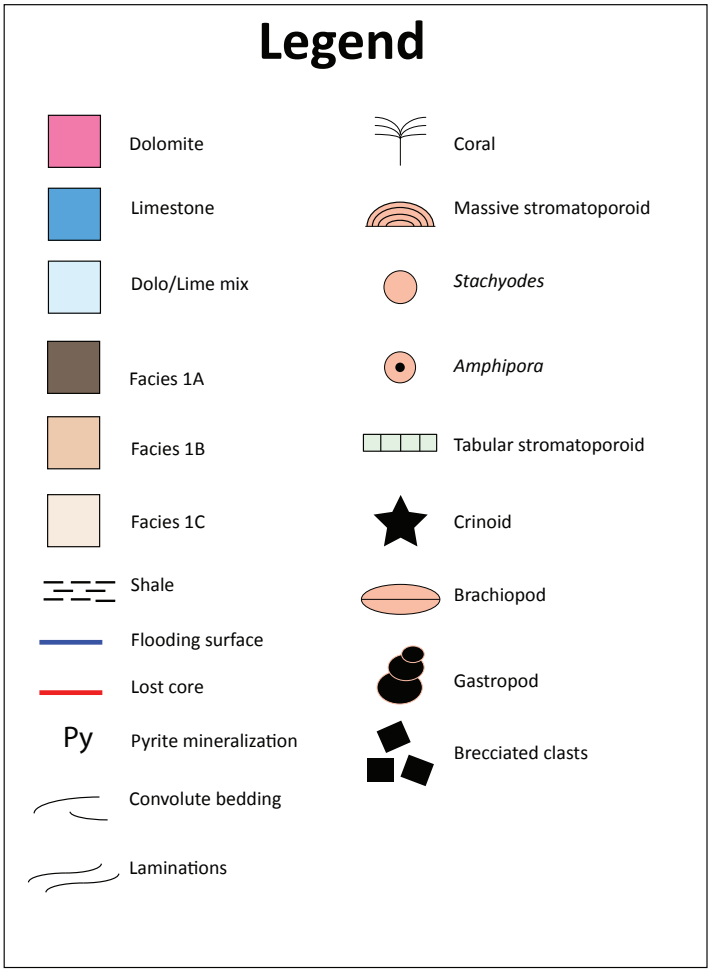

Figure B1: CANLIN ET AL CLARKE A- 061-F/094-J-10 Core Description

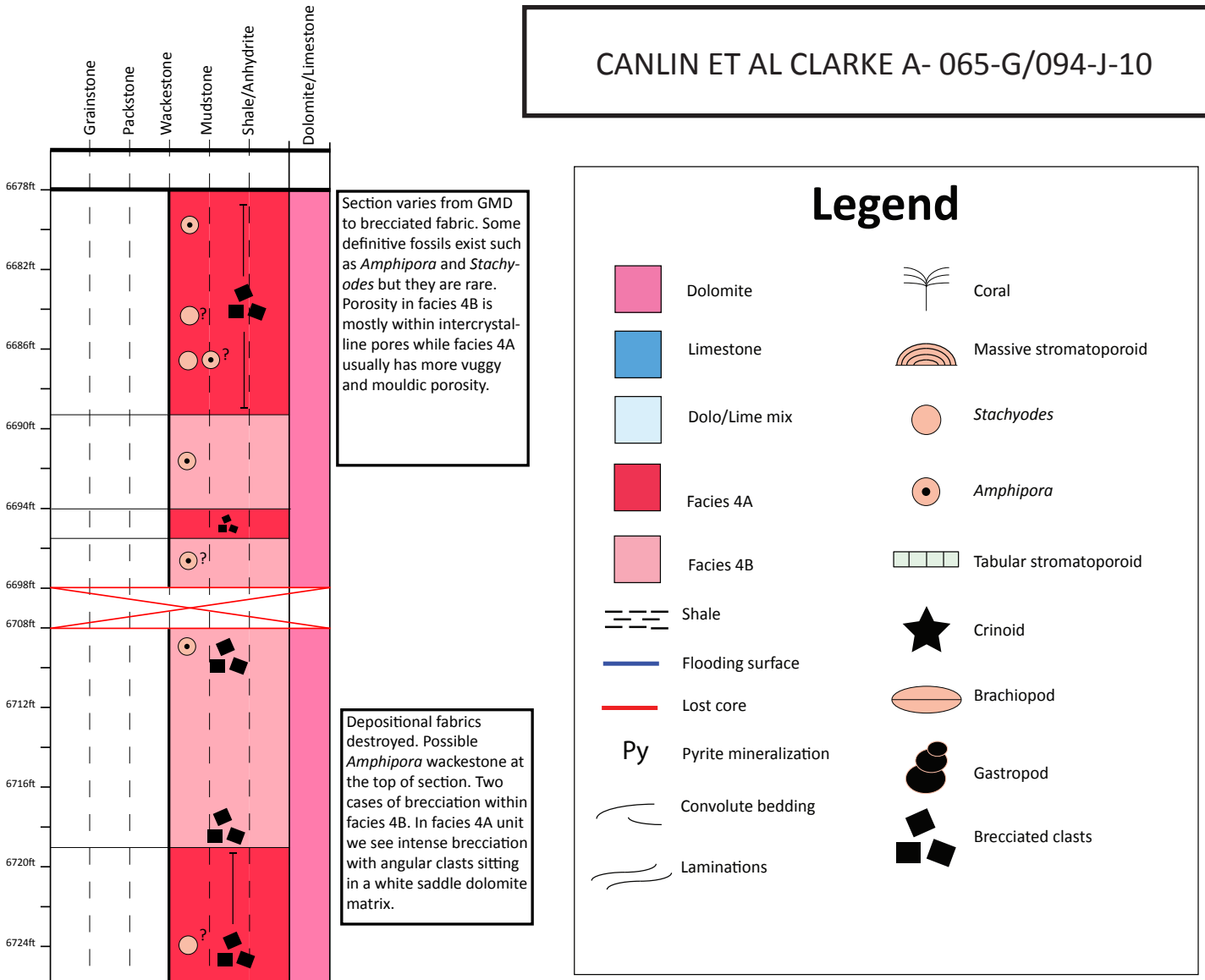

Figure B2: CANLIN ET AL CLARKE A- 065-G/094-J-10 Core Description

CANLIN CLARKE A- 083-G/094-J-10

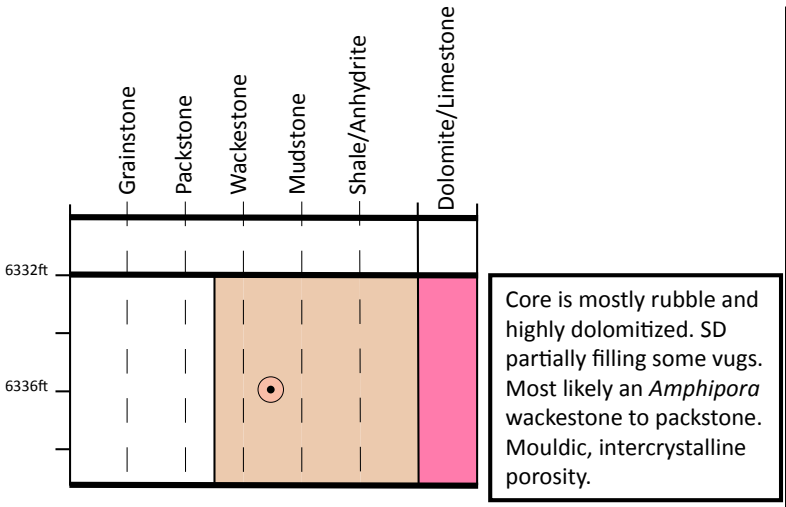

Core is mostly rubble and highly dolomitized. SD partially filling some vugs. Most likely an *Amphipora* wackestone to packstone. Mouldic, intercrystalline porosity.

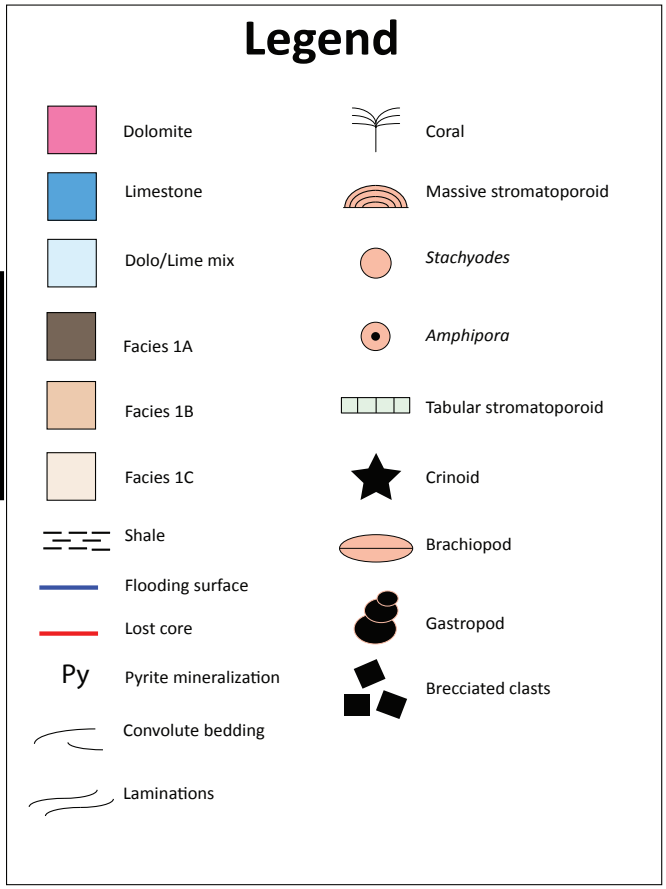

Figure B3: CANLIN CLARKE A- 083-G/094-J-10 Core Description

CANLIN CLARKE B- 010-D/094-J-16

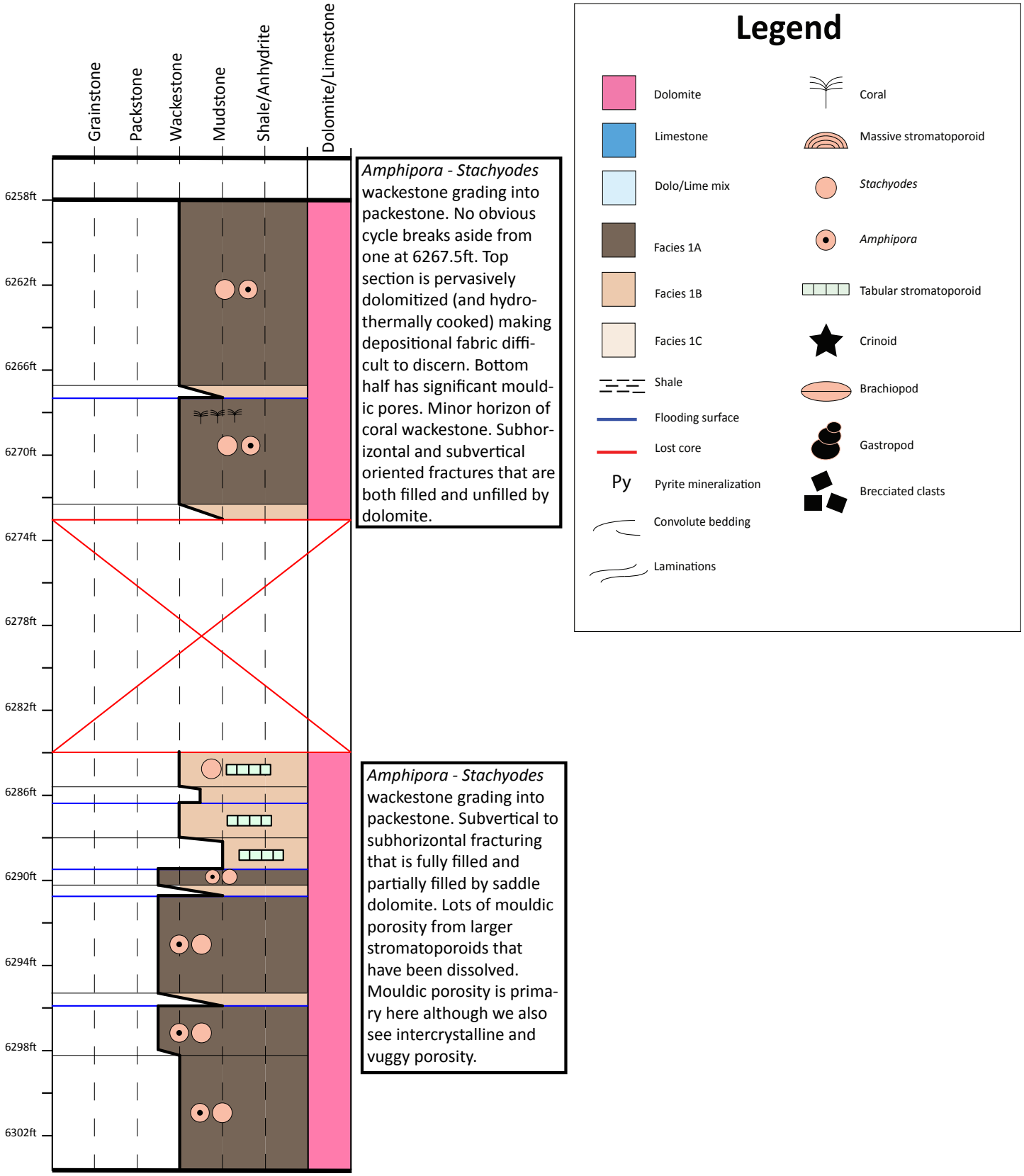

Figure B4: CANLIN CLARKE B- 010-D/094-J-16 Core Description

CANLIN ET AL HZ CLARKE B- 022-J/094-J-10

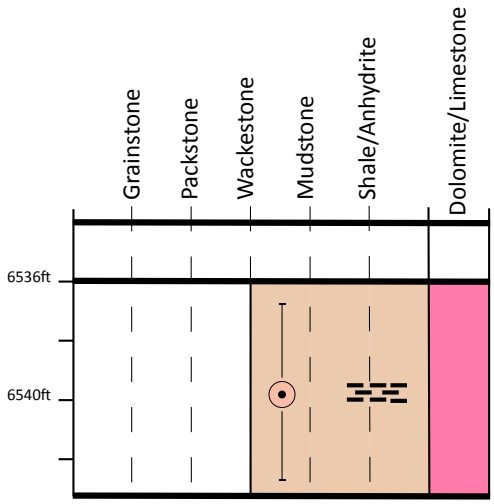

Amphipora wackstone. Highly dolomitized with pervasive gray matrix dolomite. Some minor larger stromatoporoid bioclasts. Chaotic texture near shale horizon.

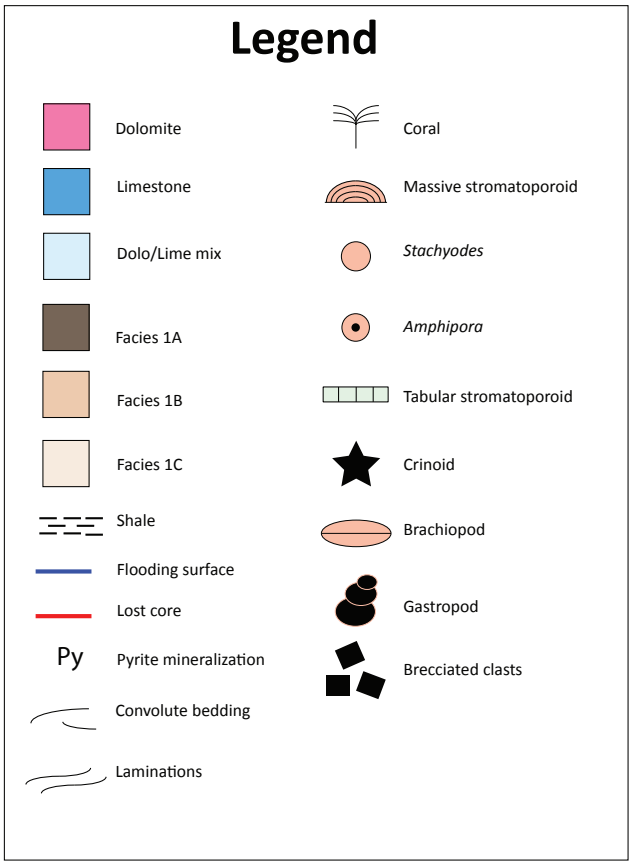

Figure B5: CANLIN ET AL HZ CLARKE B- 022-J/094-J-10 Core Description

CANLIN ET AL CLARKE B- 070-I/094-J-10

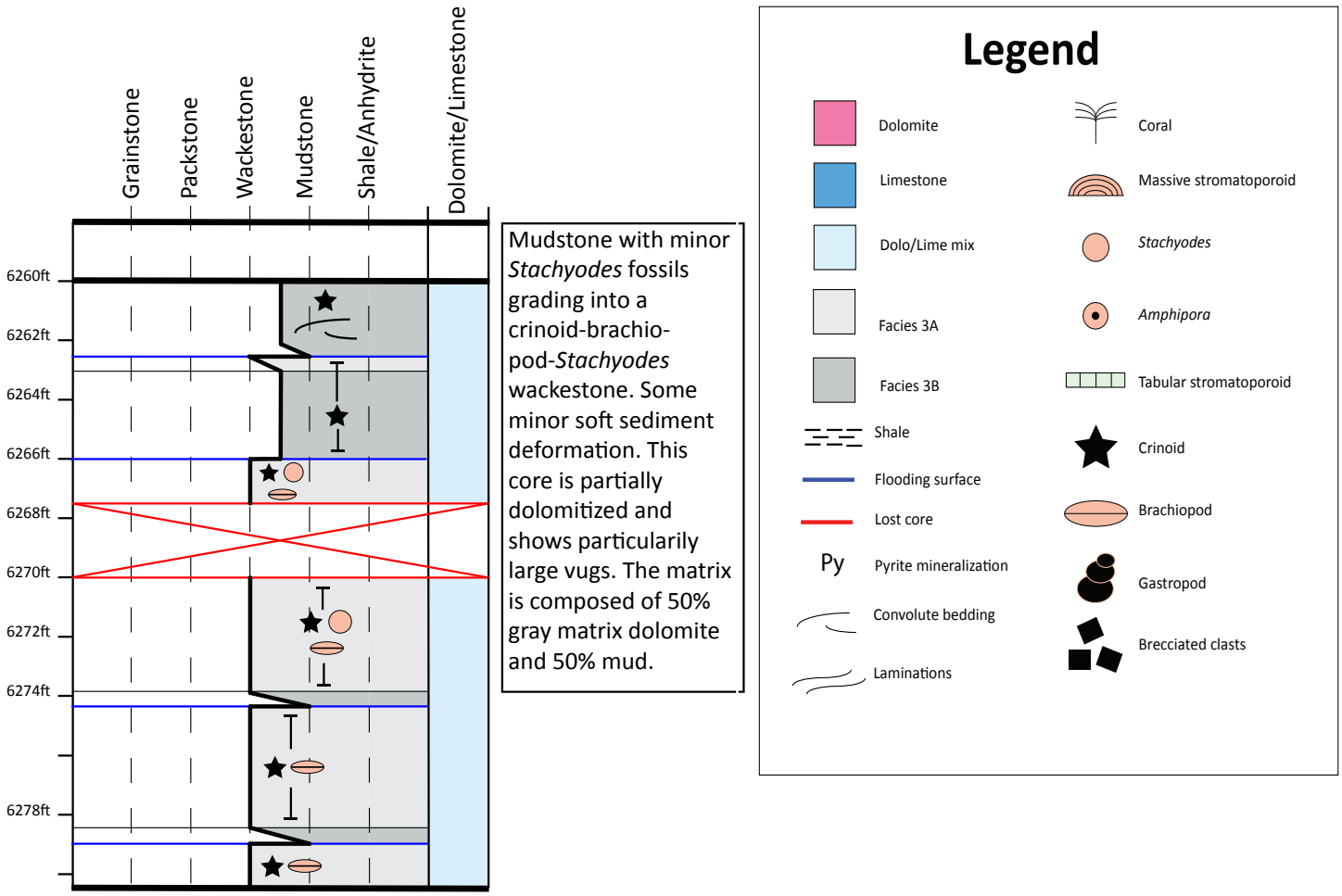

Figure B6: CANLIN ET AL CLARKE B- 070-I/094-J-10 Core Description

CANLIN CLARKE B- 072-L/094-J-09

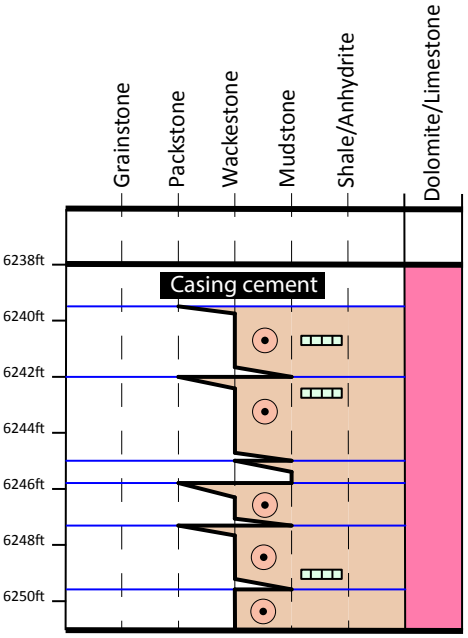

Section is dominantly composed of GMD with significant intercrystalline porosity and minor moul-dic pores from dissolution of small *Amphipora*. We have *Amphipora* mud-stones grading into *Amphipora* packstones with minor amounts of tabular stromatoporoids.

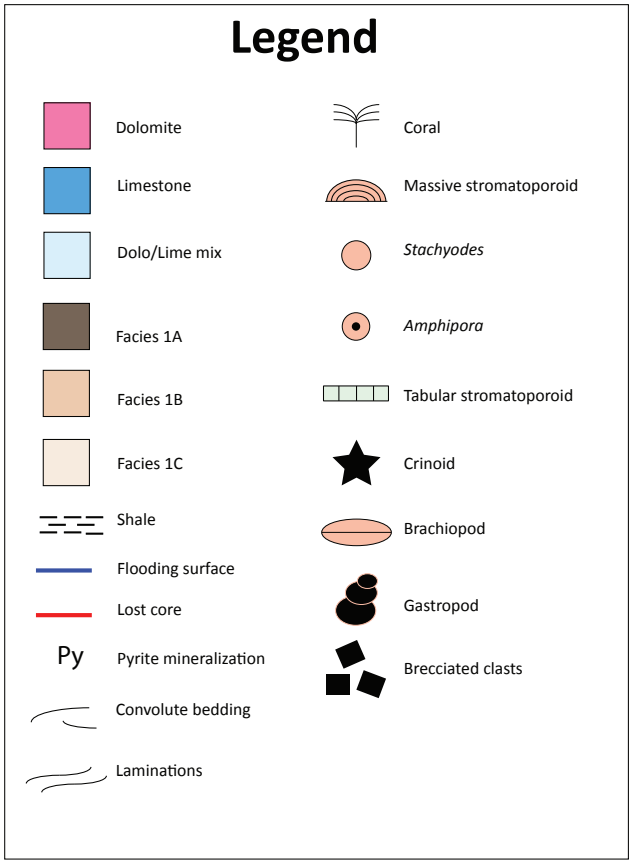

Figure B7: CANLIN CLARKE B- 072-L/094-J-09 Core Description

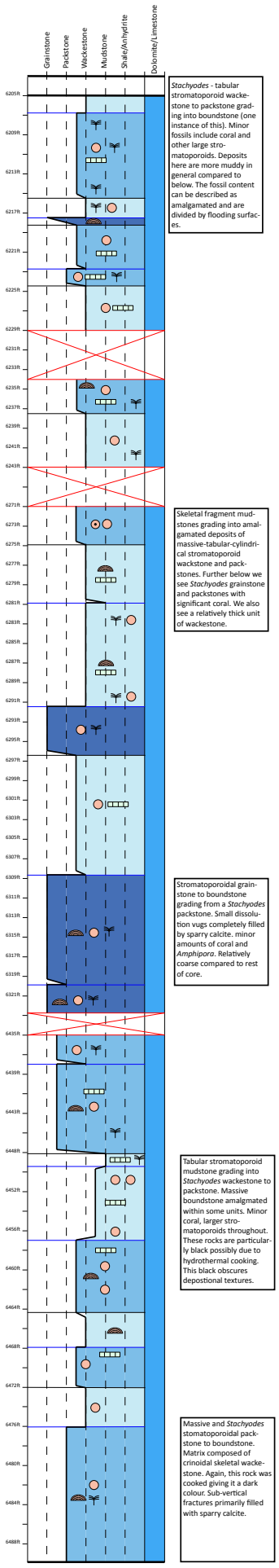

CANLIN CLARKE B- 078-J/094-J-09

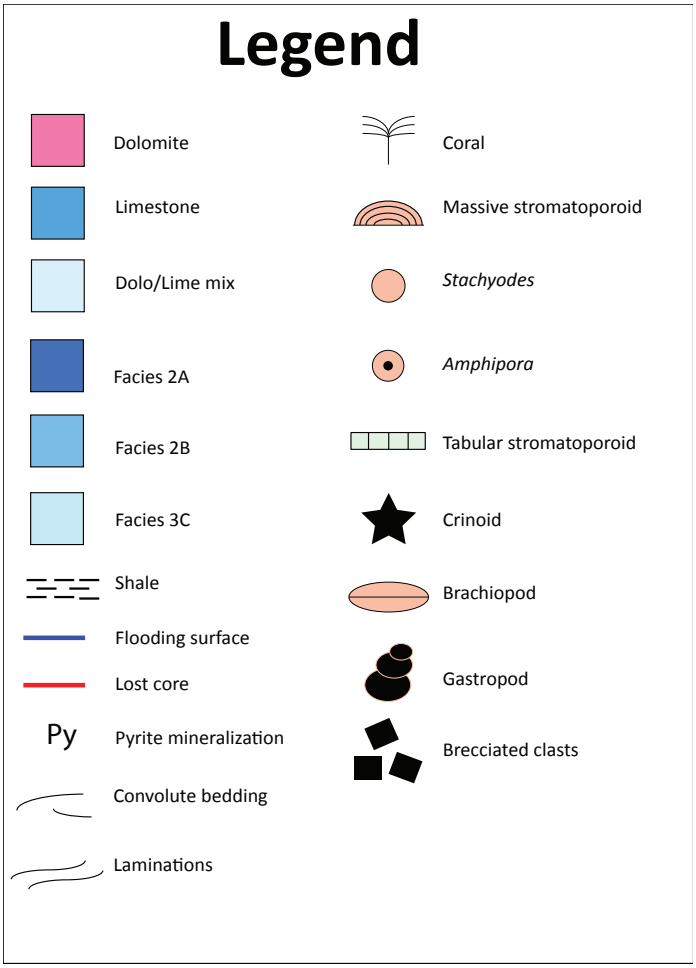

Figure B8: CANLIN CLARKE B- 078-J/094-J-09 Core Description

CANLIN CLARKE B- A018-D/094-J-09

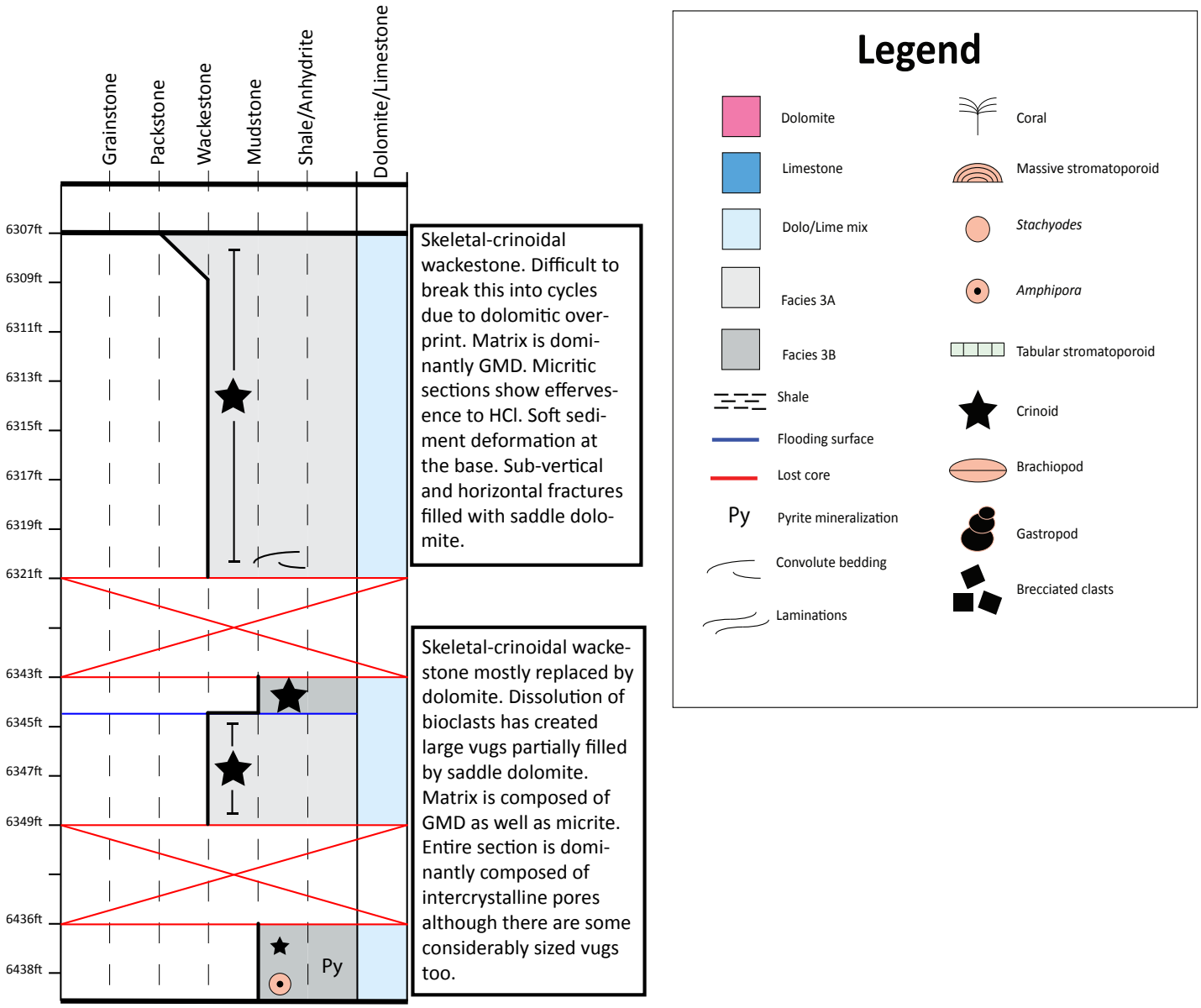

Figure B9: CANLIN CLARKE B- A018-D/094-J-09 Core Description

CANLIN CLARKE C- 047-J/094-J-10

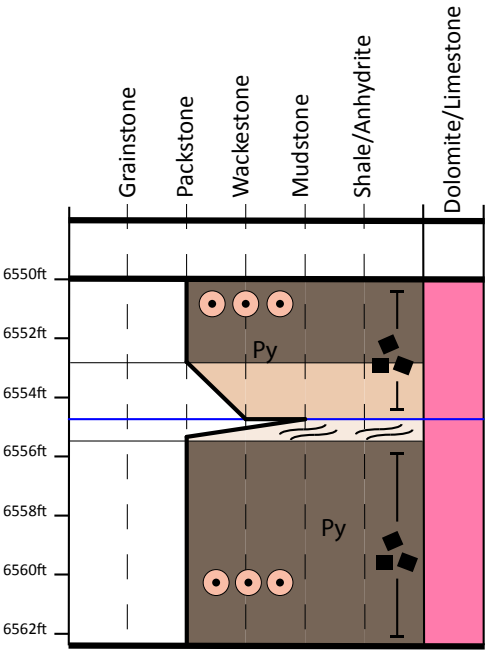

Core has a fairly high degree of dolomitization and may be better classified as breccia of Facies Zone 4. Majority of bottom section is composed of massive saddle dolomite with large fractures. Most likely an *Amphipora* packstone/wackestone thats grading into laminated mudstone. This section shows vuggy and intercrystalline porosity.

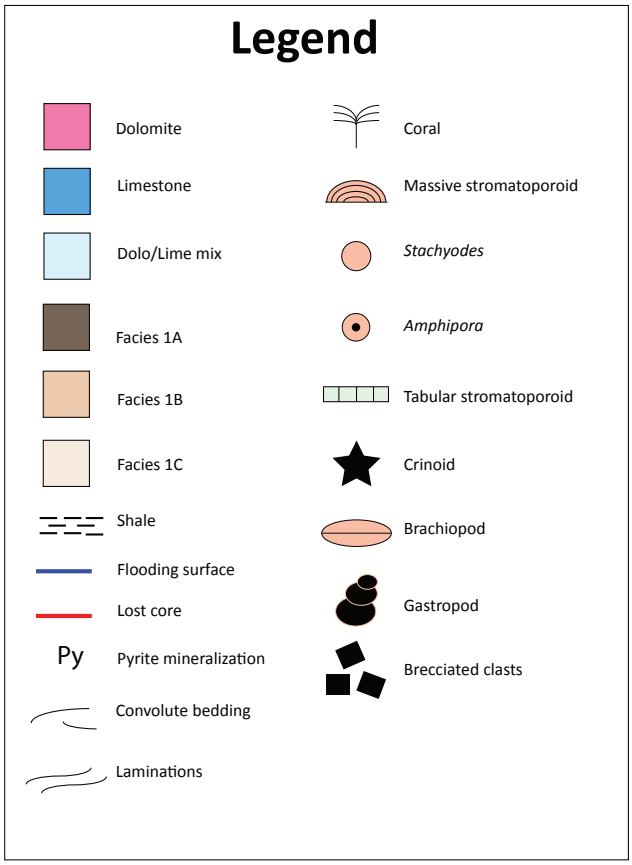

Figure B10: CANLIN CLARKE C- 047-J/094-J-10 Core Description

CANLIN CLARKE C- 050-K/094-J-09

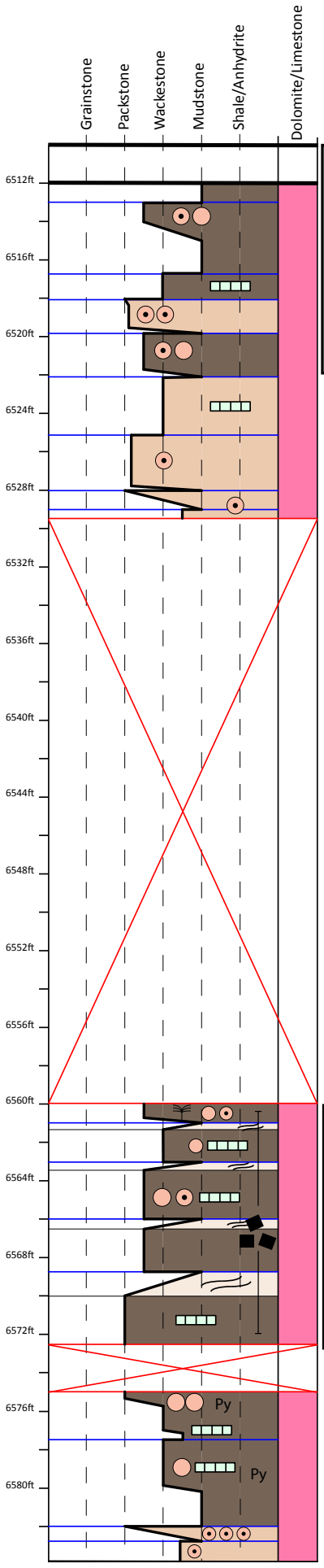

Mudstone grading into *Amphipora - Stachyodes* wackestone to packstone. Some intervals are strictly *Amphipora*. Sub horizontal fracturing infilled by coarse saddle dolomite. Porosity in this interval is dominantly intercrystalline with few mouldic and vuggy pores.

This section has a very high degree of dolomitization and depositional character is difficult to discern. This interval may be more realistically referred to as breccia of facies 4A. Potentially we see *Amphipora - Stachyodes* packstones and wackestones grading into mudstone.

Very similar to what we see just above except for the lack of brown mudstone. Dolomitization of fine grained units (such as a dark mudstone vs a brown laminated mudstone) leaves them difficult to identify. Based on this, brown mudstones in this interval could potentially be dark mudstone/wackestones.

Legend

- Dolomite
- Limestone
- Dolo/Lime mix
- Facies 1A
- Facies 1B
- Facies 1C
- Shale
- Flooding surface
- Lost core
- Py — Pyrite mineralization
- Convolute bedding
- Laminations
- Coral
- Massive stromatoporoid
- *Stachyodes*
- *Amphipora*
- Tabular stromatoporoid
- Crinoid
- Brachiopod
- Gastropod
- Brecciated clasts

Figure B11: CANLIN CLARKE C- 050-K/094-J-09 Core Description

CANLIN ET AL CLARKE C- 056-L/094-J-09

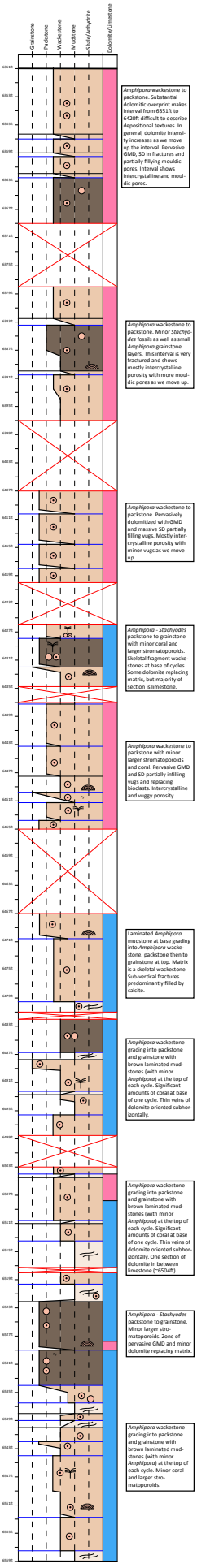

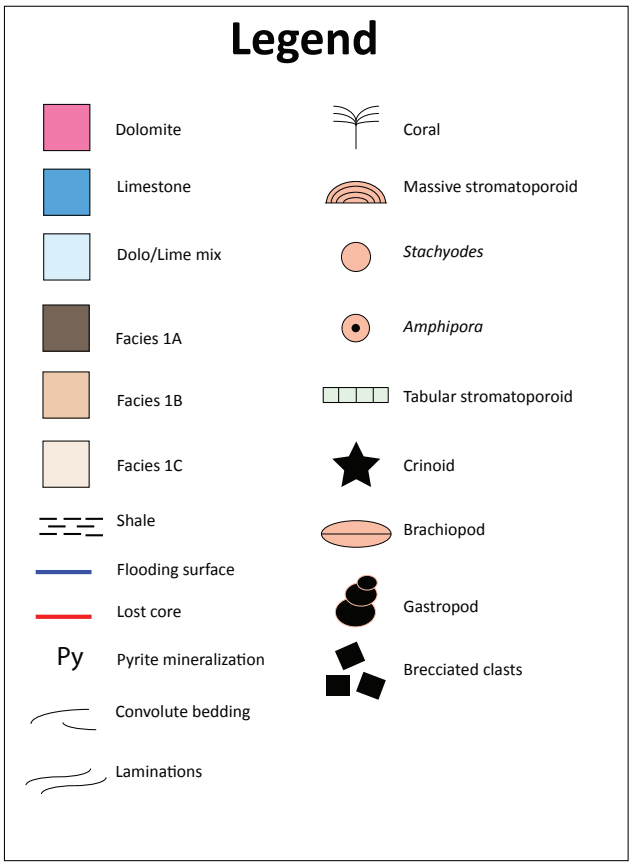

Figure B12: CANLIN ET AL CLARKE C- 056-L/094-J-09 Core Description

GULF STATES IMP CLARKE LAKE C- 064-I/094-J-10

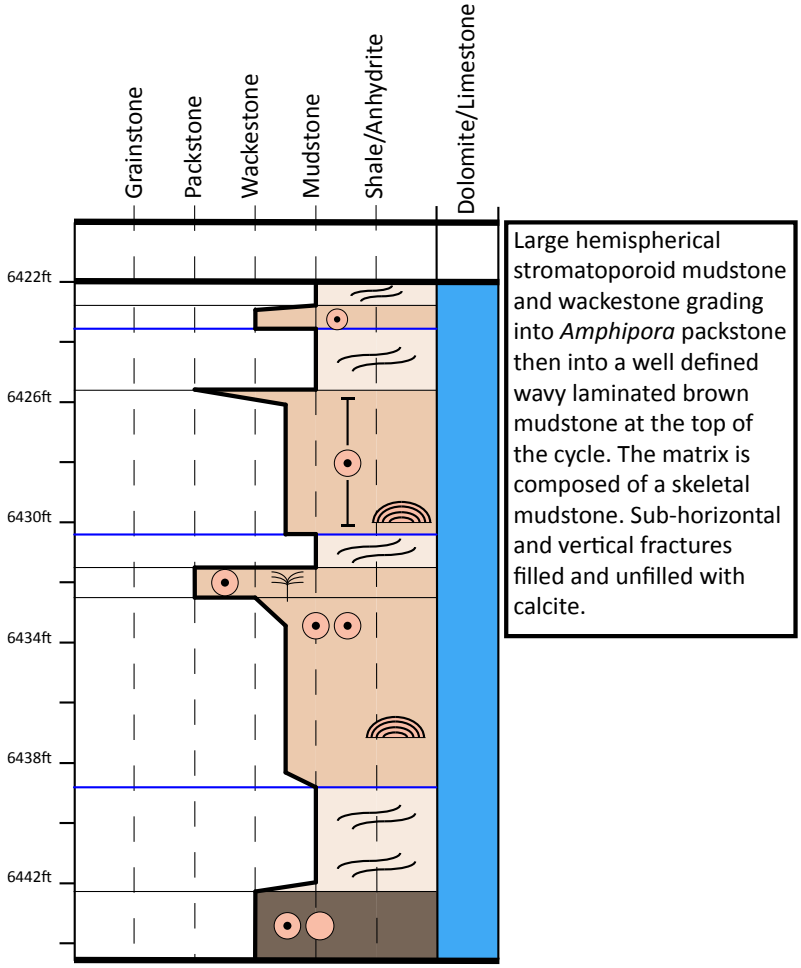

Large hemispherical stromatoporoid mudstone and wackestone grading into *Amphipora* packstone then into a well defined wavy laminated brown mudstone at the top of the cycle. The matrix is composed of a skeletal mudstone. Sub-horizontal and vertical fractures filled and unfilled with calcite.

Legend

- Dolomite
- Limestone
- Dolo/Lime mix
- Facies 1A
- Facies 1B
- Facies 1C
- Shale
- Flooding surface
- Lost core
- Py — Pyrite mineralization
- Convolute bedding
- Laminations
- Coral
- Massive stromatoporoid
- *Stachyodes*
- *Amphipora*
- Tabular stromatoporoid
- Crinoid
- Brachiopod
- Gastropod
- Brecciated clasts

Figure B13: GULF STATES IMP CLARKE LAKE C- 064-I/094-J-10 Core Description

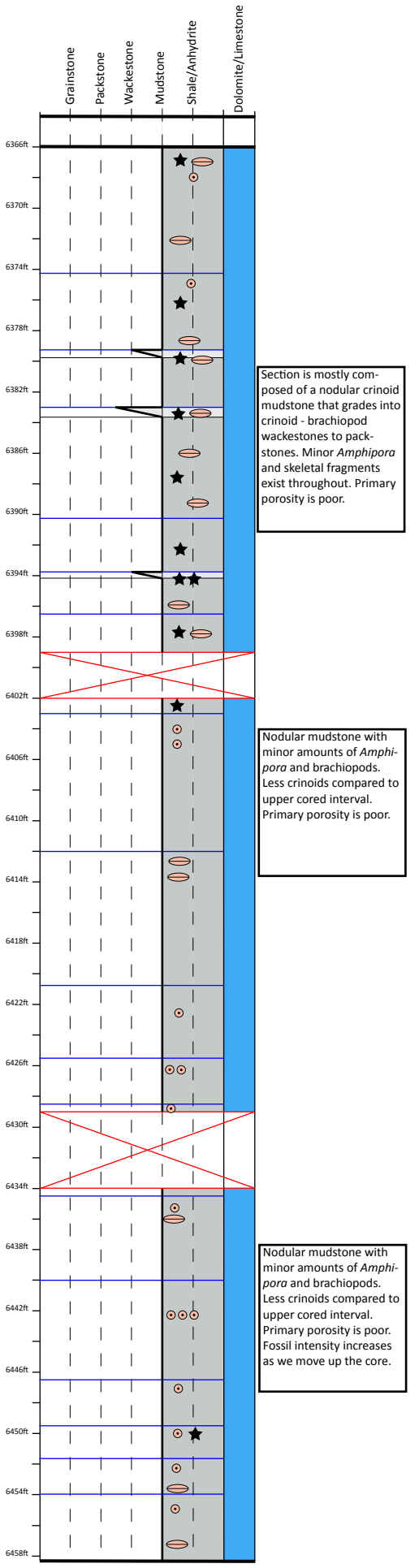

BA SHELL KLUA C- 070-E/094-J-10

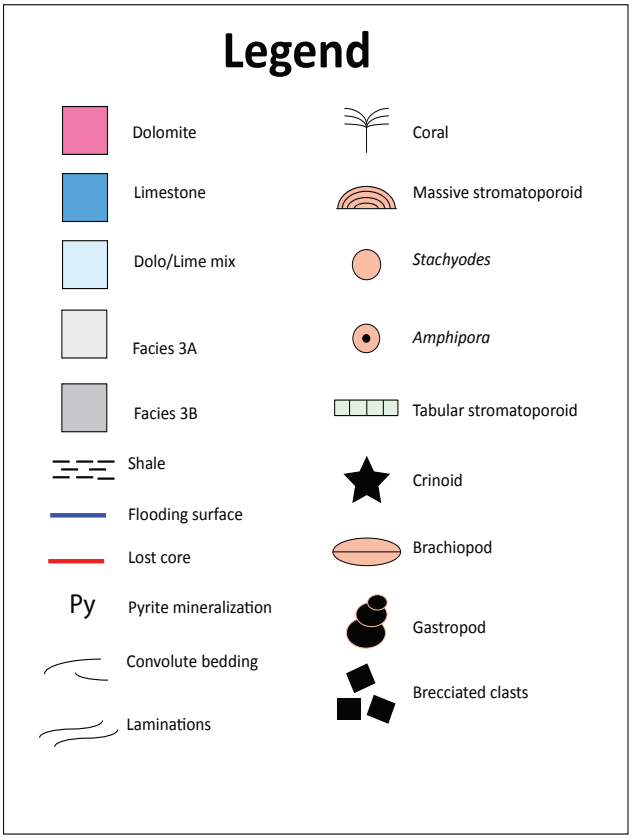

Figure B14: BA SHELL KLUA C- 070-E/094-J-10 Core Description

CANLIN ET AL CLARKE C- 078-I/094-J-10

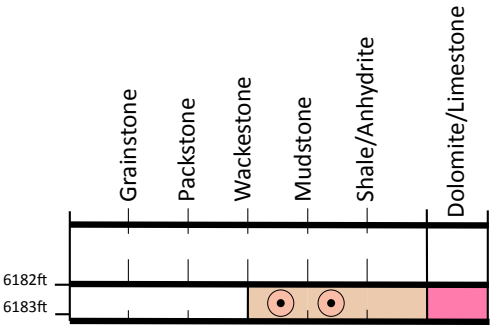

Highly fractured rubble. Possibly an *Amphipora* wackestone to packstone although a high degree of dolomitization makes descriptions difficult.

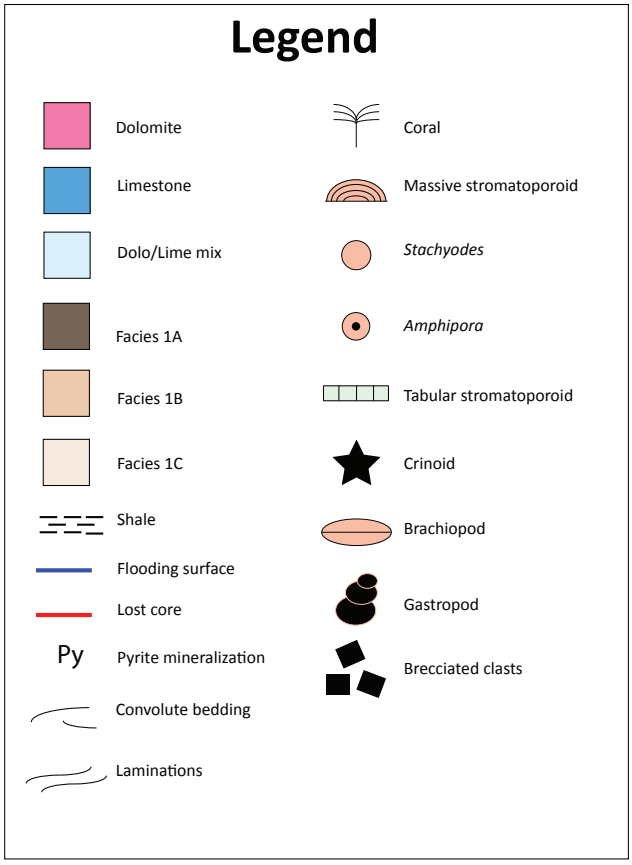

Figure B15: CANLIN ET AL CLARKE C- 078-I/094-J-10 Core Description

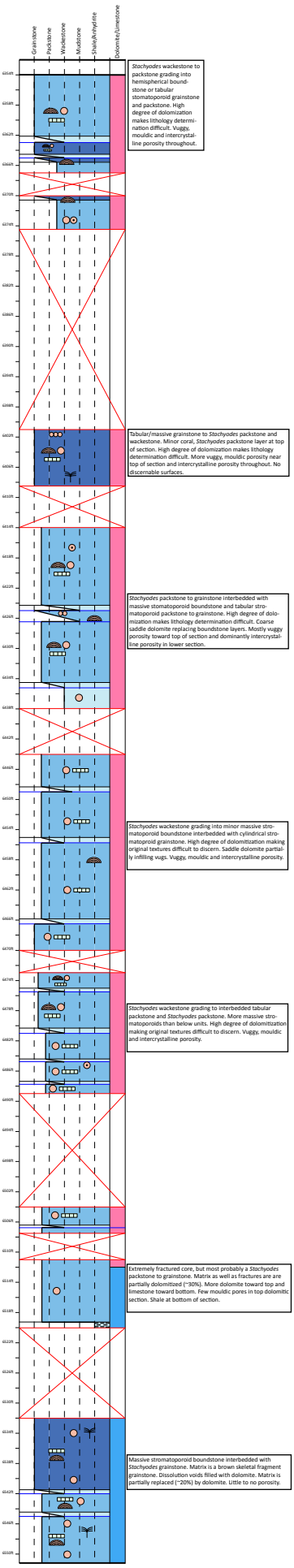

CANLIN CLARKE C- 094-L/094-J-09

Legend

- Dolomite
- Limestone
- Dolo/Lime mix
- Facies 2A
- Facies 2B
- Facies 3C
- Shale
- Flooding surface
- Lost core
- Py — Pyrite mineralization
- Convolute bedding
- Laminations
- Coral
- Massive stromatoporoid
- *Stachyodes*
- *Amphipora*
- Tabular stromatoporoid
- Crinoid
- Brachiopod
- Gastropod
- Brecciated clasts

Figure B16: CANLIN CLARKE C- 094-L/094-J-09 Core Description

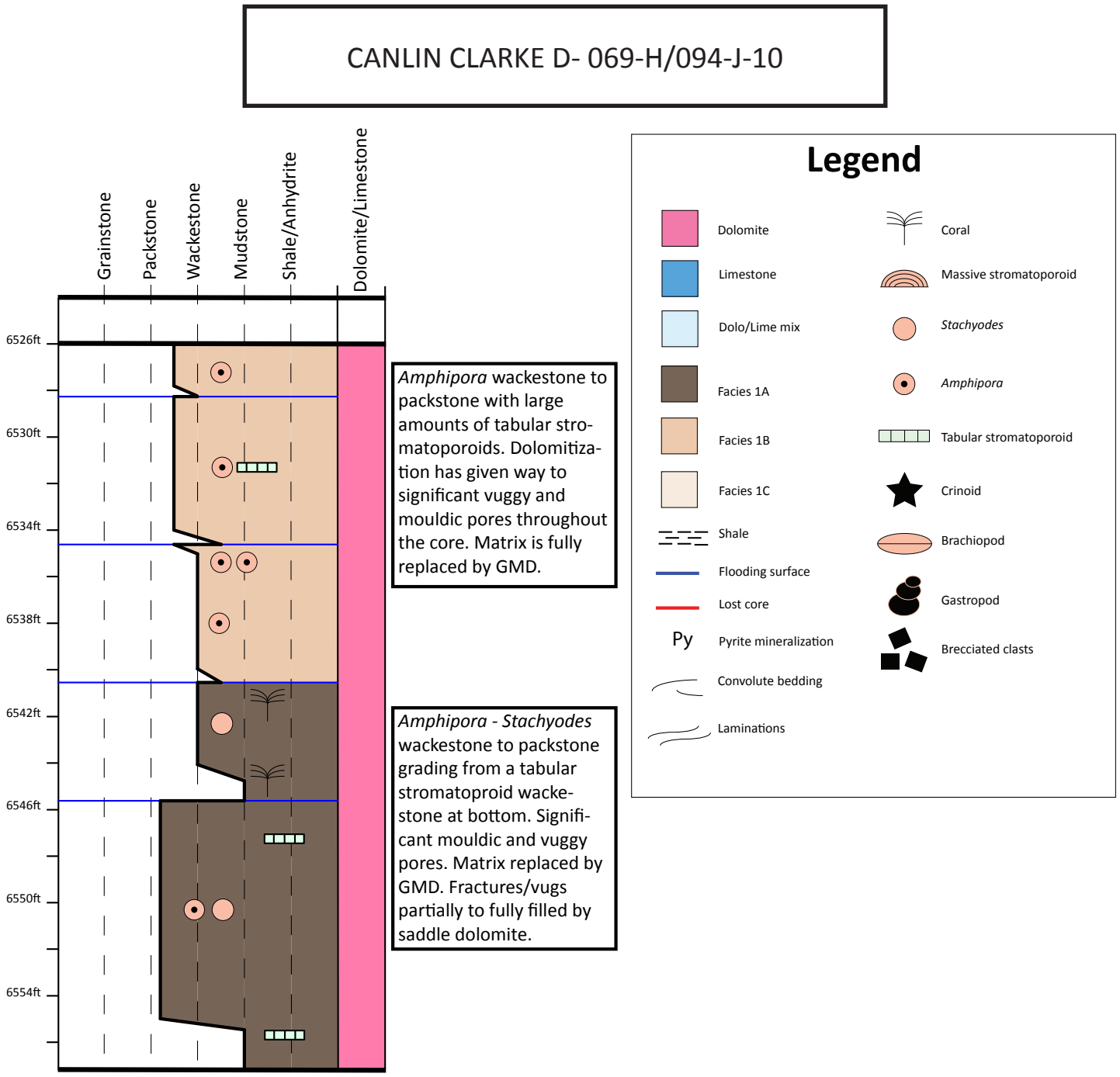

Figure B17: CANLIN CLARKE D- 069-H/094-J-10 Core Description

CANLIN CLARKE D- 072-G/094-J-10

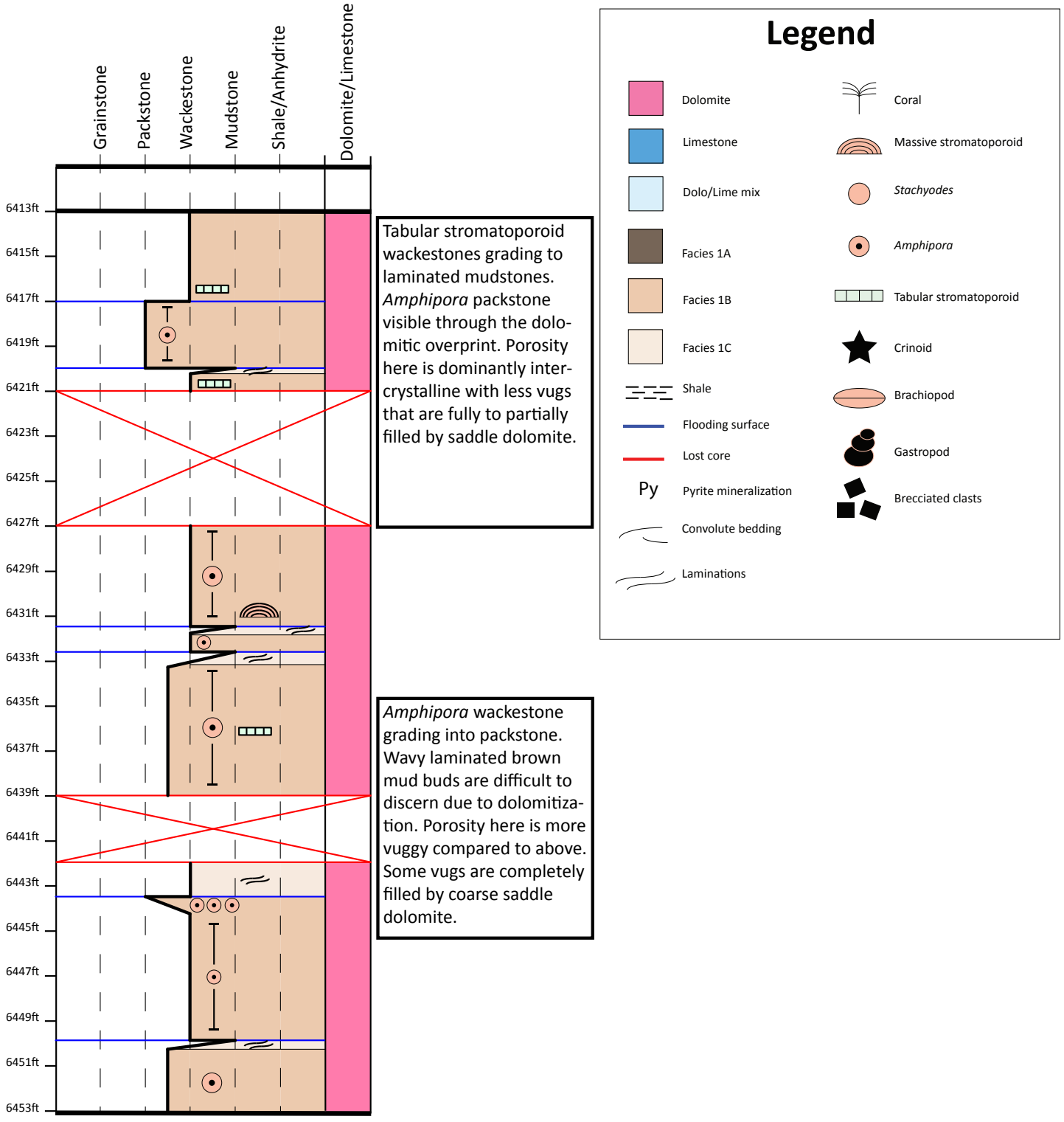

Figure B18: CANLIN CLARKE D- 072-G/094-J-10 Core Description

CHEVRON MILO D- 079-F/094-J-10

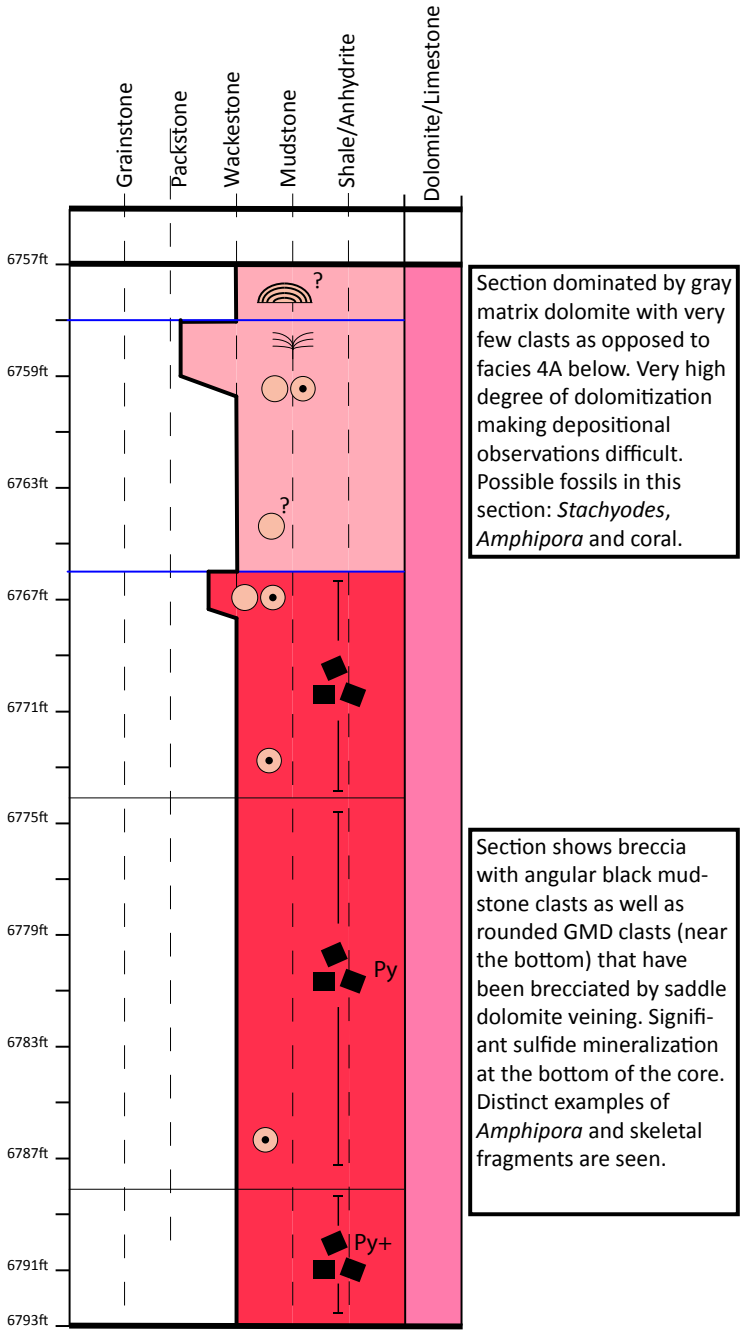

Section dominated by gray matrix dolomite with very few clasts as opposed to facies 4A below. Very high degree of dolomitization making depositional observations difficult. Possible fossils in this section: *Stachyodes*, *Amphipora* and coral.

Section shows breccia with angular black mudstone clasts as well as rounded GMD clasts (near the bottom) that have been brecciated by saddle dolomite veining. Significant sulfide mineralization at the bottom of the core. Distinct examples of *Amphipora* and skeletal fragments are seen.

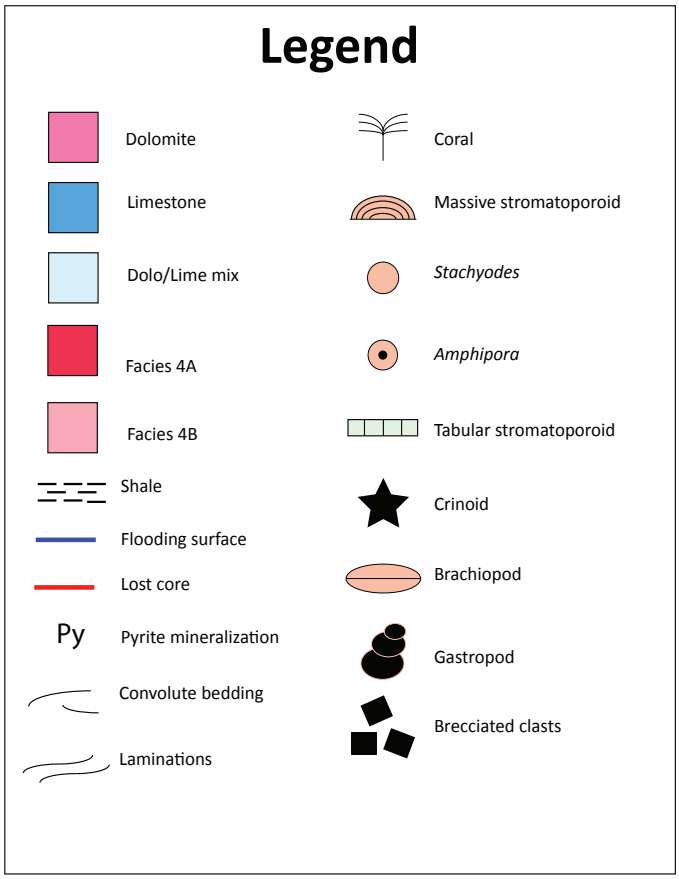

Figure B19: CHEVRON MILO D- 079-F/094-J-10 Core Description

CANLIN CLARKE D- 091-L/094-J-09

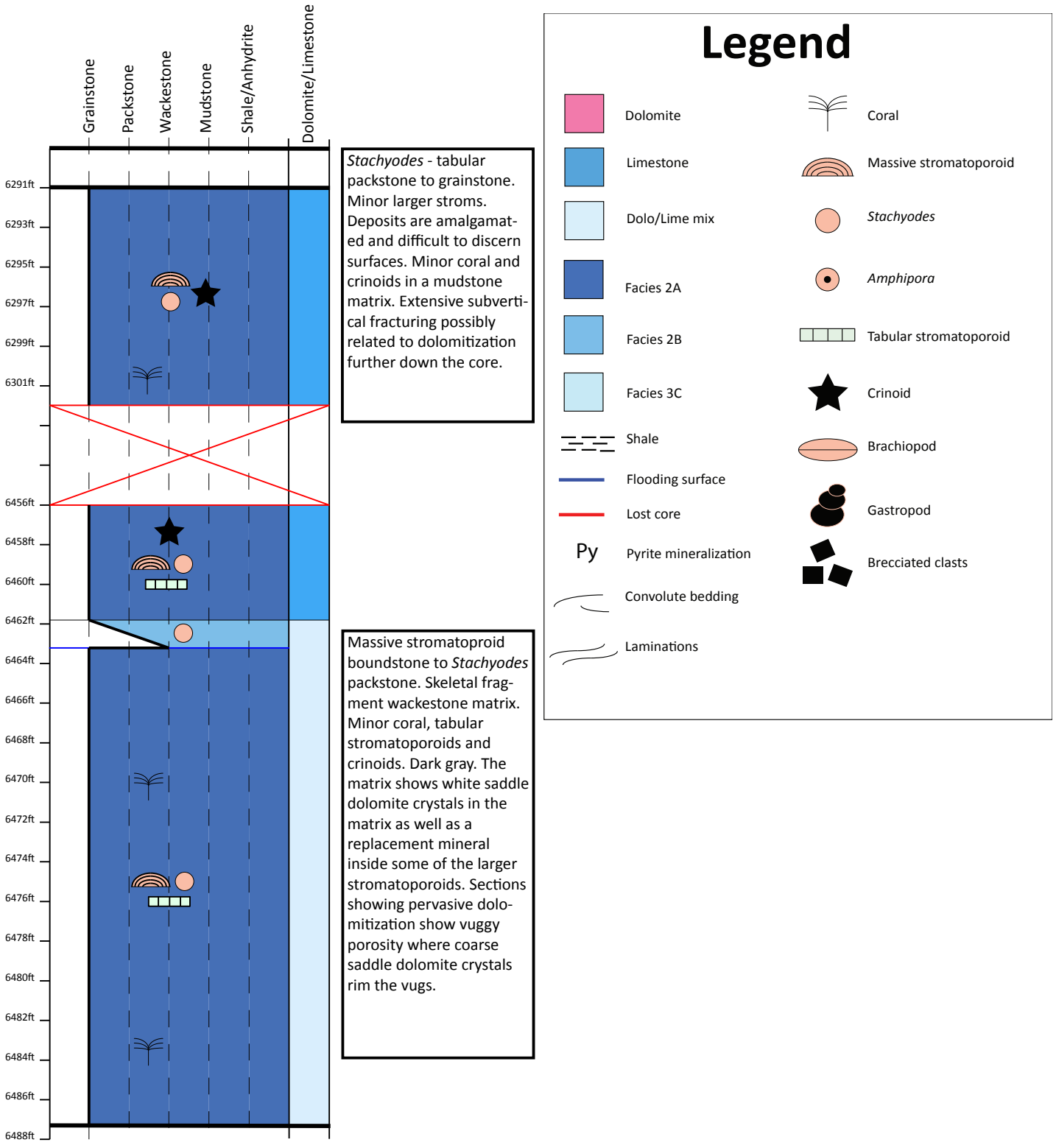

Figure B20: CANLIN CLARKE D- 091-L/094-J-09 Core Description

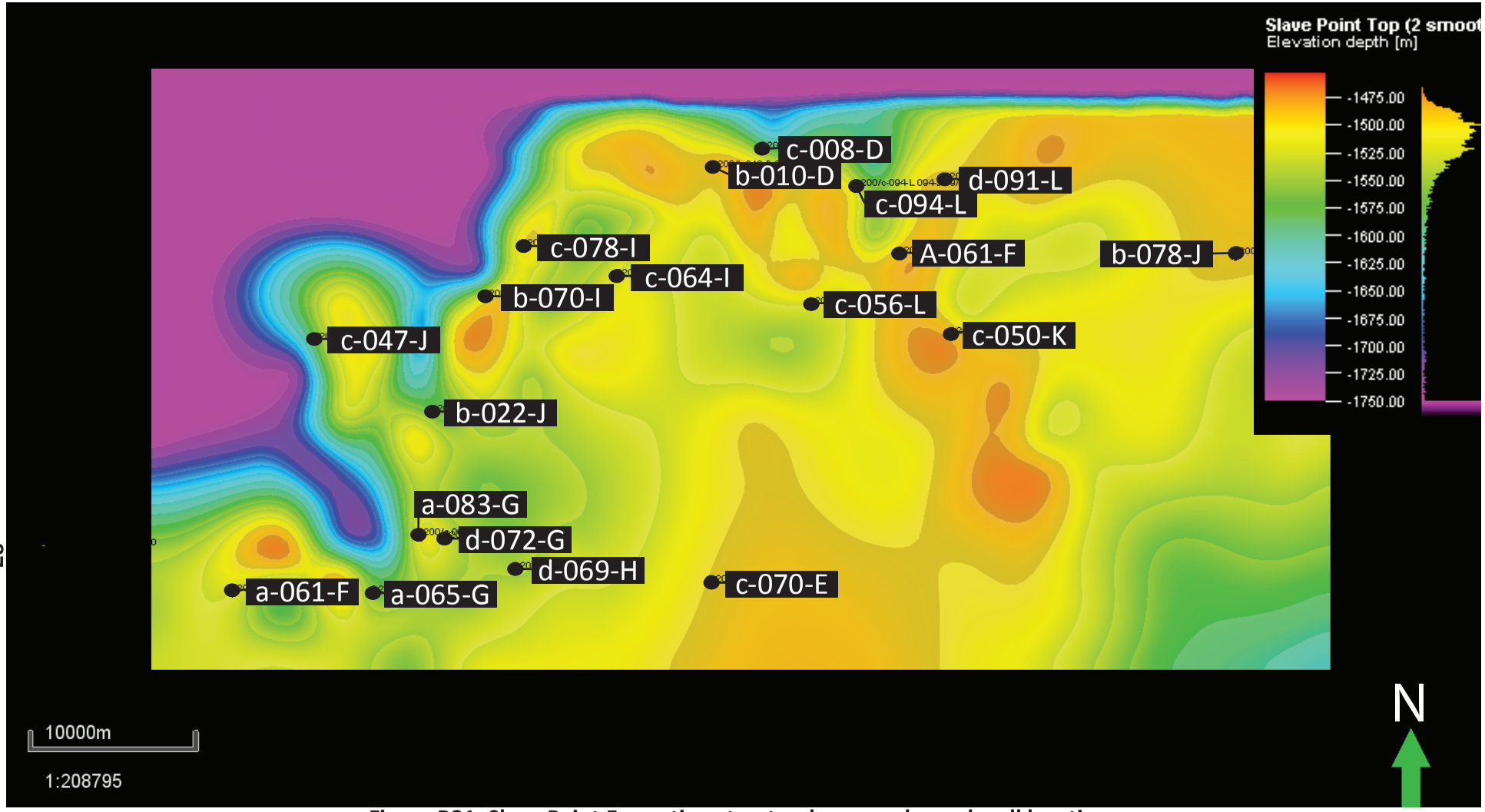

Figure B21: Slave Point Formation structural map and cored well locations

Location of cored wells plotted on top of a structure map (TVD) of the Slave Point Formation at Clarke Lake field.